Durham E-Theses

Wireless Power Transfer Technology for Electric Vehicle Charging

MOU, XIAOLIN

How to cite:

Use policy

Wireless Power Transfer Technology for Electric Vehicle Charging

Xiaolin Mou

A Thesis Presented for The Degree of
Doctor of Philosophy

Department of Engineering
Durham University
United Kingdom

June 2017

Wireless Power Transfer Technology for Electric Vehicle Charging

Xiaolin Mou

Submitted for the degree of Doctor of Philosophy

June 2017

Abstract

In the years 1884-1889, after Nicola Tesla invented "Tesla Coil", wireless power transfer (WPT) technology is in front of the world. WPT technologies can be categorized into three groups: inductive based WPT, magnetic resonate coupling (MRC) based WPT and electromagnetic radiation based WPT. MRC-WPT is advantageous with respect to its high safety and long transmission distance. Thus it plays an important role in the design of wireless electric vehicle (EV) charging systems. The most significant drawback of all WPT systems is the low efficiency of the energy transferred. Most losses happen during the transfer from coil to coil. This thesis proposes a novel coil design and adaptive hardware to improve power transfer efficiency (PTE) in magnetic resonant coupling WPT and mitigate coil misalignment, a crucial roadblock in the acceptance of WPT for EV. In addition, I do some analysis of multiple segmented transmitters design for dynamic wireless EVs charging and propose an adaptive renewable (wind) energy-powered dynamic wireless charging system for EV.

Declaration

The work in this thesis is based on research carried out at the Energy Group, the Department of Engineering, Durham University, UK. No part of this thesis has been submitted elsewhere for any other degree or qualification and it is all my own work unless referenced to the contrary in the text.

Acknowledgements

There are so many people to thank for helping me during the three years and a half.

First, I would like to appreciate my supervisor Dr.Hongjian Sun for the continuing supports; from his valuable guidances, encouragements, and patiences during the period of my PhD study. Thank you so much for guiding me in both research and creativity. Your support is essential to my success here.

Additionally, I would like to be grateful for those who have worked with me in my research: Oliver Groeling and Yingji Zhang. Their contributions are appreciated as the most elemental work in my research. The discussions and built-in breaks help me avoid frustrated. Thanks for all the memorable moments we have spend together.

Meanwhile, I would also like to appreciate my colleagues: Minglei You, Qitao Liu, Jiangjiao Xu, Dan Li, Weiqi Hua, and all my friends in Durham University. Because of your companions, I spent a good time during my three years PhD time. Thank you so much for your help and encouragement.

Last but the most important, I would like to thank my family: my parents for giving birth to me and supporting me spiritually throughout my life.

Nomenclature

η Power transfer efficiency

Γ Intrinsic decay rate

κ Coupling coefficient

μ_0 permeability of free space

μ_r Relative permeability

σ Conductivity of the conductor

a Resonant coil wire radius

a_1, a_2, a_3, a_4 Predefined upper limits of traffic flow at different phases with respect to the maximum traffic flow in a specified time period

B Magnetic field intensity

C Capacitance

c Speed of light

f Resonant frequency

L Self-inductance

M Mutual inductance

M Number of pads that wind energy can charge

M_p Predicted number of pads by charging demand prediction (before Demand Response)

M_r Real number of pads after Demand Response and auto selection

N Traffic flow

n Maximum number of pads that wind energy can charge

N_{max} The maximum traffic flow in a specified time period

p Charging price, $£/kWh$

p_1 The lowest charging price when wind energy is adequate to supply all predicted demand (M_p), $£/kWh$

p_2 The medium charging price when wind energy can supply parts of the predicted demand and the Grid compensates for the supply deficit, $£/kWh$

p_3 The highest charging price when no wind energy is available and the grid supply all charging demand, $£/kWh$

P_g The amount of power from the grid, kW

P_m Maximum wind power of the system, kW

P_o Nominal charging power per charging pad, kW

P_r Total demand power after Demand Response, kW

P_{wt} The wind power of all wind turbines, kW

r Coil loop radius

R_o Ohmic resistance

R_r Radiation resistance

$s_{M_r[orM]}$ The serial number of pads to be turned on

V Wind speed, m/s

Contents

List of Figures

List of Tables

Chapter 1

Introduction

Wireless Power Transfer (WPT) is a term that includes several technologies to transmit power without connecting wires. This technology is not only useful for applications where interconnecting wire is not possible (such as charging cardiac pacemakers) but it is also useful for reducing toxic material resulted from disposing of 6 billion batteries each year used for battery operated electronic devices (e.g. laptops, mobile devices and toys). There is a need for significant research to mature the technology of wireless power transfer.

1.1 History of WPT Technology

To discuss about wireless power transfer technology, we will first acknowledge Nicola Tesla and his 'Tesla Coil'. In the years 1884-1889 Tesla got different patents for his alternating polyphase technology, which was a substantial breakthrough at that time against direct current technology. But the first patent [1], which reveals the landmark thoughts of Tesla, was filed in the year 1891 and is a full description of a high frequency lighting system. The specific feature of this system is the use of only one supplying single wire to the patented single terminal carbon lamps without a return wire, as shown in Figure 1.1.

With the first transformer P-S the alternating voltage of generator G (about 5 kHz) is transformed into high voltage. The resonance circuit S-C is then discharged along the spark gap. As a result there are high current peak in the primary winding
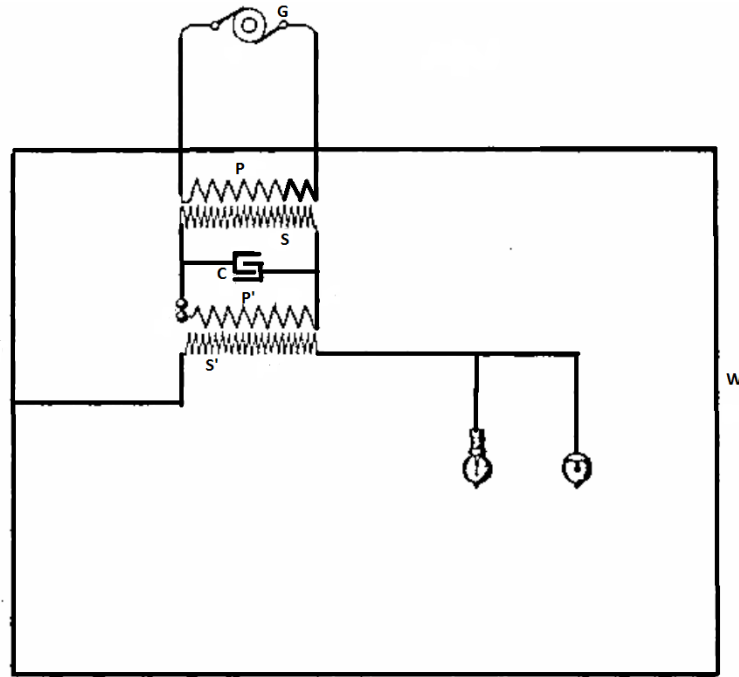
Figure 1.1: US-Patent 454,622 'System of Electric Lighting'issued on June 23rd, 1891 [1]

P' of the second transformer. With this second transformation the high frequency part of this current peaks is again transformed upwards and feeds the load circuit. One end of the second secondary S' is connected to a long wire or wire grid W positioned along the room walls. The other end is connected to Telsa's invented single terminal lamps [2]. This patent shows all the characteristics of the high frequency circuits with high voltage and high currents as used by Tesla.

In the year 1897 he applied for another patent [3] for a high frequency transformer with high power capabilities. Besides a common ground connection this transmission method needs only one transmission wire, as shown in Figure 1.2.

The generator G supplies the primary of the flat coil C. This simplified diagram does not come close to the real experimental set-up. Then as previously shown with the patent for the lighting system an intermediate step-up transformation with a spark gap and a high voltage transformer is necessary to achieve a resonant frequency of some million cycles per second. With some advantages it is also possible to use this step-up transformation after the flat secondary coil B. On one end the secondary B is connected to earth and on the other end to the transmission wire which is
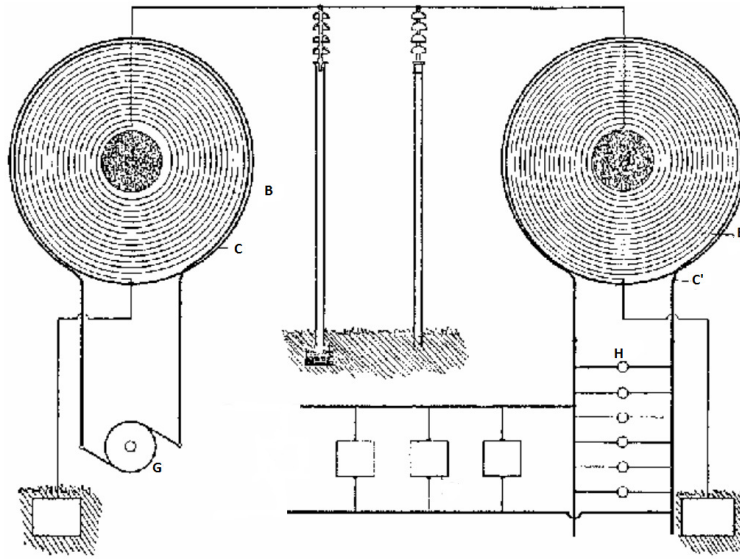
Figure 1.2: US-Patent 593,138 'Electrical Transformer' issued on November 2nd, 1897 [3]
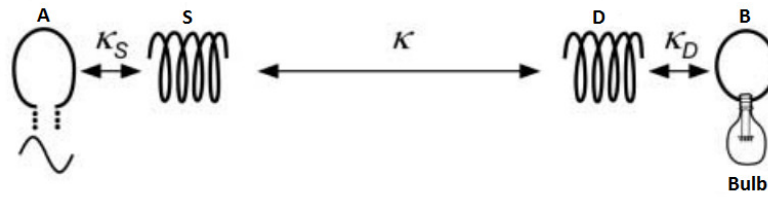
Figure 1.3: Schematic of the MIT experimental set-up [4].

connected to a receiving device with a flat coil B' of a symmetrical form. With a step-down transformation with the coil C' the electrical energy is finally transmitted from the generator G to the load H with only one conducting wire [2]. This flat coil has excellent performance with high voltage and high frequency signals and it looks like a modern four-coil wireless power transfer system model.

In 2007, a physics research group at the Massachusetts Institute of technology (MIT), led by Professor Marin Soljacic, presented a coupled magnetic resonance power transfer system 'Witricity', as shown in Figure 1.3. They experimentally demonstrated efficient nonradiative power transfers over distances up to 8 times the radius of the coils. This system was able to transfer 60 watts with 40% efficiency over distances in excess of 2 meters [4].

A is a single copper loop of radius 25 cm that is part of the driving circuit, which outputs a sine wave with frequency 9.9 MHz. S and D are respectively the source and device coils referred to in the text. B is a loop of wire attached to the load (light bulb). The various κ_s represent direct couplings between the objects indicated by the arrows. The angle between coil D and the loop A is adjusted to ensure that their direct coupling is zero. Coils S and D are aligned coaxially. The direct couplings between B and A and between B and S are negligible [4]. The emergence of this invention has attracted the attention of scientists around the world to wireless power transfer technology. In 2008, Intel reproduced the MIT group's experiment and wirelessly powering a light bulb at 75% efficiency, but for a shorter distance.

Nowadays, wireless power transfer technology is widely used in powering biomedical implants, tooth brushes, cell phones, laptops, and hybrid electric vehicles.

1.2 WPT technology for Electric Vehicle

In order to achieve the Paris Agreement, the Paris Declaration on Electro Mobility and Climate Change and Call to Action has set a global deployment target of 100 million electric cars and 400 million electric vehivles by 2030 [5]. There are only 1.26 million battery EVs (BEVs) and plug-in hybrid EVs (PHEVs) by the end of 2015 (accounting for around 8% of global vehicle threshold) even though it almost doubles that of 2014 [6]. The main obstacles for larger take-up of EVs, from the consumers' perspective, are the limited driving range, long charging time, lack of convenient charging infrastructure and relatively high purchase price compared with conventional internal combustion engine vehicles (ICEVs) [7]. On the other hand, governments also have concerns about the potential increase in electricity consumption and carbon emissions due to EV charging, especially during peak demand periods, even though many of them have launched preferential purchase policies to advocate EV. To tackle these constraints, wireless power transfer technologies for EV charging seem most promising.

WPT technology could revolutionise global transportation and accelerate growth

in the EV market, offering an attractive alternative to cabled charging. The need for a sustainable means of transportation, caused by the depletion of fossil fuels and increase in carbon output severely polluting our environment, has led to a growth in the research and innovation of EV technologies. The available range of conventional EV is a well-known constraint for customers who are yet to fully adopt eco-friendly motorisation. Furthermore, drawbacks, such as large and heavy batteries, high prices and long charging times, are issues which are not easily solved with current battery technology. Since EV is slowly becoming a more popular choice amongst vehicle owners, especially with government incentives and tax breaks, a more user-friendly means of charging makes economic sense. WPT offers an attractive alternative to a cabled charging system as the driver would simply park their vehicle above a TX coil embedded in the ground, whilst the chassis mounted RX coil initiates charging.

Wireless EV charging would solve one of the primary headaches: the trouble of having to get out of the vehicle and make the connections for charging. The advantages of wireless EVs charging can be summarized as follows [8]:

1) The elimination of the galvanic connection between the charging station and the vehicle simplifies the charging process and removes safety concerns related to the handling of the electrical equipment.

2) Automatic power transfer without the need for moving mechanical components is particularly attractive for charging public transportation EVs because it enables the charging process to be integrated with regular vehicle operation via 'opportunity charging' at bus stations, taxicab stands, or traffic lights along the route.

3) More frequent recharging reduces the battery's depth of discharge, which extends battery lifetime and allows dimensioning EVs with a smaller on-board energy storage capacity, thus lowering initial costs.

4) Moreover, the lack of a galvanic connection frees the charging station from moving mechanical components, which reduces the required maintenance.

There are two interesting fields in WPT for EV applications: static and dynamic charging WPT. For the static scenario, the EV may be charged in a modified car

park or garage. In a dynamic WPT system, the EV is continuously charged in a dedicated charging lane using multiple coils embedded in the road [9]. This makes charging more convenient and could result in downsized batteries, reducing their required capacity by 20% and permitting shorter charging times [10] [11].

The key challenge of the WPT technology is its lower transfer efficiency and lower pickup power than the conductive power transmission [12]. It is caused by multiple reasons and much research in recent years has focused on the methods of improving the PTE in EV wireless charging systems. Theodoropoulos *et al.* [13] presented a load balancing control algorithm for EV wireless charging to improve the efficiency. Some research examined different kinds of the primary supply architectures used for EV wireless charging to get the maximum efficiency [14]. Some researchers focused on the new materials, *e.g.*Y.D.Chung *et al.* proposed a high-temperature superconducting resonant coil to improve PTE [15]. The coil structure design and location can also affect the PTE in EV wireless charging [16] [17] [18]. In practice, the most immediate cause in its lower transfer efficiency is its low coupling coefficient of the loosely coupled transformer adapted in the WPT. A bipolar coupler was proposed to improve the coupling [19]. The misalignment between the transmitter and receiver coils can lead to a weak coupling thus reducing the efficiency. Existing WPT technology is bulky and highly sensitive to axial and angular coil misalignment [20] [21] [22] [23] [24] with limitations on the TX and RX coil sizes due to packaging constraints of most vehicles [25].

Recent research explored mitigating techniques such as optimal methods (adaptive rectification, adaptive frequency tuning or adaptive impedance matching [26]) and the arrayed TX coil structures [27] [28] [29]. Although adaptive frequency tuning is widely used in Kilohertz WPT system, the used ISM band is too narrow to accommodate the frequency tracking [30]. This method also needs additional circuitry at the transmitter and receiver [31]. Using impedance matching, the network itself may introduce additional power loss due to unavoidable nonideal capacitors and inductors, and it also leads to increased system complexity [30]. The key benefit of the proposed design of arrayed TX coil structure is that each coil can be individually turned on and off. But there always exists a tradeoff between coil size,

performance and cost.

For the arrayed TX coil structure, L.C.Meng *et al.* [32] studied two kinds of multi-coil format design for the induction cooker. The seven-circle coils structure and the hexagon like seven-coils structure can significantly improve the heating efficiency compared with the traditional single coil induction cooker. A single-layer winding array and coil structure for portable electronic products was presented [33] [34]. Hui and Ho [35] proposed a new multilayer PCB winding structure. Many hexagonal spiral windings were arranged as a transmitter array, and two more layers of PCB winding arrays were added in this design. This invention can successfully solve the problem of charging different types of mobile phone or portable electronic equipment placed on the same charging platform. [36] provided other useful details about WPT system design, particularly the power transmitter and power receiver designs and requirements. Generally, ferrite cores with high permeability and low magnetic loss tangent are useful in the enhancement of the magnetic coupling and consequently leading to high PTE. Hence, ferrite shielding plays an important role in WPT technologies [34].

One potential solution to the coil misalignment is an intelligent parking assist system developed by Toyota [37] which uses guidance systems and parking sensors to auto-pilot the vehicle more accurately to its charging bay. A major drawback, however, is the need for further fine tuning hardware to ensure millimeter precise alignment between both coils once the car is stationary. A further patent [38] proposed a light-activated mechanical positioning system that uses an array of photoelectric detectors coupled with a servo control system and an X-Y-Z mechanical driver to position the charging coils. This is less desirable due to the complexity and potential wear of moving parts and is less economical in mass production. The patent [39] depicts an upright inductive charger that stands in front of the car, where the RX coil is placed behind the license plate.

There are many companies focusing on these technologies, *e.g.* Evatran Wireless Charging Station, Volvo Wireless Charging for Electric Cars and Delphi Wireless Charging System.

Figure 1.4: Evatran Wireless Charging System [40]

Evatran Wireless Charging System, as shown in Figure 1.4.

Evatran has come up with a new method of recharging your EV with 'electric juice' which is an adapter (size of a shoebox) called Plugless Power, it is a new wireless charging system for EVs that makes use of electrical induction. The plugless charging system includes a parking pad over which the car is required to be placed. A control tower keeps a check on the system working properly and charging your vehicle. There is no particular modification required in the automobile to charge this way, other than a 10-pound adapter mounted to the undercarriage of the vehicle. There is no actual flow of electricity between the parking block and the adapter but instead charge is induced to the batteries generated by an electromagnetic field created by the magnetic coil housed in the adapter and parking pad. One can also use a normal plug in system for charging the EV [40].

Volvo Wireless Charging for Electric Cars, as shown in Figure 1.5.

Swedish car maker Volvo is developing wireless charging stations for electric cars. This project is officially named Continuous Electric Drive that allows EVs to charge without any hassle of either power sockets or charging wires. The new technology makes use of inductive charging and thus restoring the EV's battery power. The application of the new technology is simple. A charging plate that consists of a coil to produce the magnetic field is embedded within the ground. The EV, the base of
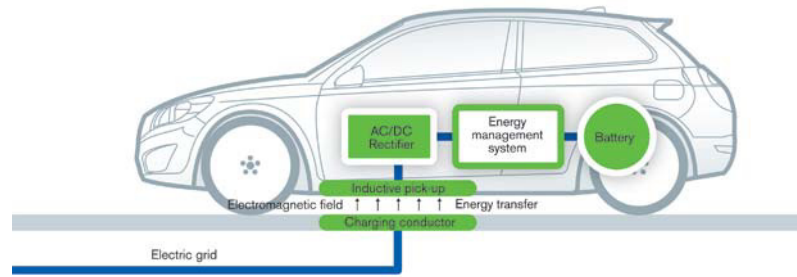
Figure 1.5: Volvo Wireless Charging for Electric Cars [40]
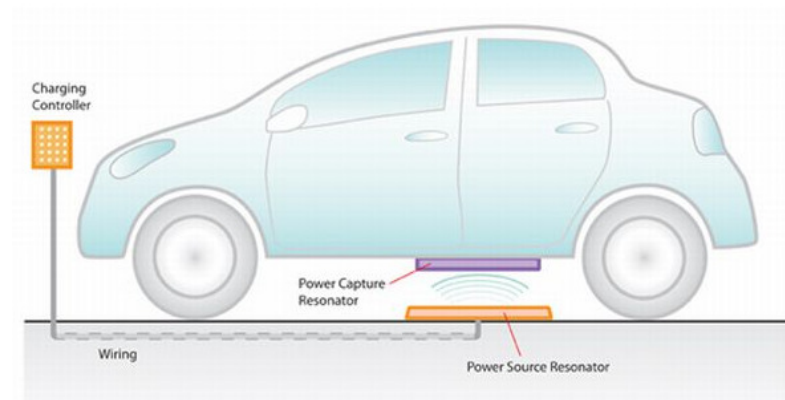
Figure 1.6: Delphi Wireless Charging System [40]

which consists of an inductive pick up plate, has to be parked above the plate where the energy produced by the magnetic field is transferred to the car's battery without any physical contact. The Volvo C30 Electric vehicle is furnished to get power with this new method. It is estimated that the C30 would take one and a half hours to be fully charged [40].

Delphi Wireless Charging System, as shown in Figure 1.6.

Delphi, an automotive parts supplier company has collaborated with WiTricity, a wireless energy transfer company to build a wireless charging system for electric vehicles. The technology used by the system is based on sharply resonant magnetic coupling. The system consists of a resonating pad mounted on the ground that carries power to the EV's battery pack. The power generated by the strong coupling

Figure 1.7: Model of Dynamic wireless EV Charging [41]

is efficiently transferred without any contact, thus charging the battery of the EV safely and in an easier way, without the requirement of any wires and sockets [40].

In a dynamic WPT system, as shown in Figure 1.7, the EV is continuously charged in a dedicated charging lane using multiple coils embedded in the road. This makes charging more convenient and can result in downsized batteries, reducing their required capacity by 20% and permitting shorter charging times. The dynamic WPT system is still at the laboratory stage, because it should be considered many restrictions, *e.g.* governmental support. The details will be mentioned in Chapter 3.

1.3 Motivation and Research Objective

The current problems of WPT system are summarized as below:

1. The power transfer efficiency is very low. Most losses happen during the transfer from coil to coil. *e.g.* Misalignment between transmitter coil and receiver coil.

2. The installation cost of WPT charging systems maybe higher than that of plug-in charging methods. *e.g.* The cost of infrastructure, and safety/shielding requirements.

3. Concern of RF radiation [42].

The transmission efficiency of magnetic resonant coupling WPT systems is defined by the size of the transmitter coils, the air gap between the transmitter coils, the selected resonant frequency and many other factors. [8] proposed that the magnetic coupling is mainly a function of the ratio between the air gap and the size of the transmitter coil. Large transmitter coils lead to higher efficiency for a given transmission distance.

The calculated results shown that increasing the radius of the receiver coil can improve mutual inductance, thus improving power transfer efficiency. However, there is a decreasing trend in power transfer efficiency when increasing the radius of the transmitter coil. That means large transmitter coils may not lead to higher efficiency. So there is a design trade off between the coil size and the power transfer efficiency in the system. In addition, the magnetic coupling decreases rapidly with misalignment. The misalignment between the transmitter coil and the receiver coil is inevitable, especially in the dynamic EV charging case. Therefore the outline of our research objectives can be defined as follows:

• **Improve the power transfer efficiency (PTE) for static wireless EV charging.**

Considering the design trade-off among the transfer coil size and the PTE, I proposes a novel coil design and adaptive hardware to improve PTE in magnetic resonant coupling WPT to mitigate coil misalignment, a crucial roadblock in the acceptance of WPT for EV. The new design was verified using an Advanced Design System (ADS), providing a good match to theoretical analysis. Custom designed receiver and transmitter circuitry was used to simulate vehicle and parking bay conditions and obtain PTE data in a small-scale set-up. Experimental results showed that PTE can be improved by 30% at the array's centre, and an impressive 90% when misaligned by 3/4 of the arrays radius. The proposed novel coil array achieves overall higher PTE compared to the benchmark single coil design.

• **Analysis of multiple segmented transmitters design for dynamic wire-**

less EV charging.

Multiple segmented transmitters rail for dynamic wireless power transfer (DWPT) electric vehicle charging can supply high power transfer efficiency. Previous research discussed the vehicles' speed as a key factor that can affect the design of the rail (especially, the distance between two neighboring segmented transmitters T) to maximize the system's PTE. However, this research finds it is not the vehicle's speed but the size of the transmitter rail that can affect the design of T for optimizing the PTE if the charging rail has a infinite length. Otherwise, I proposed an adaptive renewable (wind) energy-powered dynamic wireless charging system for EV.

- **Renewable (wind) energy-powered dynamic wireless charging system design.**

In order to increase rational utilization of wind energy resources to power EV thus enabling near zero lifetime carbon emission for EV systems (including their charging infrastructure), and to extend the range of EV for addressing consumers' range anxiety thus enhancing take-up of EV, an adaptive renewable (wind) energy-powered dynamic wireless charging system for EV is proposed. This system can adaptively choose how many EVs to be charged, and how to use available energy sources to charge them.

This thesis has 6 chapters: Chapter 2 reviews the theories of wireless power transfer technologies. Chapter 3 reviews the wireless power transfer technologies for electric vehicles charging. Chapter 4 presents a novel transmitter coil design for static wireless EVs charging which can solve the misalignment problem, thus improving the PTE. Chapter 5 presents the research of dynamic wireless power transfer for electric vehicle charging and Chapter 6 gives the conclusion and future work.

Chapter 2

WPT Technologies Overview

WPT technologies can be categorized in many different ways. M.Hassan [43] presented a method for classifying WPT technologies that depended on the range of power delivery: far field WPT technologies and near field WPT technologies. The far field WPT technologies are based on the electromagnetic radiation technique, and the near field WPT technologies can be further categorized as magnetic induction WPT and electric induction WPT. The differences between these two types of field are illustrated in Table 2.1:

WPT	Far Field	Near Field
Range	Long	Short
Phenomenon	Coupled mode theory	Induction theory
Frequency	Mega Hertz	Kilo Hertz
Efficiency	Low	High

Table 2.1: Main differences between Far field WPT and Near field WPT [43]

Near-field WPT technology can be categorised into two methods: magnetic induction (or inductive power transfer-IPT) and electrostatic induction (or capacitor power transfer-CPT) [44]. IPT system usually uses helically or flat cooper windings as resonant coils, as shown in Figure 2.1. Firstly, the alternating power is converted to a direct current using an AC to DC converter. Then the DC power is converted to high frequency AC power to drive the transmitting coil through a compensation network. Secondly, in the primary and the secondary coil, the high frequency current in the primary side coil generates an alternating magnetic fields, which induces an
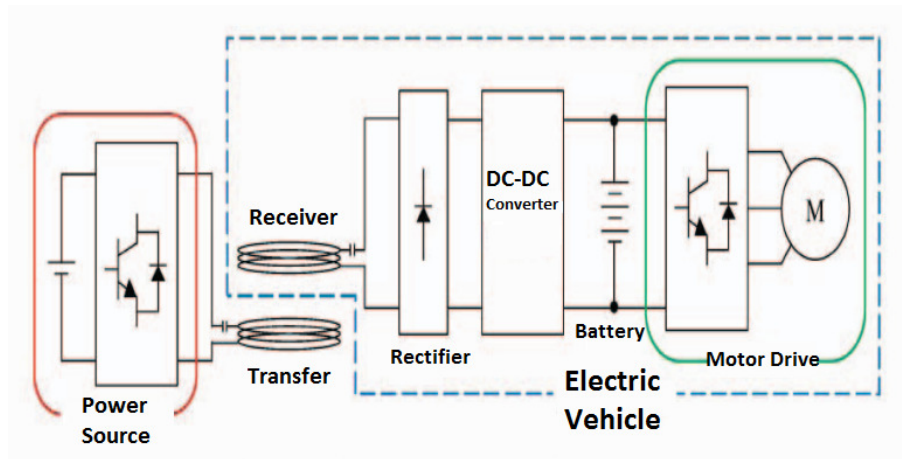
Figure 2.1: Typical schematic of the wireless inductive power transfer [45]
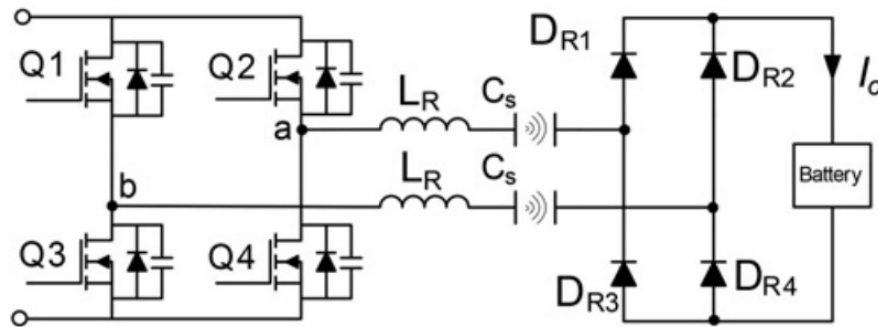
Figure 2.2: Typical schematic of the wireless coupling capacitor transfer [42]

AC voltage on the receiving coil. By resonating with the secondary compensation network, the transferred power and efficiency are significantly improved. At last, the AC power obtained is rectified to charge the battery.

Wireless capacitive power transfer (CPT) technology has been proposed recently as an alternate contactless power transfer solution. The CPT interface is constructed around a pair of coupling capacitors, as shown in Figure 2.2. Foil plates as coupling capacitors for a CPT system are potentially more cost effective than complex copper winding. The remainder of the power conversion system, including the inverter and rectifier structures, remains the same.

Moreover, from an alignment perspective, CPT only has one dimension (vertical z axis) [46]. Because of the low value of coupling capacitance, the CPT technology has an average efficiency range between 60-80% and the gap distance is less than

1mm. The IPT system not only has a vertical z axis dimension but also has a dimension in the horizontal surface. The gap distance is more than 10 cm. Another way of classifyina WPT technologies is categorising them into three groups, namely inductive coupling WPT, magnetic resonant coupling (MRC) WPT, and electromagnetic radiation-based WPT [47]. MRC-WPT is advantageous with respect to its high safety and long transmission distance. Thus it plays an important role in the design of wireless EV charging systems. Table.2.2 shows a summary of advantages and disadvantages of different wireless power transfer technologies.

WPT Technology Category	Advantages	Disadvantages
Inductive	Sample, safe, and high transfer efficiency in short distance	Short transmission distance, needs accurate alignment
Magnetic Resonant Coupling	Long transmission, distance no radiation	Difficult to adjust resonant frequency for multiple devices
Electromagnetic Radiation	Very high transmission efficiency over long distance	Radiation, needs line of sight

Table 2.2: Summary of advantages and disadvantages of different wireless power transfer technologies

2.1 Inductive Power Transfer

Inductive WPT is a technique which can deliver power contactless to devices with high efficiency. Typical inductive WPT systems employ two separate coils, one on the primary side as transmitter coil, the other coil on the secondary side as the receiver coil and the power transfered cross an air-gap between the two coils, shown in Figure 2.3. An electrical transformer is a good example of inductive WPT. Alternating current in the transmitter coil generates a magnetic field which induces
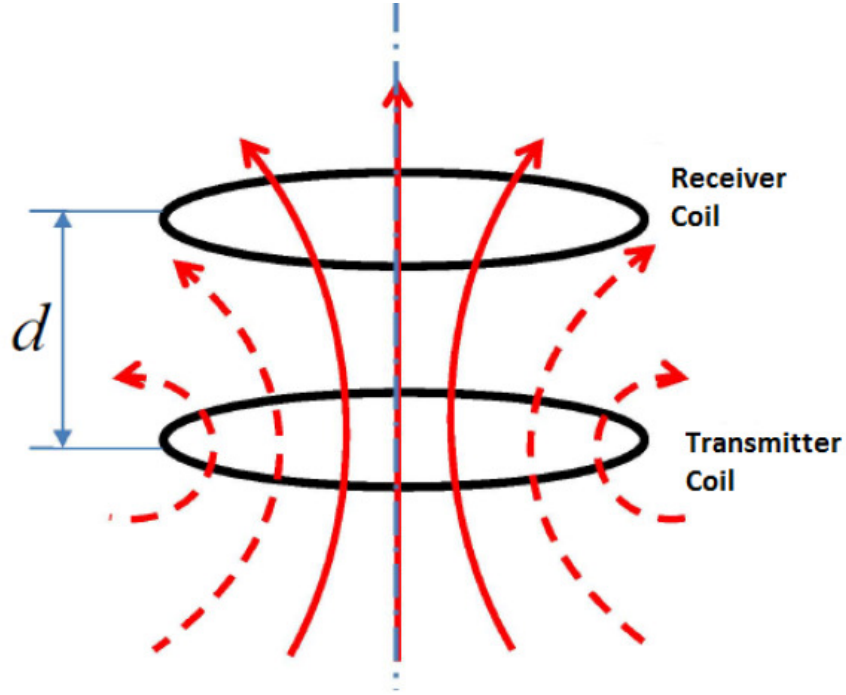
Figure 2.3: Scheme of Inductive Power Transfer Technique.

a voltage in the receiver coil. This voltage can be used to power the devices or charge a battery. It is a near-field transmission technique, which can support a transmission distance in mm or cm [48]

2.1.1 Theory

The fundamental theories of inductive WPT include the use of Biot-Savart's Law and Faraday's Law. Biot-Savart's Law is used for calculating the magnetic field produced by an arbitrary current distribution:

$$\mathbf{B} = \frac{\mu_0}{4\pi} \oint \frac{\mathbf{I}d_{\mathbf{I}} \times \mathbf{r}}{|\mathbf{r}|^3} \tag{2.1.1}$$

where μ_0 is the magnetic constant, $\mathbf{I}$ is the current in the transmitter coil, $d_{\mathbf{I}}$ is a vector whose magnitude is the length of the differential element of the wire, and $\mathbf{r}$ is the full displacement vector from the wire element to the point at which the field is being computed. Faraday's Law can then be used for calculating the induced voltage V_{Ind} over the receiver coil as the rate of magnetic field $\mathbf{B}$ change through an

effective surface area S by [49]:

$$V_{Ind} = -\frac{\partial}{\partial t} \oint \mathbf{B} \cdot d_s.$$ (2.1.2)

This technique is gaining popularity and wide acceptance for numerous applications as it offers the advantages of high transfer efficiency over short distances (1-5 cm). One significant drawback of the inductive WPT is its short transmission distance. Moreover, when the transmitter coil and the receiver coil are not well aligned, the power transmission efficiency (PTE) drops significantly. Despite these weaknesses, inductive WPT is often advantageous with respect to its simple design and high safety, therefore it has been broadly used in many applications including the charging of toothbrushes, mobile phones, watches and medical implants [50].

2.1.2 Inductive WPT Applications

Electronic Equipments

1. Oral-B rechargeable toothbrushes by the Braun company have used inductive charging since the early 1990s, as shown in Figure 2.4(a).

2. On March 15, 2013, Samsung launched the Samsung Galaxy S4, which supports inductive charging with an accessory back, as shown in Figure 2.4(b).

3. On September 9, 2014, Apple announced the Apple Watch (released on April 24, 2015), which uses wireless inductive charging, as shown in Figure 2.4(c).

Medical Implants

One important application of inductive WPT technology is the medical implant (*e.g.,* nerve stimulators, implantable monitor, endoscopic capsules) The power modules of the medical implants are implanted inside the human body, so a continuous and stable power supply is necessary. J.D.Kim *et al.* [51] proposed that penetrability was an important parameter in wireless charging for medical implants applications. Inductive WPT technology has been more often used in medical implants application, even though the magnetic resonance coupling WPT and microwave WPT

Figure 2.4: Scheme of Inductive Power Transfer Technique.

have advantages of a longer transmission range. However, a microwave might show negative aspects on wireless powered medical implants applications because it might influence human health.

A WPT system for medical implants applications usually consists of a power transmitter which is outside the human body, and a power receiver, which is inside the body or patched on the human skin. A typical endoscopic capsule requires 10-30 mW of power with a peak demand of 10 W, and a PTE within 5%. Figure 2.4 (d) shows a video endoscopy capsule. This capsule has a power provider, image sensor, image data buffer, coding correction, modulation, control logic and wireless transceiver.

2.2   Electromagnetic Radiation Power Transfer

Low PTE is one issue in the development of WPT technologies. In order to solve this problem, a strong directional, energy concentrated laser beam, which has similar properties as a microwave beam is worth considering. The Radio-frequency (RF)/microwave and laser-based systems can be used in electromagnetic radiation WPT, and they also belong to far field WPT.

2.2.1   Theory

In RF/ microwave WPT systems, there are several core components that transfer energy between two points in space, as shown in Figure 2.5. In the transmitter part, RF/microwave power must be generated at the base station, typically via a microwave source. After the base station, the radiated energy propagates through the channel. In the receiver part, the energy harvesting node has an energy conversion circuit consisting of a receiving antenna(s), a combination matching network/bandpass filter, a rectifying circuit, and a low-pass filter. The band-pass filter helps to ensure that the antenna is correctly matched to the rectifying circuit, and harmonics generated by the rectifying element are not reradiated to the environment. Finally, an output low-pass filter removes the fundamental and harmonic frequencies from the output, sets the output impedance, and stores charge for consumptions [52].

The one other technique of electromagnetic radiation power transfer involves using a laser beam. Laser beam power transmission is the only available technology for powering the space elevator into a low earth-orbit and it has also been demonstrated for use in biomedical applications. However, for these applications, the safety issues are not considered [53]. A laser beam system has several technological challenges that are limited by weather, beam safety and current cost.

A.Massa *et al.* [54] proposed a summary of the key-roles and challenges in designing transmitting and receiving antenna arrays to reach high-efficiency power transfer in a RF long-distance WPT system, as shown in Figure 2.6. In this antenna arrays based RF-WPT system, a transmitting array is fed by a DC source with power. The
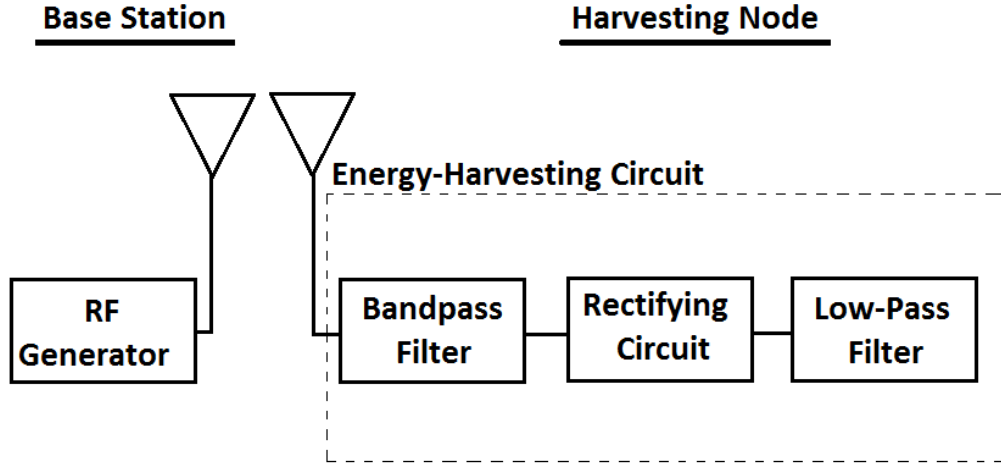
Figure 2.5: Scheme of Microwave WPT system

feeding network consists of the DC-to-RF conversion and the powering of radiating elements (*e.g.,* dipoles, waveguide slots and microstrip patches). In the receiving array side, antennas are responsible for gathering the RF wave to convert it to DC power. The first thing to consider in a RF-WPT system design is end-to-end RF-WPT system efficiency. This efficiency is mainly related to the performance of each part of the system. (*e.g.,* the efficiency of the DC-to-RF conversion in transmission and radiation and the efficiency of the RF-to-DC conversion in reception, the capability to suitably shape the radiated beam towards the collection area.) The challenges in transmitting array design include the real-time steering problem and the beam shaping problem. In other words, the transmitting must be steering the beam toward the receiver direction, and shaping the radiated beam through suitable weighting strategies, so that the power transmitted is maximized. The challenge in receiving array parts is finding out the most widely adopted strategy which is preferred over a standard phase array. This paper [54] proposes an innovative receiving network scheme for rectenna arrays to obtain high average efficiency: the subarray-based architectures and the combination of rectenna-collected signals architectures.

The main advantage of the electromagnetic radiation power transfer approach is its high PTE over long distances. But it often has radiation concerns and requires
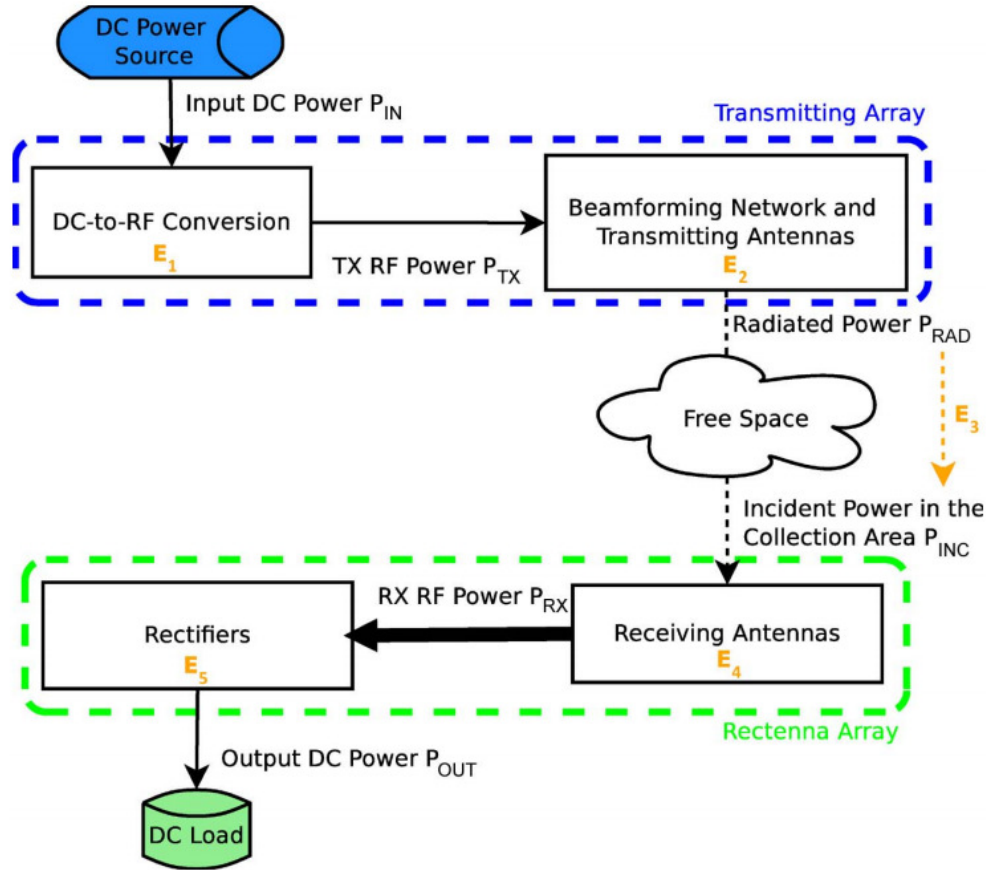
Figure 2.6: Schematic diagram of a long-range WPT system [54]

line of sight transmission. The various microwave frequencies suggested in many electromagnetic radiation WPT studies are at or around 2.45, 5.8, 8.51, 35, 94, 140 and 170 GHz. Lower frequencies have more efficient energy converters, larger antenna tolerances and lower cost. The higher frequencies can reduce the diameter of antennas and rectennas but we should consider propagation impairment [55]. The electromagnetic radiation WPT has made significant contributions to space-based solar power (SSP) or solar powered satellites (SPS). Moreover, this technique can be used for enabling energy harvesting (EH) in wireless powered communication networks (WPCN) (*e.g.,* cellular network, wireless sensor networks (WSNs) or named wireless power networks (WPNs).)

2.2.2 Electromagnetic Radiation WPT Applications

Solar Powered Satellite

Solar powered satellite (SPS) is a technology which can collect a massive amount of solar energy in orbit and transfer it via wireless power transmission for use on earth. Several different approaches of solar powered satellites have been proposed. The fundamental structure of SPS has a solar energy collection and a method for conveying the collected energy to the ground. For energy collection, photovoltaics (PVs), solar thermal, solar- pumped lasers and simple reflection have been considered. For transmission, microwave frequencies and lasers have been examined in literature. Each collection and transmission have their own distinct advantages and disadvantages. PVs are considered for their simplicity, while solar thermal is advocated for its theoretical ability to achieve high efficiencies transcending the schockley- Quessier limit that bounds PVs. Laser transmission is advanced for its ability to utilize smaller transmitter and receiver apertures, whereas microwave transmission is favored for its greatly reduced susceptibility to attenuation from ropospheric effects.

Common technical concerns for all solar powered satellite implementations include total space segment mass, transmitted energy density on the ground, conversion efficiencies of the space and ground segments, power beam pointing and control, interaction between the power beam and the ionosphere and troposphere, and electromagnetic compatibility with other satellites and terrestrial services [56]. The original model of the solar powered satellite was proposed by the Solar High Study Group of the DOE/NASA in 1978. It consists of an enormous satellite in geosynchronous orbit with separate solar collection and power transmission surface. The satellite would send many gigawatts of electricity to the utility grid via a microwave downlink operating at either 2.45 or 5.8 GHz, which would be collected by large rectifying antenna (rectenna) receiving stations [56].

Wireless Powered Communication Networks (WPCN)

Wireless powered communication network (WPCN) means the energy is transmitted from the energy transmitter to the wireless devices over the downlink and in-

formation is transmitted from the wireless devices to the access point over the up-link [57] [58]. It can be used in many areas including cellular networks, wireless sensor networks, smart grids [59] [60] etc. C.Kyprianou *et al.* [61] presented a green wireless powered communication network, which is usually achieved by harvesting energy from natural resources (sun, wind *etc.*) Some papers also use wireless power transfer networks (WPTNs) to define it, however, the basic theory in both is the same. Wireless power transfer networks (WPTNs) are deployed to transfer suffi-cient power to nearby energy receiver devices over the air. The major physical layer technique of WPTNs is through microwave/ RF. Energy transmitter devices form-ing WPTNs are capable of controlling their transmitter power and frequency of the waveforms in order to charge different types of energy receivers demanding differ-ent levels of energy. Each energy receiver is equipped with a harvester circuit that converts the received RF signal to a DC signal to charge its built-in battery [62].

Cellular Networks

Using microwave power transfer (MPT) for delivering energy wirelessly from power beacons (PBs) to mobile devices was presented in [63], as shown in Figure 2.7(a). This hybrid-network model can provide mobiles with practically infinite battery life and eliminate the need for power cords and chargers. The hybrid-network consists of two main parts: power beacons (PBs) and base stations (BSs). In this model, PBs power uplink transmissions by isotropic radiation, called isotropic MPT, or direct energy towards target mobiles by beamforming, called directed MPT. The model consists of three main parts: the Access-Network Model, Power-Beacon Network Model, Metrics and Constraints. Access-Network Model uses coordinates of the BSs to confirm the locations of mobiles which are associated with the nearest BSs. In the power-Beacon network model, each mobile deploys a microwave-power receiver with a dedicated antenna to intercept microwave energy transmitted by PBs. Moreover, there are two energy storage units in one mobile, as shown in Figure 2.7(b). One is used as the microwave power receiver and the other one is used for powering the transmitter. When the transmitter is inactive, the microwave-power receiver remains active utill all units are fully recharged. The metrics and constraints are
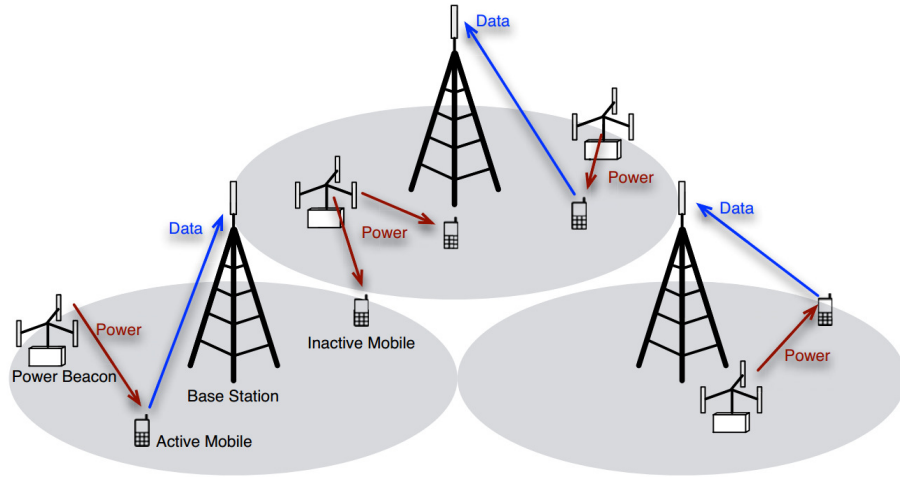
(a) The scheme of the hybrid-network model
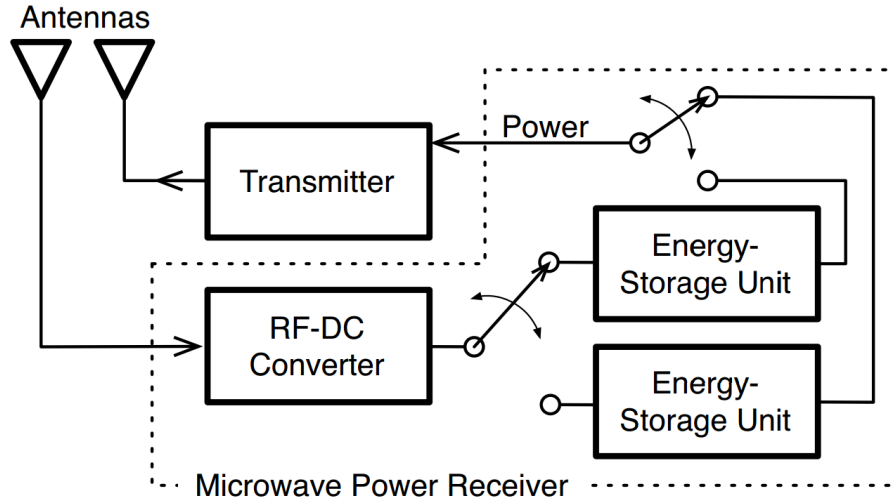
(b) A mobile consists of a transmitter and a microwave-power receiver

Figure 2.7: Microwave WPT technology for a cellular network [63]

considered from two aspects: the information outage constraint at BSs, and power outage constraint at PBs. One more important contribution of [63] is the analysis of the tradeoffs between the network parameters and PB/BS densities for different network configurations according to isotropic/ directed MPT and mobiles having large/small energy storage.

Wireless Sensor Networks

Wireless sensor networks (WSNs) (as shown in Figure 2.8) play a critical role in numerous applications including Internet of Things (IoT), smart homes, smart grids,
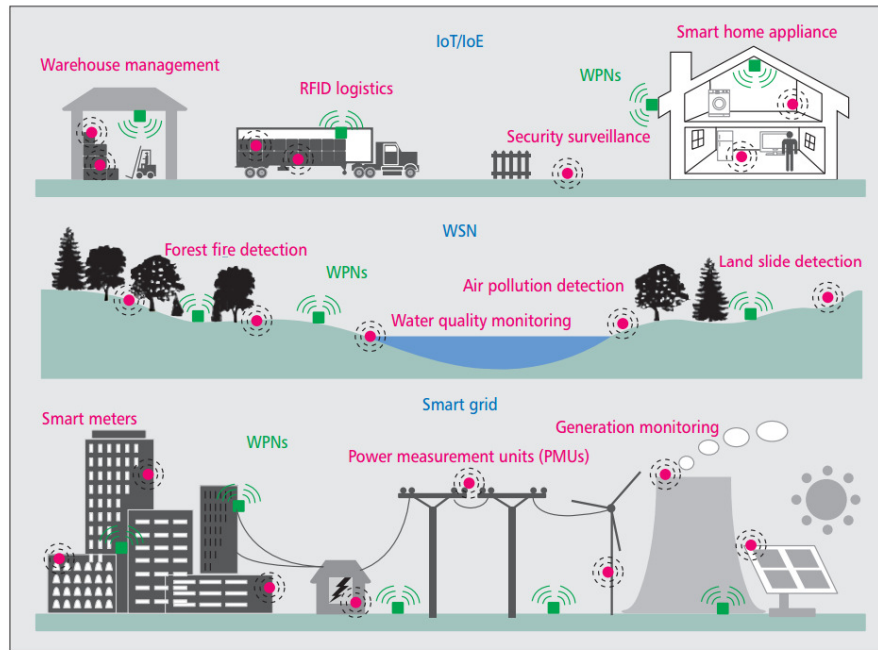
Figure 2.8: Example applications of WSNs in IoT/IoE systems [65]

health care *etc.*. In Figure 2.8, the green nodes are wireless power networks nodes, which transmit RF energy to wireless powered devices. The red nodes are wireless sensor networks, which transmit the information to devices. Naoki [64] proposed a microwave WPT system design for a ZigBee sensor. In this WPT-ZigBee system, the frequency for the WPT and the ZigBee wireless communication are at the same 2.45 GHz band. The power transfer efficiency is mainly related to RF-DC conversion efficiency and DC-DC conversion efficiency. The loss transfer efficiency was always caused by the mismatching of the impedance between the rectifying circuit and DC-DC converter, or re-radiation from the rectenna. So they proposed a rectifying circuit with a recollection circuit of reflected waves to decrease the reflected microwave, thus increasing efficiency.

In general, the static sensor nodes' battery of the rechargeable WSNs can be recharged using solar power harvesting. In addition, these sensor nodes can also be recharged via WPT. The key concern in rechargeable or energy harvesting wireless sensor networks is the max flow or data rate at one or more sinks, and this data rate is constrained by the available energy at each node as well as link capacity. T.He *et al.* [66] [67] presented a novel approach that sensor nodes can be recharged via

WPT. Moreover, an additional node, which is called an auxiliary charger (AC), is used to upgrade the recharging rate of a finite number of low energy nodes, thereby improving the max flow of rechargeable WSNs. They proposed three algorithms to place ACs in large scale WSNs, namely *path*, *Tabu* and *lagOP*. According to the results in large networks, *Tabu* has the best performance but the highest running time. However, this work did not consider random energy harvesting rates, and the numerous of sampling is limited.

2.3 Magnetic Resonant Coupling Power Transfer

At first glance, magnetic resonant coupling WPT technology reminds us of inductive coupling power transfer, and in some sense, it can be considered a special case of inductive coupling power transfer where the primary and secondary coils are tuned in resonant frequency by adding compensation capacitors. Some papers defined it as inductively coupled power transfer [inductively coupled power transfer (ICPT) for electric vehicle charging, elsevier]. This thesis defines it as magnetic resonant coupling (MRC) power transfer.

2.3.1 Theory

The scheme of MRC-system:

In previous research, a typical MRC-system is generally classified as either a two-coil or a four-coil system. Figure 2.9 shows the two-coil MRC-system. The two-coil MRC-system consists of two electromagnetic subsystems with the same natural resonance frequency, and it is the original type of the MRC-system.

To improve PTE at longer transmission distance, the four-coil system has been proposed. Figure 2.10 shows the four-coil MRC-system. In this system, the transmitter includes a source coil and a sending coil (or primary coil), the receiver includes a receiving coil (or secondary coil) and a load coil.

A four-coil system offers the advantage of two degrees of freedom such that the source coil can be mounted and coupled with the sending coil to adjust the system input impedance, and the load coil can be mounted and coupled with the receiving
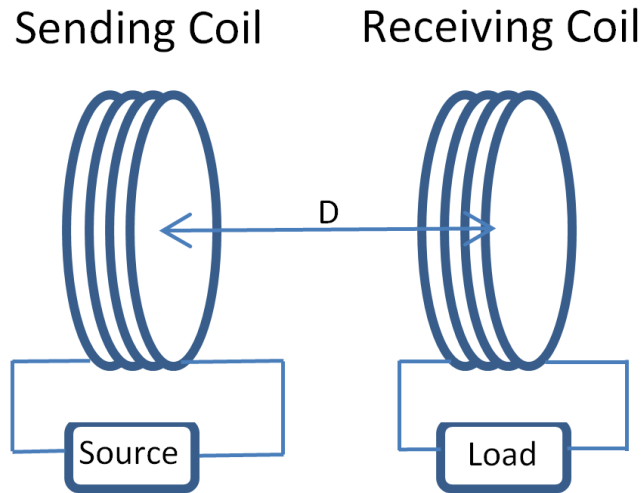
Figure 2.9: Scheme of tow-coil MRC-system
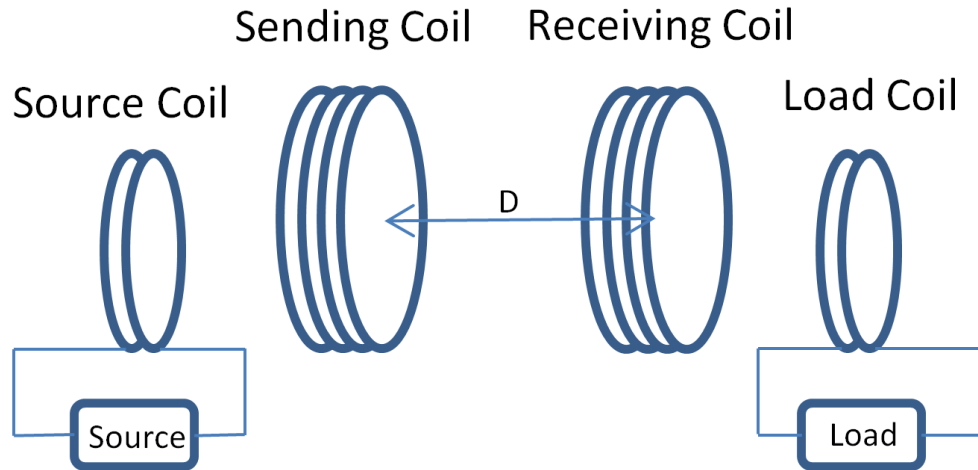
Figure 2.10: Scheme of four-coil MRC-system

coil to adjust the equivalent load resistance seen from the receiving coil to match the load condition. A four-coil system is suitable for mid-range applications while a two-coil system gives better performance in short-range applications. Applications are considered short-range or mid-range based on whether the transmission distance is smaller or larger than the coil dimension. *e.g.,* in electric vehicle (EV) applications, the transmission distance, also known as air gap, ranges typically from 100 mm to 300 mm, and the coil dimension is always larger than the transmission distance. Therefore, a two-coil system is adopted for this short-range or mid-range application.

The four-coil system can improve the PTE at large transmission distance, how-
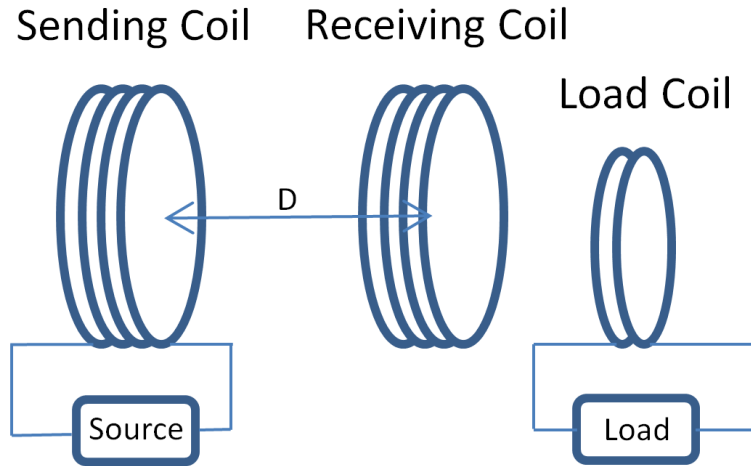
Figure 2.11: Scheme of three-coil MRC-system

ever, it causes a significant reduction in power delivered to load (PDL) [68]. M.Kiani *et al.* [68] proposed a three-coil MRC-system, as shown in Figure 2.11. This topology not only provides a high PTE as the four-coil method but also offers a PDL that is significantly higher than the four-coil MRC-system at large transmission distance.

The compensation topology of the MRC-system:

The compensation circuit is often required for both transmitter and receiver in MRC-system to improve the power transfer capability. The compensation circuit can not only make the system resonant, but also minimizes the volt-ampere (VA) rating of the power supply, and regulate the value of current in the supply loop and voltage of the receiving loop with a higher efficiency. There are several compensation topologies studied in literature, the basic compensation topologies are: series-series (S-S) compensated, parallel-parallel (P-P) compensated, series-parallel (S-P) compensated and parallel-series (P-S) compensated, as shown in Figure 2.12. With series compensation, a compensation capacitor is placed in series with the primary or secondary leakage inductance, whereas with the parallel compensation the compensation capacitor is in parallel with the primary or secondary.

The basic one series-series (S-S) compensation topology is shown in Figure 2.12. The transformer inductances Lp in the primary side and Ls in the secondary side, respectively. Cp and Cs are the primary and secondary compensation capacitors,
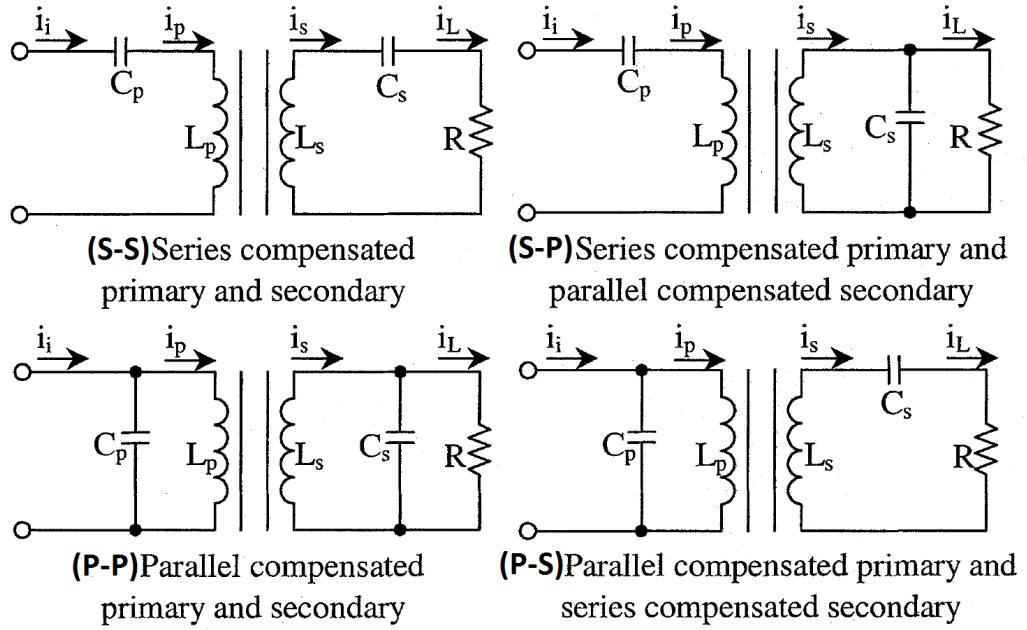
Figure 2.12: The compensation circuit topologies of MRC-system [69]

for enhancing energy transfered from an AC source to an output loading resistance R. The AC source as input value is generally an equivalent voltage generated from a half-bridge or full-bridge switching circuit.

The standard of choosing the compensation topology in primary and secondary is different. In primary side, the compensation topology depends on the application environment, the transmission range or voltage requirement. Series compensation topology is useful in short transmission distance. If the primary coil requires large current, this makes parallel compensation more attractive. In the secondary part, series compensation has voltage source characteristics, thus it is well suited for systems that have an intermediate DC bus. Parallel compensation in the secondary part has current source characteristics and is well suited for battery charging [70]. For instance, a wireless electric vehicle battery charging system is suitable for using a parallel-parallel (P-P) compensation topology.

Besides the above mentioned four basic compensation topology circuits, there are several hybrid series-parallel compensation topology circuits found in literature. (*e.g.,*LCL, LCC,LCCL.)

Wu *et al.* [71] discussed the LCL compensation circuit that uses WPT system. There are several advantages of LCL compensation topology circuits: constant cur-
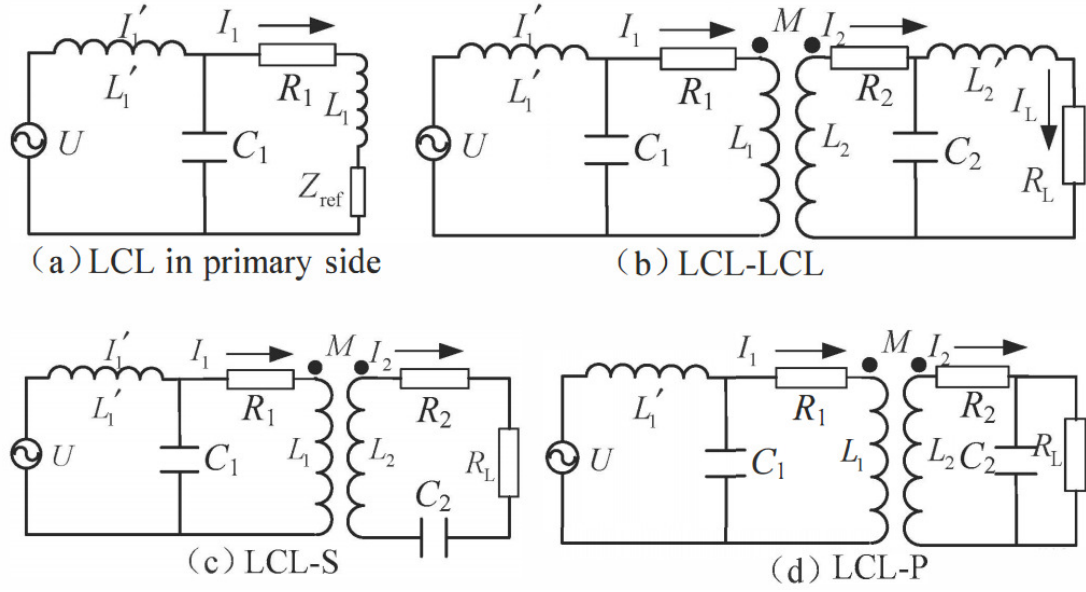
Figure 2.13: Double-sided LCC compensation topology [72]

rent source property, high efficiency at light load (unity power factor) and harmonic filtering capabilities. F.Liu [72] gives comparisons of the four topologies of LCL compensation circuits (LCL-S, LCL-P, LCL-LCL), shown in Figure 2.13 on their load characteristics comprehensively and systematically. It pointed out that the primary inductance has an influence on the load characteristics when the LCL topology is utilized in the primary side.

One more recent compensation topology called double-sided LCC compensation circuit topology was proposed by T.Kan and F.Lu [73] [74]. Figure 2.14 shows a wireless charging system using the double-sided LCC compensation circuit topology. The DC input is transformed to a high frequency AC power by a full-bridge inverter, which is formed by MOSFET switches $S1-S4$. At the transmitting side, $Lf1$, $Cf1$, $C1$, and $L1$ form the primary resonant part, which is tuned to have a resonant frequency the same as the switching frequency of the full-bridge inverter. The high frequency AC power resonates in the primary resonant part. At the receiving side, $Lf2$, $Cf2$, $C2$, and $L2$ make up the secondary resonant part. Both the primary resonant part and the secondary resonant part have the same resonant frequency. Since there is no wire connection between the transmitting side and the receiving side, the high frequency AC power is transmitted wirelessly through the main cou-
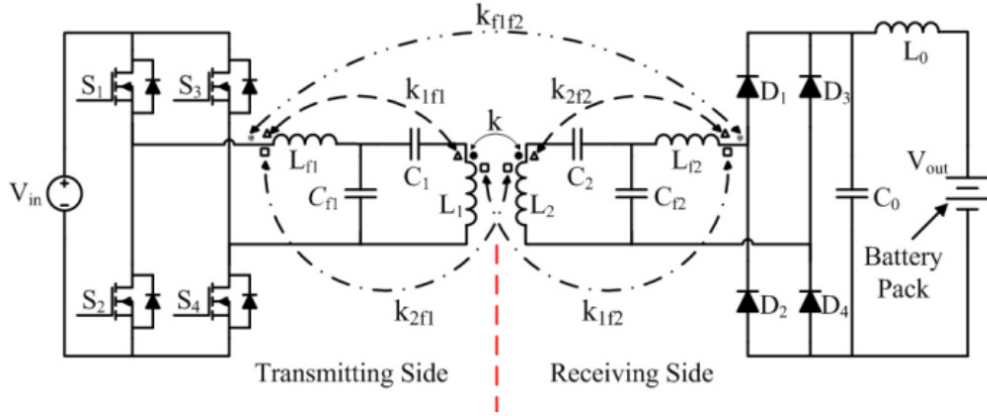
Figure 2.14: Double-sided LCC compensation topology [73]

pling between the main coils $L1$ and $L2$. Afterwards, AC power is converted back to DC by the rectifier consist of four diodes $D1 - D4$. After being further filtered by the CL-filter, the power is qualified to charge the battery packs.

In double-sited LCC compensation topology, $L1$ and $L2$ indicate the main coil inductance while k is the coupling of these two coils; $Lf1$ and $Lf2$ denote the compensation coil inductance; $k1f1$ and $k1f2$ are used to denote the coupling between $L1$ and $Lf1$, $L1$ and $Lf2$, respectively. $k1f1$, $k2f2$ are the same-side coupling. J.Deng *et al.* [75] proposed that the vertical gap has the greatest impact on the cross-side couplings (k, $k1f2$, $k2f1$, and $kf1f2$) and the main coils' self-inductance. Remarkably, the coupling between the compensation coils $kf1f2$ increases quickly when the vertical clearance is smaller than 140 mm. To avoid the energy exchange between the compensation inductors, the range of the vertical gap should be 140 mm-200 mm. The nominal gap is set to be 150 mm accordingly. The advantage of this topology is that it performs as a current source to both the input and output, and it can maintain relatively high efficiency at both light and heavy load conditions [74]. However, one drawback of this topology is its large complex due to the compensated coils [73].

A.Ong [76] proposed a compensation topology circuit where a parallel resonant tank is added to the series compensation, named as the LCCL compensation topology circuit, as shown in Figure 2.15.

Compared to the series compensation circuit, the LCCL circuit produces high
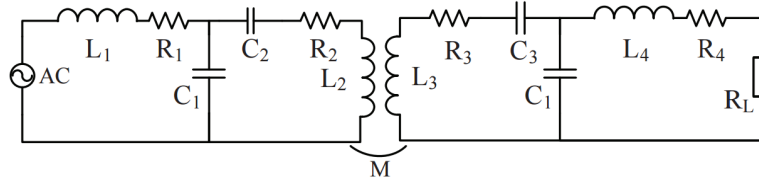
Figure 2.15: LCCL compensation topology [76]

Table 2.3: The summary of impact factors

Impact Factor	Description [reference]
Coil Design	Coil material [77, 78]
	Coil size [79, 80]
	Coil geometry [80–86]
Coil Alignment	Lateral misalignment [87, 88]
	Angle misalignment [88]
Circuit Design	Frequency [79, 89]
	Compensating circuit [90]
Environmental Analysis	Temperature, humidity [79, 91]
	Ferrite Core
Multiple Transmitters	Add additional coils [92].

maximum transfer power. In addition, LCCL circuit produces high efficiencies with high transfer power levels with high coupling coefficients.

2.3.2 Main Research Themes

Although MRC-WPT technology has been successfully utilized to develop a number of commercial products, there are still many areas for improvement. Reviewing the literature, the main research themes on MRC-WPT can be summarized as:

1. Improving the transmission efficiency and distance,

2. Multiple transmitters/receivers design.

Improving the transmission efficiency and distance

There are several impact factors affecting the PTE and the transmission distance that are summarized in Table 2.3.

Coil Design

Optimizing the coil material can improve the system's PTE. In [77], it was shown that using a high Q planar-Litz coil can lead to almost 40 % efficiency improvement when the transfer distance is 0.5 cm. The coil is designed by dividing the wide planar conductor lengthwise into multiple stands to reduce the high frequency conduction losses and improve the Q-factor. T.Mizuno *et al.* [78] proposed a magnetoplated copper wire whose circumference is plated with a magnetic thin film. Due to the magnetic thin film, the inductance is increased. Meanwhile, the resistance due to the proximity effect is decreased because eddy current loss is reduced.

The coil size is one important parameter in MRC-WPT system design. A major design constraint for the coil is space limitation [80], *e.g.,* receiver coil size for biomedical implants should be small, while the transmitter coil size can be large. However, for electric vehicle charging or industrial applications, both transmitter coil and receiver coil can occupy large space. The ratio of the coil diameter and transmit distance (air gap) can also affect transmission efficiency. Assuming a constant Q-factor, if the air gap (L) is smaller than the half of the coil diameter (R), i.e., $L/R < 0.5$, the transmission efficiency will become greater than 80%. Furthermore, if $L/R < 0.25$, the transmission efficiency can reach 90% [79].

The coil geometry also has an effect on the PTE. Solenoidal coil, flat (or spiral) coil, square coil, and circular coil have different efficiencies according to the literature. X.J.Song *et al.* [81] gave an analysis and experiments of solenoidal coil, however, a flat coil is widely used in a MRC-WPT system. Z.Pantic [82] gives some experimental comparisons between the solenoidal coil and spiral coil. J.P.K Sampath *et al.* [80] and M.Q.Nguyen *et al.* [83] proposed experiment analysis of different types of flat (or spiral) coil design. For a spiral coil, the geometric parameters determine the radiation patterns and can be optimized to obtain maximum power transfer and transmission link efficiency for particular requirements in targeted applications. Three parameters are considered: inner radius , outer radius , and turn number. M.Q.Nguyen [83] presented a method to determine of these three parameters thus optimizing the design of spiral antenna considering both field intensity and circuit efficiency. M.Q.Nguyen and Ishizaki [83, 84] proposed comparisons of two typical
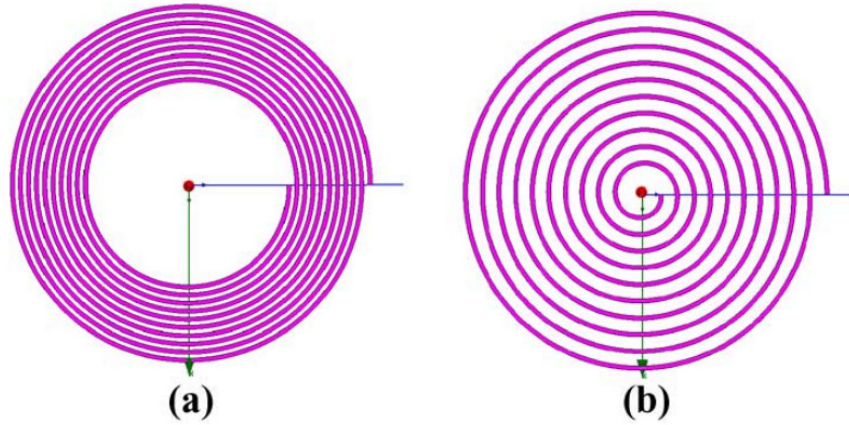
Figure 2.16: spiral coil design in different types [83]

flat (or spiral) coil design as shown in Figure 2.16. In the same area, the physical lengths of coil(a) are longer than coil (b), however, coil (a) is capable of maintaining 90% of the maximum field intensity while coil (b) can only maintain about 50% within the same area.

The other coil geometry is defined from the coil's appearance, *e.g.,* circular coil, square coil, rectangular coil or coil array *etc..* Optimizing the geometry can maximize system PTE. This optimization is only possible when maximizing the value of the quality factor and coupling coefficient. S.Mehri *et al.* [85] proposed a variable width square coil geometry based on single and double layer. Using a single lager variable width square coil, the quality factors can improve 8.2% in comparison with a conventional uniform square width coil geometry, and double layer can reach 11% higher in quality factors in comparison with single layer coil. F.Jolani *et al.* [86] proposed a four square coils array in the transmitter part. This coil array can increase the PTE when the receiver is moving. The coil design of small electrical devices (*e.g.,* mobile phone) always chose a coil array in PCB. Large devices (*e.g.,* electric vehicle) have more coil geometry design cases *e.g.,* double-D (DD), double-D-quadrature (DDQ), and details will be given in Chapter 3. Figure 2.17 shows the comparison of the coil topologies [93].
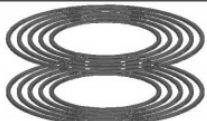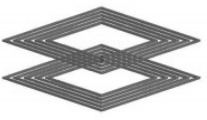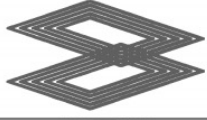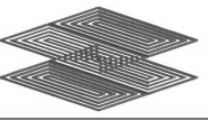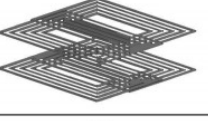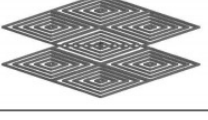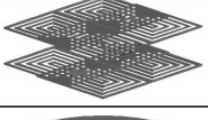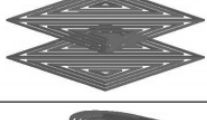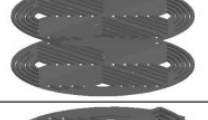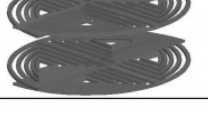
Circular		DD Overlapped	
Square		DDQ	
Rectangular		Two Squares	
Compensation Winding Primary		Two Squares Overlapped	
Compensation Winding Secondary		Four Squares	
Compensation Winding Both-Sided		Four Squares Overlapped	
Triangular		Circular Quartered	
DD		Circular Quartered Overlapped	

Figure 2.17: List of coil topologies [93]

Coil Misalignment

One of the important factors affecting the PTE is the coil misalignment between the transmitter coil and the receiver coil [88,94–96]. There are two forms of misalignment [88,95]

- Lateral misalignment: when the transmitter coil and the receiver coil are placed in parallel, their centres do not only have horizontal distance Δ, but also have the vertical distance d, as shown in Figure 2.18.

- Angular misalignment: the receiver coil is turned by an angle ϑ when the centres of the transmitter coil and the receiver coil are well aligned, as shown in Figure 2.19.
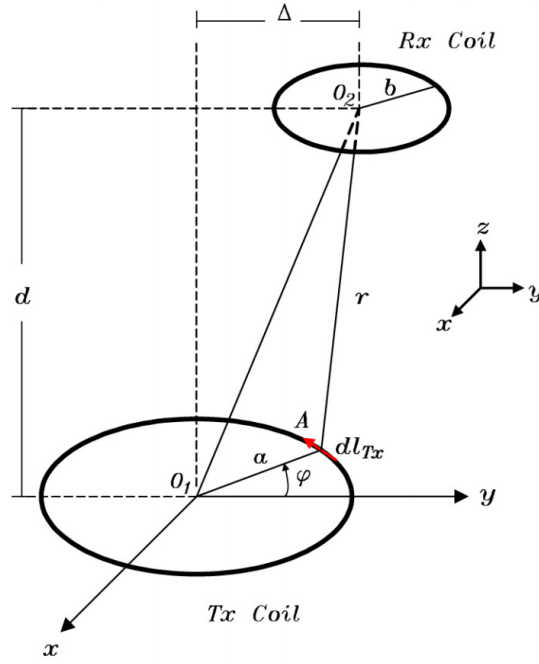
Figure 2.18: Lateral misalignment
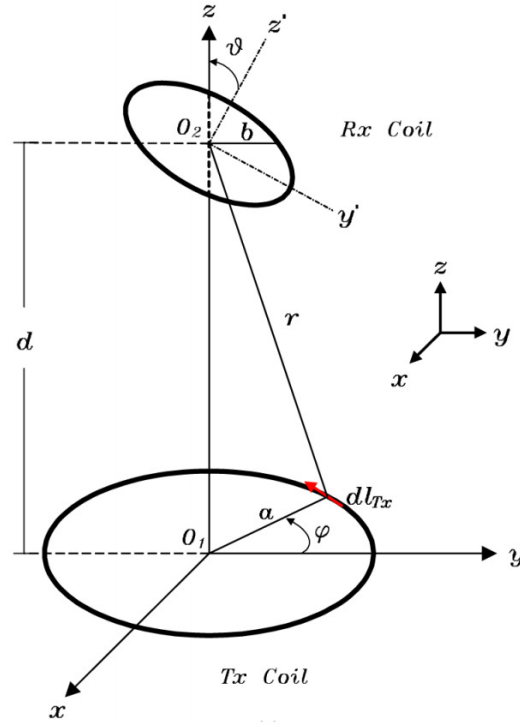
Figure 2.19: Angular misalignment

The magnetic resonance coupling WPT system with lateral misalignment was studied in [87] that used an ANSYS model to simulate the relationship between the transfer efficiency and the lateral misalignment distance. The high efficiency misalignment range can then be determined. In practice, the coils' lateral and angular

misalignment may happen together. However, most of existing work analysed the lateral misalignment and the angular misalignment, respectively. Therefore, there exists a research gap here. (*e.g.* in static electric vehicle wireless charging, the research almost ignores the angular misalignment, however, in dynamic electric vehicle wireless charging, the angular misalignment should not be ignored. Because the charging environment is complex.) D.Liu *et al.* [97] proposed a two orthogonal coils topology to provide misalignment insensitivity. The result shows that the proposed misalignment system can improve efficiency when the transmitter and receiver are under angular misalignment.

Circuit Design

To maintain a high PTE, an optimal operating frequency can be found *e.g.,* by frequency tracking. In [89], an automatic frequency turning method was proposed to find the possible maximum PTE. However, due to the skin effect and the proximity effect increasing winding resistances, the operating frequency shall not be too high [79]. In [90], a compensating system was proposed to improve the PTE by using a serious-shunt mixed-resonant circuit, resulting in a high transmission efficiency over long distance.

The Environmental Analysis

Temperature and humidity [91] are also important factors that affect the PTE. Some semiconductors are sensitive to temperature [79]. In addition, ferrite cores with high permeability and low magnetic loss tangent are generally useful in the enhancement of the magnetic coupling and consequently lead to high PTE. Hence, the electrostatic shielding plays an important role in WPT technologies. J.Mclean [98] presented a primary winding coupler with an electrostatic shield and a magnetic core. The presence of the ferrite core increases the field significantly in the immediate vicinity of the couplers. Moreover, adding a third coil may also improve the PTE. In [92], an optimal design was proposed that makes use of an intermediate coil between the primary coil and the secondary coil. It can boost the effective self-inductance and magnetizing inductance in the primary coil, thereby increasing the apparent

coupling coefficient.

Multiple transmitters/receivers design

Exploring the use of multiple transmitters and receivers is another important research theme. This is because the ability of transferring power from a single transmitter to multiple receivers is often required in practice [99]. Moreover, the transmission efficiency varies as the number of the transmitters/receivers changes.

In [99], a method was proposed to analyse the influence of multiple transmitters or multiple receivers in the WPT system. Compared with the single transmitter/receiver coil case, it was found that increasing the receiver coils can improve the transmission efficiency. In contrast, increasing the number of transmitter coils could degrade the transmission efficiency if the coupling coefficient from a newly added transmitter to the receiver is small.

Matching the resonant frequency in multiple transmitters/receivers in the magnetic resonant coupling-based WPT system was found difficult [100]. An algorithm was studied to determine the resonant frequency in a 2 by 2 array multiple transmitters/receivers WPT system. The PTE can be maintained at a certain high level without changing the system operating frequency. In [101], a multi-receiver WPT system was presented that analyses both the PTE and the power distribution among the receivers. The power distribution depends on both the load impedances and the relative position of the receivers to the transmitter. In addition, it was found that using a repeater can extend the transmission distance.

Compared with the inductive WPT approach, there are some fundamental advances with magnetic resonant coupling (MRC) power transfer. The MRC-WPT approach can transfer power to a longer distance. Furthermore, it is non-radiative, so it does not require line of sight and gives almost no harm to humans [50]. However, similar to the inductive WPT approach, the MRC-WPT approach is also sensitive to misalignment. Another problem is that it is difficult to adjust the resonance frequency when charging multiple devices [102].

2.3.3 MRC-WPT Applications

Home Electronics

The MRC-WPT technologies can be used for charging high power devices with mid-range distance. *e.g.,* LED television or other home electronics. In [103], a 150 watt wireless charging circuit was presented that makes use of three self-resonators for charging a 150 watt, 47 inch LED TV. The transmitter resonator and the intermediate resonator were placed vertical, whilst the receiver resonator and the intermediate resonator were placed in parallel. The PTE was up to 80% when the frequency was 250 MHz.

Electric Vehicles

In recent years, wireless electric vehicle charging technology has made rapid developments. Along with further increases in transmission power and efficiency, stationary wireless charging is likely to replace traditional conductive charging in the near future. In addition, dynamic wireless charging has been proposed. In [104], the concept of the roadway-powered electric vehicle was proposed, which can achieve 100 kW power output with 80% PTE at the 26 cm transmitter/receiver distance. In order to compensate the reactive power, a series compensation system was adopted that was proved with high PTE and high tolerance of lateral misalignment. Such a system consists of two main parts: transmitter part with an inverter and the power line, and the receiver part with pick-up modules, rectifiers, and regulators.

Chapter 3

WPT Technologies for Electric Vehicles (EVs) Charging Review

For energy and environmental reasons, electrification of transportation has been carried out for many years. Electric vehicles (EVs) were attractive to consumers with many government incentive programs. Government subsidy and tax incentives were key to increase the market of EVs today. Nowadays, car companies have been developing various EVs such as pure battery EVs, hybrid EVs, plug-in hybrid EVs and roadway powered EVs. The hybrid EVs were more popular in worldwide markets among all EVs. However, electricity storage technology was one key problem for EVs. The battery of the electric vehicle was not easy to design due to its high energy /power density, affordable cost, long cycle life time, good safety, reliability and many other requirements that should be met simultaneously. Until now, most EVs were using plug-in charging. There were several weaknesses of the plug-in charging, *e.g.,* it really brought some trouble as people might forget to plug-in and thus find themselves out of battery energy later on. The charging cables on the floor might bring tripping hazards. Leakage from cracked old cables, in particular in cold zones, could bring additional hazardous conditions to the owner. Also, people might have to brave the wind, rain, ice, or snow to plug-in with the risk of an electric shock [105].

The WPT technologies for EV charging could eliminate charging troubles and make charging much more convenient for EV owners. Wireless EVs charging has

two categories, static EV charging and dynamic EV charging. Static EV charging means the driver just need to park their car and leave. For a dynamic charging, the EVs could be powered while driving. Additional batteries are not required because the car could get the power directly from a road while they were moving.

3.1 Static EVs Charging

There are several constraints for static EVs charging system design that should be considered :

- Increase magnetic coupling as much as possible in order to get higher induced voltage;

- Increase power transfer efficiency for a given power capacity and cost;

- Make the model as compact as possible to accommodate for given space and weight;

- Manage resonant frequency variation and coupling factor change due to misalignment of pick-up position, air-gap change.

The main issues of a static EVs charging system could be summarized as follows:

1) Power Transfer Efficiency:

The key challenge of the EVs-WPT technology was its lower transfer efficiency and lower pickup power than the conductive power transmission [106]. It was caused by multiple reasons; recent research was focused on the methods of improving the PTE in wireless EVs charging systems. Theodoropoulos *et al.* [107] presented a load balancing control algorithm for wireless EVs charging to improve the efficiency. Some research examined different kinds of primary supply architectures used for EV wireless charging to get maximum efficiency [108]. Some researchers focused on the new materials, like Y.D.Chung *et al.* proposing a high-temperature superconducting (HTS) resonant coil to improve PTE [109]. The coil structure design and location could also affect the PTE in wireless EVs

charging [110] [111] [112]. In practice, the most immediate cause in its lower transfer efficiency was its low coupling coefficient of the loosely coupled transformer adapted in the WPT. The misalignment between the transmitter and receiver coils could lead to a weak coupling thus reducing efficiency. Existing WPT technologies were bulky and highly sensitive to axial and angular coil misalignment [113] [114] [115] [116] [117] with limitations on the TX and RX coil sizes due to packaging constraints of most vehicles [118]. Recent research explored mitigating techniques such as adaptive matching networks [119] and arrayed TX coil structures [120] [121] [122].

2) Coil Design:

The Litz wire diameter and the number of turns were two parameters for coil design. The Litz wire diameter should be selected by the current of the coil, and the number of turns, which should be designed by the mutual inductance or the required power output. The space between wires influenced the coupling since the leakage flux tended to directly close from the wire space. The smaller wire space leaded to a higher coupling coefficient [110]. Ferrite cores were widely used in wireless EVs charging designs to increase the PTE. However, it had a tradeoff between the weight and coupling coefficient. The shielding which was added to both the primary and secondary coils was an important design for the wireless EVs charging system. The shielding in the primary coil was to block the magnetic flux from going down to the metal plate below the floor-board of the garage to cause eddy current loss. The shielding in the secondary coil was to prevent the magnetic flux from entering the vehicle chassis (iron) and causing losses and to protect humans sitting inside the vehicle.

In static EVs charging, the coupler was usually designed in a pad form. The circular-topology pad could work at relatively high efficiency, however it had limitations of air gap length and high output power [123]. [124] proposed a flux-pipe topology which was formed by a coil along an H-shape ferrite bar. In the wireless EVs charging system, the rectangular bipolar coil had better misalignment tolerance than the circular type [125]. The popular bipolar coil topologies for
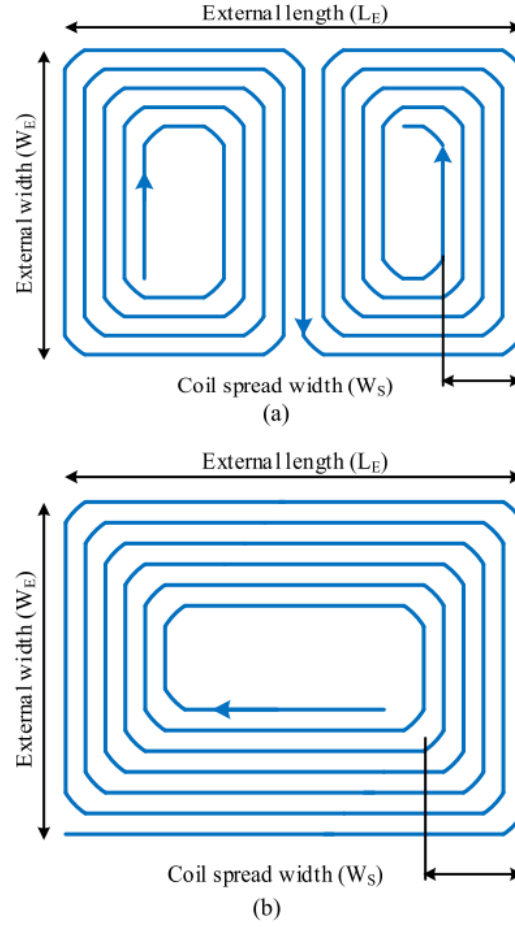
Figure 3.1: DD coil and unipolar coil [126]

wireless EVs charging were double D(DD) coil and double D quadrature (DDQ) coil, shown as in Figure 3.1. Paper [126] presented a double D (DD) coil and compared it to the unipolar coil. The DDQ pad had an overlapping coil between the two D coils, and it was always used as a secondary pad. The result showed that the double D coil structure could achieve the maximum coupling coefficient as well as maximum efficiency with misalignment.

3.2 Dynamic EVs Charging

Most roadway wireless power transfer systems so far (given different names such as: roadway-powered EVs (RPEVs), online EVs system (OLEV)) used an elongate loop of wire as the primary line of the power supply, some research teams chose

circular-type coils. The requirements of a dynamic EV charging design are different from the static EV charging system: larger lateral misalignment, higher air gap, and lower construction cost should be considered for dynamic EV charging. Moreover, dynamic EVs charging should survive in harsh road and weather conditions, such as high and low temperature, high humidity, mechanical shocks and maintenance which were not so important for static EVs. There were several design issues of dynamic EV charging as follow:

- Switching Frequency: The switching frequency of the inverter and rectifier used in the dynamic EV charging system tended to be no less than 20 kHz but not far beyond 50 kHz. That because if the switching frequency is lower than 20 kHz, acoustic noise may be a problem. Otherwise, if the switching frequency is higher than 50 kHz, the switching loss and core loss would increase due to the skin effect increase [127].

- Segmentation of Power Supply Rail: The segmentation power supply rail was an optimal choice for the dynamic EV charging rail. Each segment should be independently turned ON and OFF. The length of the segment rail was an important design issue because it would be too expensive if the length was very short due to an increased number of inverters or switch boxes. Otherwise, the power transfer efficiency would decrease if the length was very long due to increased resistance. Besides these issues, the amount of segments, the distance between neighboring segments and car length should be considered in a dynamic EV charging scheme.

- Resonant Frequency Variation: The resonant frequencies of a dynamic EV charging system varied significantly as the magnetic coupling between a power supply rail and pick-up charges, since the lateral misalignment and air-gap change were more likely to occur in dynamic EV charging cases. Moreover, the frequency changes were different from time to time for different cars and different numbers of cars on a power supply rail. There should be either a smart coil design or an inverter design to cope with these frequency changes.

- Roadway Construction: For static EV charging, the charger could be designed as a pad which was fixed on the garage floor or under the car park. Dynamic

Generation	Core Type	Distance (cm)	Output Power (kW)	Efficiency (%)
1G	E	1	3	80
2G	U	17	6	72
3G	W	17	17	71
4G	I	20	27	74
5G	S	20	22	71
6G	coreless	10-30	3.3	N/A
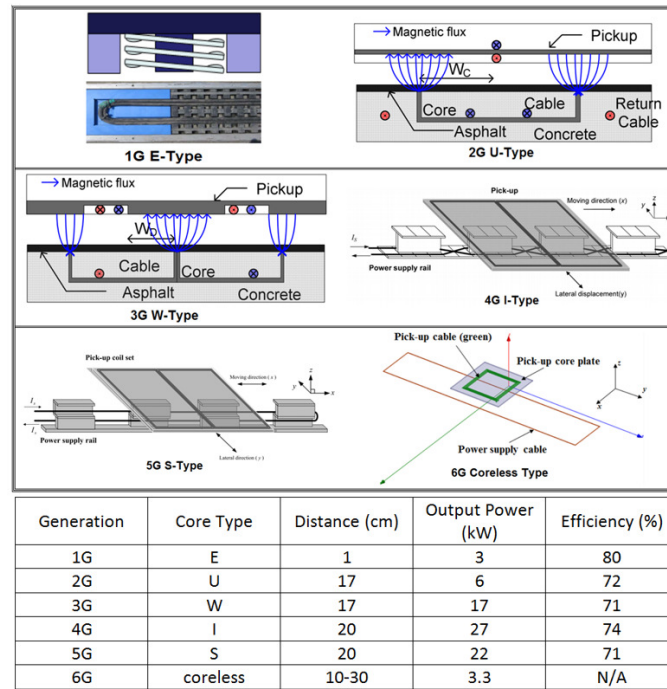
Figure 3.2: The Summary of OLEV project by KAIST

EV charging was survived in roadway, there were many difficulties in roadway work because of debris, dirt or snow. Keeping all of the electrical components of the charging clean during roadway construction was a serous problem in practice. In order to minimize traffic obstruction, the roadway construction time of the charging should be as short as possible.

3.2.1 Research Trends of Dynamic EVs Charging

1.Korea Railroad Research Team

The OLEV project was started in 2009 by a research team led by KAIST, Korea. This project solved several problems such as: Low EMF characteristics, further reduction of the construction cost of time for OLEV with narrow-width power rail, large lateral tolerances and segmentations of power rails. The comparison of OLEV project shows as Figure. 3.2.

- **The 1st generation of OLEV:**

The 1G OLEV golf bus was announced on 27 February 2009, and used an E-type core power supply rail. Basically its structure was similar to the E-type cored trans-

(a) Primary coil

(b) Pick-up coil
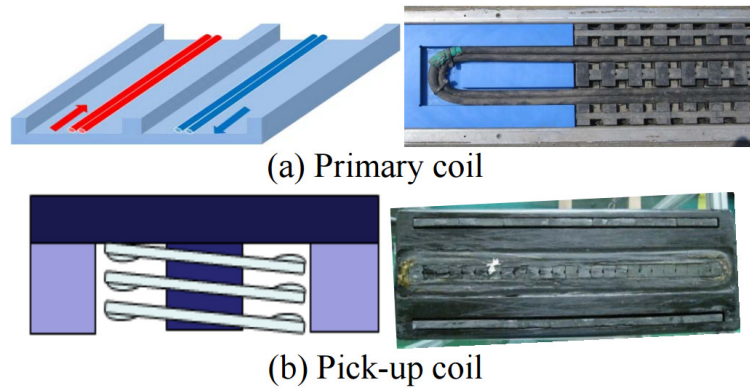
Figure 3.3: The 1G OLEV with E-type primary coil [128]

former, shown in Figure 3.3. The primary core was an E-type segmented structure with mechanical supporter, and the secondary pick-up was a conventional E-type structure. As a transformer, lateral misalignment of both cores severely degraded output power. This misalignment could happen frequently during driving if it was not for the mechanical lateral position control for pick-up with 3mm accuracy. Using these structures, an 80% system power efficiency was obtained with a 1cm air gap. At the primary side, the nominal frequency was 20 kHz and rated current was 100 A. At the secondary side, rated load was 2 Ohm and 3kW per pick up was obtained. The biggest weakness of the 1G OLEV is limitation of the air-gap, but it successfully demonstrated the wireless power delivery to a running car [128].

• **The 2nd generation of OLEV:**

The 2G OLEV bus was announced on 14 July 2009 and used an ultra slim U-type core power supply rail. In the 2G OLEV system, the nominal frequency of power supply was 20kHz and primary rated current was 200A. The rated load was 6kW per pick-up. Total output power of 52kW with 10 pick-ups and 72% power efficiency was accomplished with a 17cm air gap.

Figure 3.4 shows the primary coil (ultra slim U-type core power supply rail) and pick-up coil of the 2G OLEV. The distinction of the 2G OLEV was the direction of magnetic flux. The U-type core power supply rail structure was proposed with the direction of magnetic flux at center position was parallel to the ground, and each
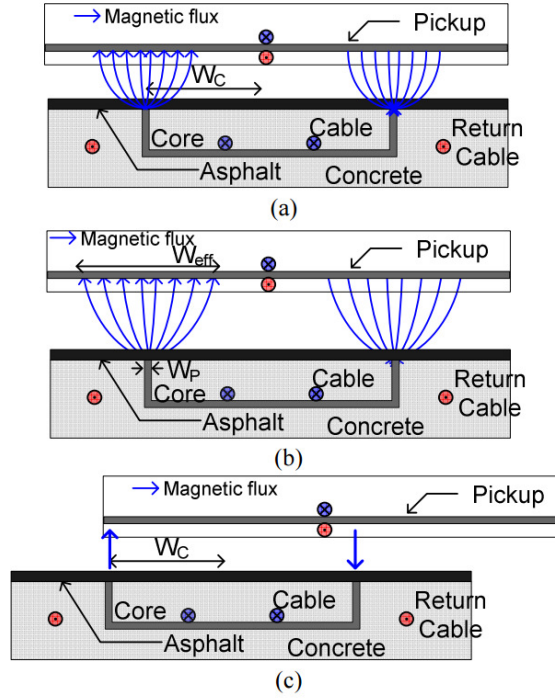
Figure 3.4: The 2G OLEV with U-type primary coil [128]

end the position had lots of fringe effects.

As shown in Figure 3.4(b) the pole width of the primary core (W_P) was much smaller than the length of the pick-up coil. So the effective pick-up width (W_{eff}) increased as the air gap increased. Therefore the magnetic flux transferred from the primary coil to the pick-up coil was proportional to the root of the air gap.

As shown in Figure 3.4(c), the maximum allowable lateral misalignment was roughly half of the length of the primary core (W_C). The proposed core structure made it possible to achieve about 50% power transfer from the primary coil to the pick-up coil with 20 cm misalignment.

Comprision with the 1G OLEV, the air-gap increased from 1cm to 17cm, and without mechanical control apparatus. However, the primary rail length of the 2G OLEV increased to 140cm due to the return cables for reducing EMF. That meant the construction cost increased and out power was limited. To solve this problem, the 3rd generation of OLEV was proposed [128].

• **The 3rd Generation of OLEV:**
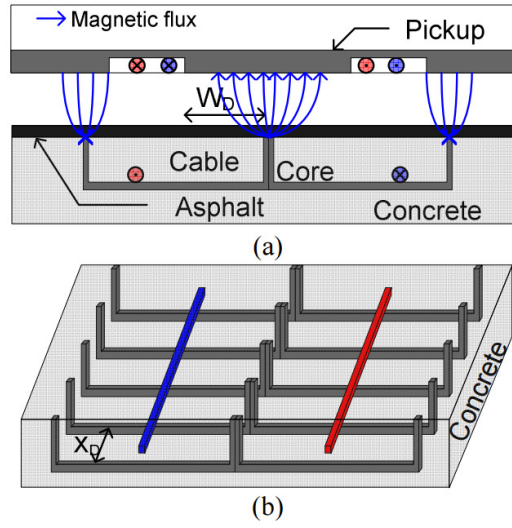
Figure 3.5: The 3G OLEV with W-type primary coil [128]

The 3G OLEV sports utility vehicle was launched on 14 August 2009 and used an ultra slim W-type structure which did not need the return cables. As shown in Figure 3.5(a), the ultra slim W-type had narrow a primary core pole width and wide pick-up core length. So the ultra slim W-type could transfer power with a large air gap. The return path of the magnetic flux in the ultra slim W-type was doubled. So the transferred power from the primary core to the pick-up could be increased. But the maximum allowable lateral misalignment (W_D) was roughly a quarter of the length of the primary coil [128].

In the 3G OLEV with a fish bone like core structure, shown in Figure 3.5(b), the amount of the core was reduced by 1/5 compared to the 2G OLEV, but the output power was improved to 17kW per pick-up. The measured power efficiency for the 3G OLEV SUV was 71% with a 17cm air gap at the same nominal primary frequency and current as the 2G OLEV case.

• **The 4th generation of OLEV:**

The 4G OLEV bus was announced in 2010 with a narrow rail width of 10 cm, a small pickup with a large lateral displacement at about 24 cm, and a large air gap of 20 cm was proposed, shown in Figure 3.6(a). The maximum output power of 35 kW and the maximum efficiency of 74% at 27 kW was achieved. The 4G OLEV proposed
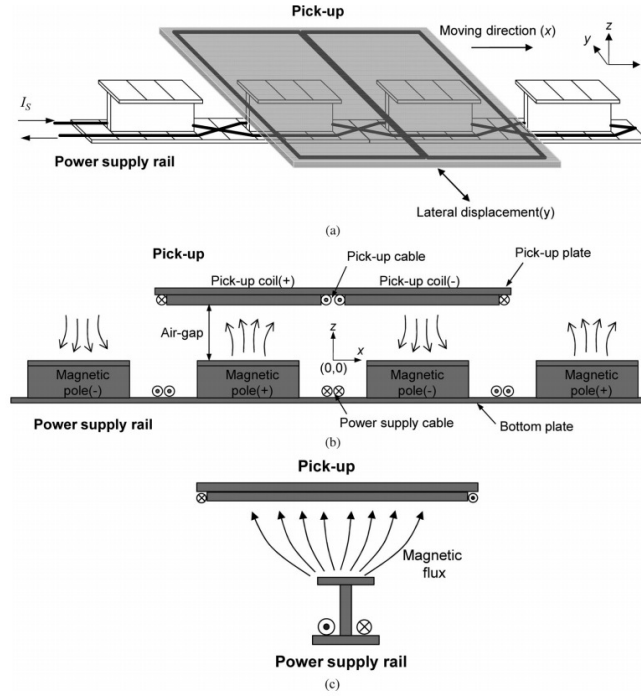
Figure 3.6: The 4G OLEV with I-type primary coil [129]

an I-type power supply rail, where the name "I-type" stems from the front shape of the power rail, as depicted in Figure 3.6(c). In an I-type structure, each magnetic pole consists of ferrite cores and a turned cable, and the poles are connected to each other with a ferrite core. Due to this alternating magnetic polarity of adjacent poles, shown in Figure 3.6(b), the EMF for pedestrians around the power supply rail could be drastically reduced and large lateral displacement could also be achieved by the wide pick-up [129] [130].

A significant improvement of 4G OLEV was lateral tolerance as well as a large air gap, high power efficiency, lower construction cost, and time reduction. However, the construction cost and time of the power supply rail should be further reduced for better commercialization because the construction cost of the power supply rail was critical for deploying the dynamic EV charging and longer construction time resulted in more traffic jams and extra deployment costs.

- **The 5th generation of OLEV:**
The 5G OLEV bus was announced in 2012. It proposed an ultra slim S-type
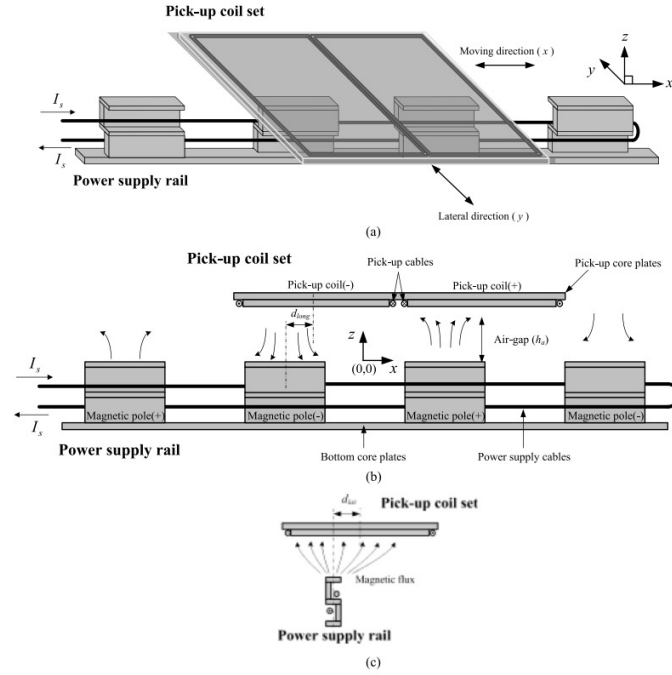
Figure 3.7: The 5G OLEV with S-type primary coil [131]

power supply module with a 4cm width which could further reduce the construction time and cost for commercialization. The name "S-type" stems from the front shape of the power supply rail, shown in Figure 3.7(c).

Each magnetic pole consisted of ferrite core plates and power cables, and adjacent magnetic poles were connected by bottom core plates, shown in Figure 3.7(a). The EMF of pedestrians around the power supply rail could be significantly reduced due to the opposite magnetic polarity of adjacent poles, shown in Figure 3.7(b). From this result, it was estimated that the S-type version has a lower EMF than the I-type version because the width of the S-type was narrower than that of I-type.

The maximum efficiency of the 5G OLEV was 91% at 9.5kW and the maximum pick-up power was 22kW with an air gap of 20cm. The S-type one led to reduction in the construction cost and time for commercialization of dynamic EV charging and further reduction for the EMF generated from a power supply rail for pedestrians. Moreover, it could lead to larger lateral tolerance of a charging system [131].

- **The 6th generation of OLEV:**

The 6G OLEV proposed a universal wireless power transfer (U-WPT) system
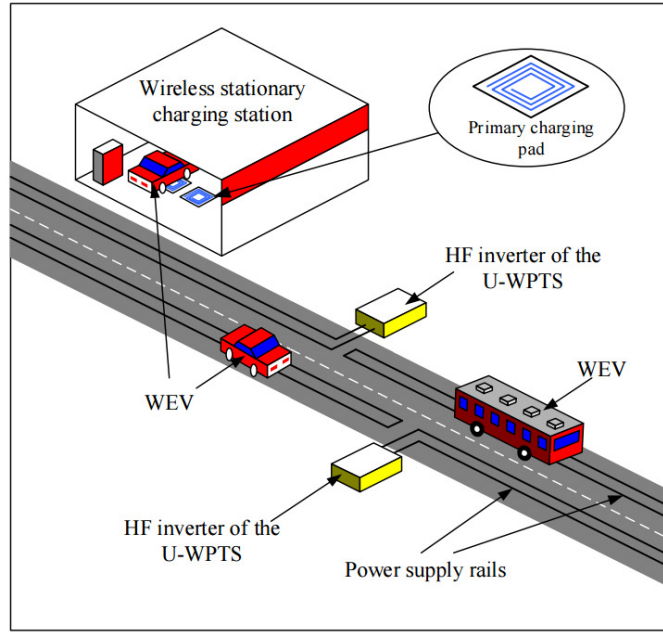
Figure 3.8: U-WPT used for general EVs [132]

which could be applied to both road-powered EVs and general EVs, as shown in Figure 3.8. General EVs could not only be charged in a conventional stationary charging station but also could be charged when they were moving along a road by the power supply rails of the proposed U-WPT system installed underneath the road. This U-WPT adopted a new coreless power supply rail to increase its operating frequency from 20kHz to 85kHz, shown in Figure 3.9. The coreless type meant that no ferrite core plate was installed under the power supply cable.

The power supply rail was an important part for a dynamic EV charging system design, and the shape of the proposed coreless power supply rail was basically the same as the U-type and W-type power supply rail [132]. For road-powered EVs, the power supply rail of an OLEV design was developed by KAIST, which showed good performance with a high efficiency rate of 83% and a long air gap of 20 cm, and operated at the frequency of 85 kHz used by general EVs. The coreless power supply rail had several benefits compared to the with-core power supply rail, such as a lower cost, less insulation voltage stress, the absence of core loss, and less sensitivity to lateral misalignments for the same power rating [133].
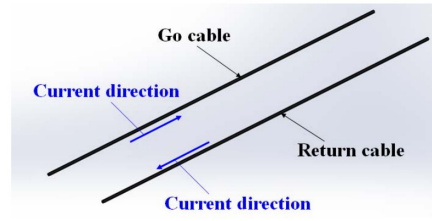
(a) coreless power supply rail
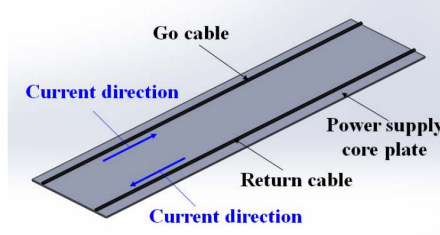
(b) with-core power supply rail

Figure 3.9: U-WPT power supply rail [132]

2. Oak Ridge National Laboratory (ORNL) Research Team

The ORNL dynamic EV charging project stared in 2011, shown in Figure 3.10. ORNL team demonstrated dynamic EV charging in test drives of the Global Electric Motors (GEM) EV over an energised track consisting of six primary coils. Each coil was planar spiral wound with seven turns using cable guides interspersed with wedge-shaped ferrite flux guides. The ferrite plates were covered with a Kapton sheet for voltage isolation. The circular coil was designed for operation at 48kHz with a working gap of 100cm, which was the ground clearance of the GEM EV [134].

Figure 3.11 shows the structure of the ORNL dynamic EV charging system. The power level was controlled by HF inverter rail voltage. The primary coils connected in pairs and in phase (*i.e.,*fountain field), singe tuned to 22 kHz. The coil sequencing was controlled by a vehicle passage using a track side photocell interruption. In this dynamic charging system, the passive and active parallel lithium-capacitor (LiC) unit was used to smooth the grid-side power and Zlinx radio communications between the vehicle and grid-side controller. The Maxwell Technologies carbon ultracapacitors (UCs) pack was used in passive parallel with a demo vehicle battery

Figure 3.10: The ORNL dynamic EVs charging system [134]
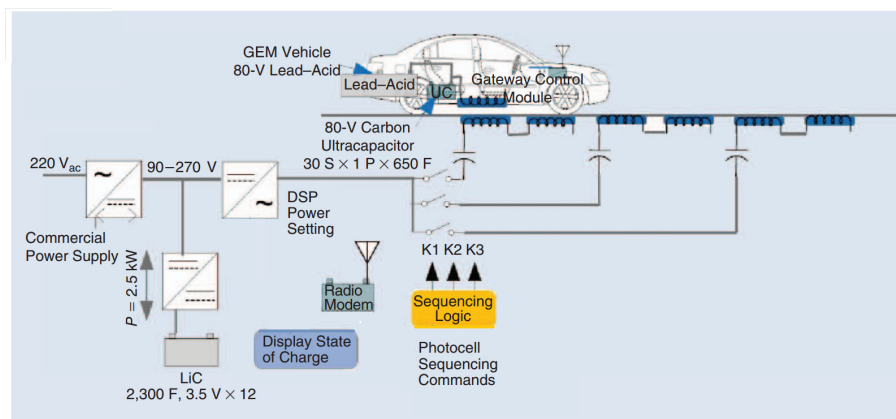
Figure 3.11: The structure of ORNL dynamic EVs charging system [134]

pack [135]

One important aim of the ORNL dynamic wireless charging system was to demonstrate grid-side and in-vehicle power smoothing. Dynamic EV charging could cause power pulsations in the vehicle battery and the grid supply. These pulsations

were due to the motion of the vehicle capture coil as it passed over a series of road-way embedded coils and the resultant pattern of alignment and straddling of their magnetic fields. The battery charging with a pulsating current could deteriorate the battery service life. In order to solve this problem, the local power storage of ORNL used two different high-power capacitor technologies: a pack of carbon UCs fabricated at ORNL and operating in passive parallel with the GEM EV battery pack and LiCs operating in active parallel with the grid-side power supply. Active parallel meant that a high-power, bidirectional controllable power flow, DC-DC converter interfaced the LiCs to the DC input of the WPT HF inverter. The experiment results showed that the vehicle charging current could be smoothed when using carbon UC. And the power pulsations were absorbed by the LiC as expected.

3. Auckland University Research Team

The project was started in the 1990s by Auckland University, New Zealand. A novel circular pads structure (as Figure 3.12) for battery charging had been proposed in [136]. The circular power pads had six main components, shown in Figure 3.13. These power pads overcame several physical limitations of common couplers by using multiple smaller bars. (*e.g.,* coil former with further protection provided by the aluminium and plastic case.) The circular power pads were relatively thinner compared to standard core topologies, and they were lighter than conventional circular coupler designs that used solid ferrite discs. Coupling could be improved in this design comparing with single ferrite bar. However, the circular-type coils were inadequate for high-power road-power EVs because of their low-power transfer capability and small lateral tolerance [127].

In 2010, they proposed a polarized pad, shown in Figure 3.14a, called the "Double D". It was formed using two coils which were wound to form a north and south pole internally due to the layout of the coils, and must be driven in series by a single phase inverter. The ferrite was placed behind the coils which had been arranged into four discrete rows with air gaps between each row. After double D structure, a Bipolar structure had been proposed which consisted primarily of two coils of wire. The coils were partially overlapped, and were coplanar except where one of them
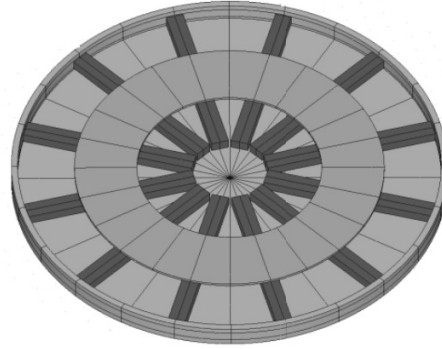
Figure 3.12: The structure of circular power pads [136]
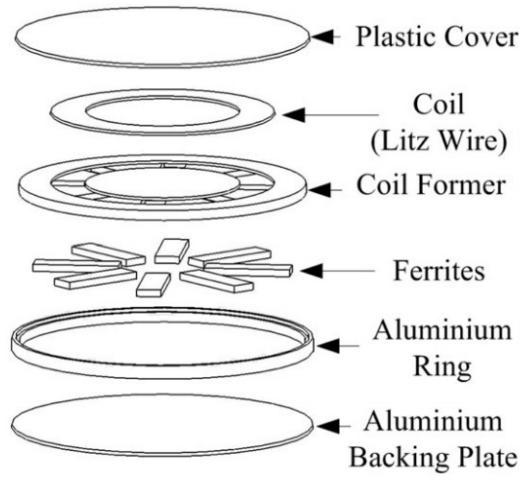
Figure 3.13: The exploded view of circular power pads [136]

must be lifted slightly to pass over the other, shown in Figure 3.14b, the amount of overlap in this case was chosen that the mutual inductance between the two coils was ideally zero. The ferrite was placed behind the coils same as double D. Excepting the novel primary polarized pad design, a new generic magnetic receiver was chosen called the "Quadrature Double D", shown in Figure 3.14c. Comprised with Double D structure, it was added a third coil in the center of the pickup. From the experiment results, power transfer in this design got significant increase and this structures could get higher tolerance to misalignment [137].

The ground-side track of power supply was a key part of the dynamic wireless EVs charging system. Single loop track was easy to supply power to and had a sample structure. But it would cause extra power losses and electromagnetic filed radiation
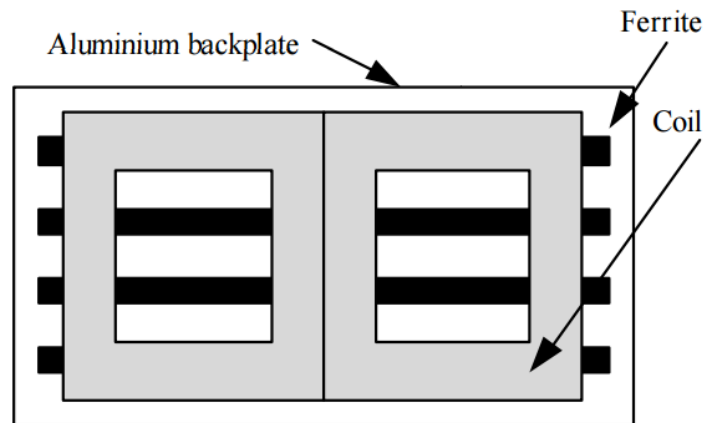
(a) Double D Structure
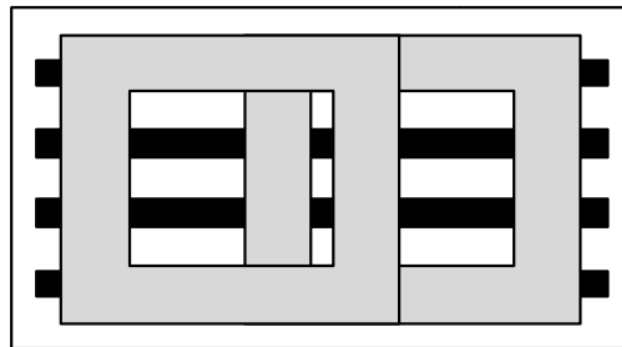
(b) Bipolar Structure
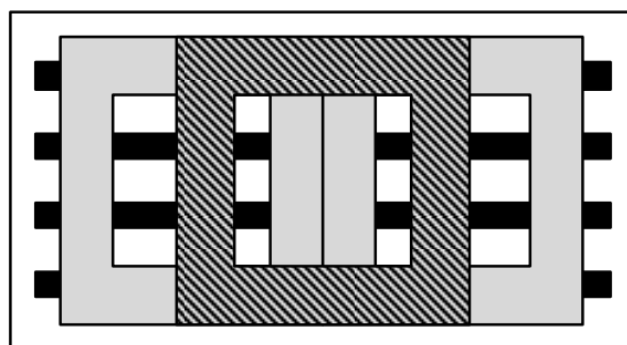
(c) Quadrature Double D Structure

Figure 3.14: The polarized pad present by Auckland Team [137]

if there was no EV charging. The segmented track could solve this problem. Several structures of the segmented tracks were presented as follow:

Figure 3.15(a) showed a simple system that extended the DC bus line of the power supply along the roadway and transfers power to individual sections through direct connections. The complexity of this system was low but it posed significant safety hazards as it run high-voltage and high-power rating DC lines underground.

Figure 3.15(b) was similar to Figure 3.15(a) in that direct connection was used between the power supply and all charging sections, the difference, however, was that instead of extending the DC bus-line, the high frequency led to the individual ground pads being extended from the central power unit [138]. While this avoided the safety hazard, shown in Figure 3.15(a), the downside was that the total track length (as well as system cost) increased exponentially with increasing number of charging sections and therefore the practical number of charging sections was very limited.

Figure 3.15(c) shows a system that transfers power from the power supply through a magnetic coupler to each charging section rather than direct connection. A simple switch (such as a bidirectional ac switch) is then used to control the turn ON and OFF of each individual section [139] [140].

Figure 3.15(d) shows a system [141] that used a two-turn primary track configuration where the current direction in one of the turns could be changed using the switch boxes to switch ON or OFF the magnetic fields around a specific section of the primary track, and therefore allowing independent control over individual charging sections. The required number of extra components was small, and all charging sections were connected in series and all the switch boxes need to be rated at the full current rating of the primary track.

In 2014, they proposed a new roadway for road-power EVs using a double-coupled system [142] which had an intermediary coupler circuit (ICC) with frequency changing capability between the power supply primary track and each ground transmitter pad/coils, shown in Figure 3.16. The proposed double-coupled system used an elongate primary track to power multiple EVs while at the same time it allowed independent control of individual charging sections through the use of an additional circuit called an intermediary coupler circuit (ICC) that allowed frequency changing
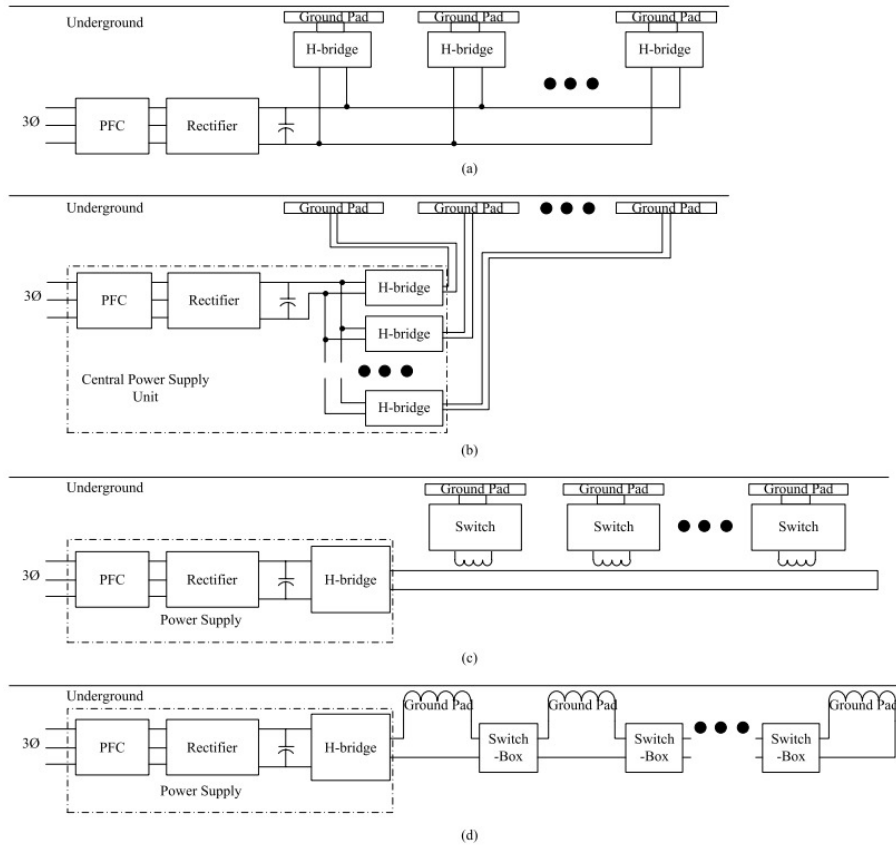
Figure 3.15: Currently proposed roadway IPT systems in the literature which allow control of individual charging sections. (a) Extended power supply dc busline. (b) Central power supply with extended connections to ground pads. (c) Double-coupled configuration with a simple ac switch. (d) Series connected ground pads with switch-boxes [142]
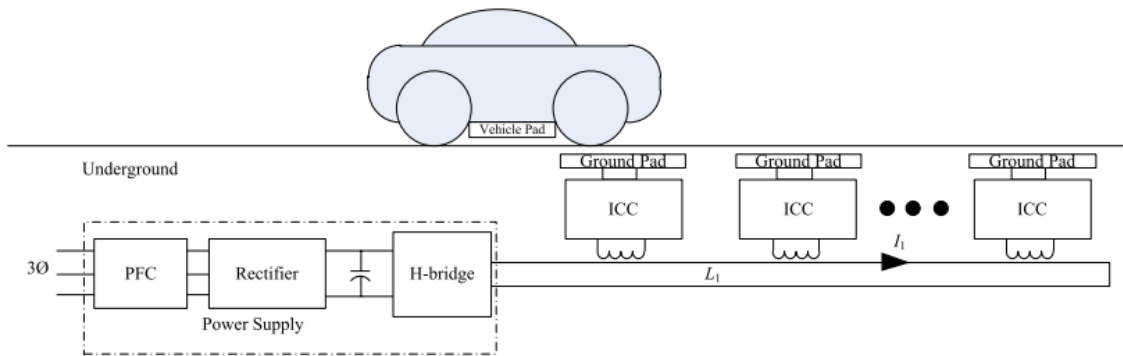
Figure 3.16: Example double-coupled system [142]

and synchronization without reflecting unwanted volt-ampere reactives (VARs) onto the backbone supply.

3.2.2 Summary

This chapter introduces the development of wireless power transfer technology for electric vehicle charging. The key issue of static wireless electric vehicle charging is low power transfer efficiency. There are many reasons affecting the power transfer efficiency, like coil size, misalignment, and circuit design. Dynamic wireless electric vehicle charging can reduce the requirement of batteries. However, it is still in laboratory status, and has not been developed in a large scale.

Chapter 4

Energy Efficient and Adaptive Design for WPT in Static EV Charging

Wireless power transfer (WPT) can revolutionize global transportation and accelerate growth in the Electric Vehicle (EV) market, offering an attractive alternative to cabled charging. Coil misalignment is inevitable due to driver parking behaviour and has a detrimental effect on power transfer efficiency (PTE). This chapter proposes a novel coil design and adaptive hardware to improve PTE in magnetic resonant coupling WPT and mitigate coil misalignment, a crucial roadblock in the acceptance of WPT for EV. The new design is verified using Advanced Design System (ADS), providing a good match to theoretical analysis. Custom design receiver and transmitter circuitry is used to simulate vehicle and parking bay conditions and obtain PTE data in a small-scale set-up. Experimental results show that PTE can be improved by 30% at the array's centre, and an impressive 90% when misaligned by 3/4 of the arrays radius. The proposed novel coil array achieves overall higher PTE compared to the benchmark single coil design.

4.1 Introduction

The key challenge of the WPT technology is its lower transfer efficiency and lower pickup power than the conductive power transmission. One of the reasons is the misalignment between the coils. The misalignment issue is critical since the electro-

magnetic energy in conventional magnetic resonant coupling wireless power transfer (MRC-WPT) rapidly decays with distance between coils. Lateral and angular misalignment analysis for inductive coupling WPT has been examined by Kyriaki [49]. Previous research was conducted to address the effect of coil design in misalignment scenarios [143] [144] [145], however, no methodology was given to mitigate the issue and no recommendations were made for an economical design to solve the problem once and for all.

To address these challenges, a new coil design and adaptive coil selection hardware is proposed. The key contributions are:

1) **New method of calculating PTE**: This design gives a new method for calculating the mutual inductance in laterally misaligned circular coils arrangement. As an important parameter of PTE calculation in MRC-WPT technology, the mutual inductance is derived that is different from J. Kim work [17] and X. Zhang *et al.* work [146].

2) **Novel EVs charging design**: The arrayed coil for the static wireless EV charging is first be proposed. The Seven-TX-Coil array design is proposed that improves the PTE in wireless charging EV systems. These seven TX coils use the isolated design, where each coil is independent, making the new design convenient for control.

3) **Smart coil selection algorithm**: A new smart coil selection algorithm is proposed in this design. Using this algorithm, only one TX coil of coils array that is nearest to receiver (highest PTE) will be selected to transmit power to the receiver. This design is not only effective in solving the misalignment problem thus keeping higher transfer efficiency, but also can reduce the electromagnetic radiation hazards (*e.g.*, caused by unnecessary electromagnetic field) on drivers' body.

4) **The integral hardware prototype**: The integral hardware prototype is developed for evaluating and verifying the new coil array design. XBee RF modules are used for enabling wireless communication. ATMega328 microcontroller is

programed to calculate real-time PTE and the OLED can display all necessary data. Moreover, the implementation results fit well with the mathematical theory results and simulation results (under allowable errors and loss).

4.2   Perfect Alignment MRC-WPT Model

A two-coil MRC-WPT system consists of a source power, a primary resonant coil (TX), a secondary resonant coil (RX) and a load, as shown in Figure 4.1. The subscripts P and Q denote the primary resonant coil and the secondary resonant coil, respectively. S and W denote the source power and load, respectively. D is the distance between the two resonant coils P and Q. The parameter r is the coil loop radius and the parameter a is the wire radius of the resonant coils. Resonant-based WPT enables efficient power transfer over acceptable distances by tuning the capacitive and inductive parameters of both RX and TX circuits to a common natural resonant frequency.

Assuming that the loop radii of the two resonant coils are identical, i.e. $a_P=a_Q$, the self-inductance L, the ohmic resistance R_o, the radiation resistance R_r and the capacitance C can be expressed as [147]:

$$L = r\mu_0\mu_r \left[ln\frac{8r}{a} - 1.75 \right] \tag{4.2.1}$$

$$R_o = \sqrt{\frac{\omega\mu_0\mu_r}{2\sigma}} \frac{r}{a} \tag{4.2.2}$$

$$R_r = 20 \left\{ \left[\frac{2f\pi}{c} \right]^2 \cdot r^2\pi \right\}^2 \tag{4.2.3}$$

$$C = \frac{1}{(2f\pi)^2 L} \tag{4.2.4}$$
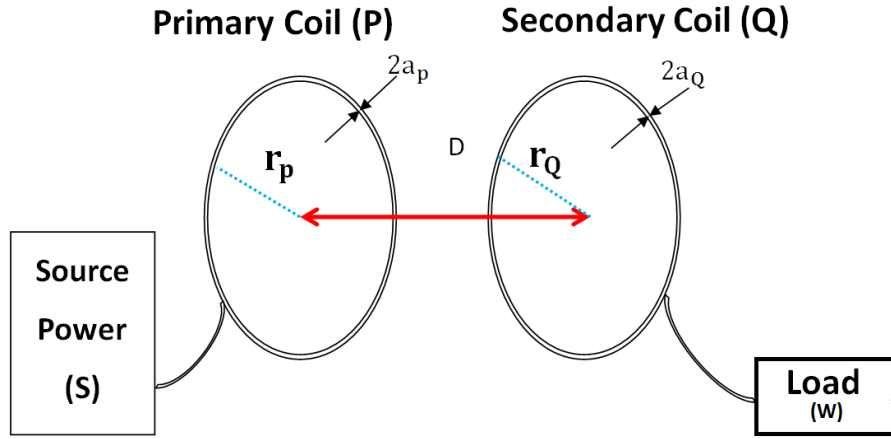
(a) Structure of perfect alignment magnetic resonant coupling WPT
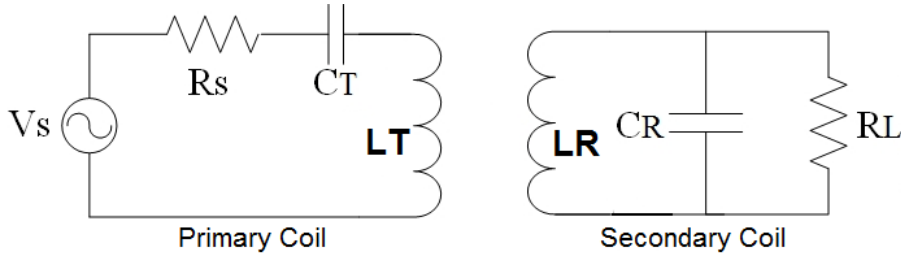
(b) Equivalent circuit of perfect alignment magnetic resonant coupling WPT

Figure 4.1: Block diagram of perfect alignment magnetic resonant coupling WPT

where μ_0 is the permeability of free space, $\omega = 2\pi f$, μ_r is the relative permeability, c is the speed of light, σ is the conductivity of the conductor and f is the resonant frequency. The total resistance of the resonant coil is $R = R_0 + R_r$. (4.2.4) indicates that the capacitance C is determined by the self-inductance L of the resonant coil and the resonant frequency f.

According to Biot-Savart's Law, when the centre of the RX resonant coil is aligned with the centre of the TX resonant coil, and $\mathbf{I}$ is the current in the TX resonant coil, the magnetic field B can be defined as:

$$B = \frac{\mu_0}{2} \cdot \frac{r_P^2 \mathbf{I}}{(r_P^2 + D^2)^{\frac{3}{2}}}. \tag{4.2.5}$$

The mutual inductance M can be given by:

$$M = \frac{\mu_0 \pi (r_P r_Q)^2 \mathbf{I}}{2(D^2 + r_P^2)^{\frac{3}{2}}}. \tag{4.2.6}$$

The PTE η can be defined as [147]:

$$\eta = \frac{\frac{\Gamma_W}{\Gamma_Q}\frac{K^2}{\Gamma_P\Gamma_Q}}{(1+\frac{\Gamma_W}{\Gamma_Q})^2 + (1+\frac{\Gamma_W}{\Gamma_Q})\frac{K^2}{\Gamma_P\Gamma_Q}} \tag{4.2.7}$$

where the PTE η is maximized when $\Gamma_W = \Gamma_Q\sqrt{1+(K^2/\Gamma_P\Gamma_Q)}$, and can be rewritten as [147]:

$$\eta = \frac{\sqrt{1+\frac{K^2}{L_P L_Q}}-1}{\sqrt{1+\frac{K^2}{L_P L_Q}}+1} \tag{4.2.8}$$

$$\Gamma_P = \frac{R_P}{2L_P}, \Gamma_Q = \frac{R_Q}{2L_Q}, K = \frac{M\omega}{2\sqrt{L_P L_Q}} \tag{4.2.9}$$

where Γ is the intrinsic decay rate, K is the coupling coefficient between the two resonant coils and M is the mutual inductance. The final equation of PTE is thus written as:

$$\eta = \frac{\sqrt{1+\frac{\mu_0^2\pi^2(r_P r_Q)^4\omega^2}{4(D^2+r_P{}^2)^3 R_P R_Q}}-1}{\sqrt{1+\frac{\mu_0^2\pi^2(r_P r_Q)^4\omega^2}{4(D^2+r_P{}^2)^3 R_P R_Q}}+1}. \tag{4.2.10}$$

In practice, the size of the TX and RX resonant coils may be different or they are in a misaligned position. The PTE of the misalignment scenario will be given in the next section.

Maple Theoretical Results:

From the calculated results, as shown in Figure 4.2, increasing the radius of the receiver coil can improve the power transfer efficiency. However, there has a decreasing trend of power transfer efficiency when increasing the radius of the transfer coil, as shown in Figure 4.3. That means large transfer coil maybe can not lead to higher efficiency. So there has a design trade-off among the transfer coil size and the power transfer efficiency for the system.
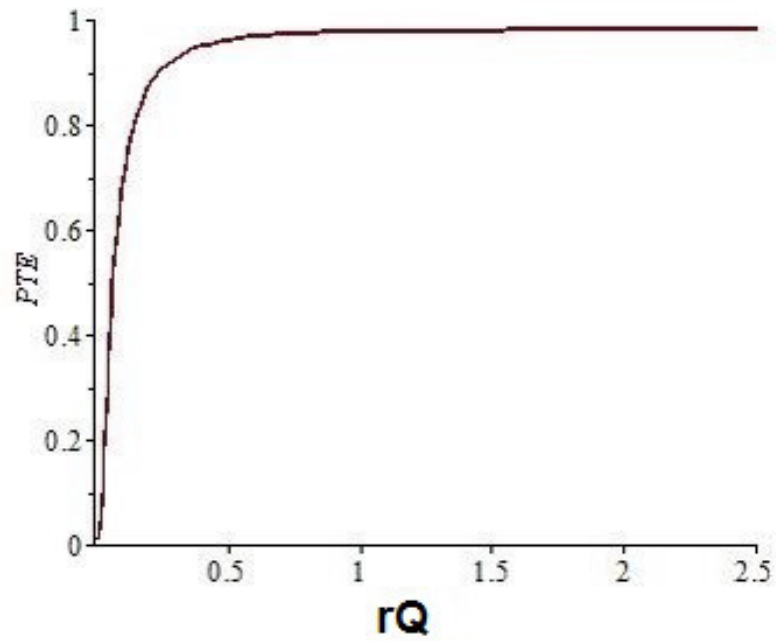
Figure 4.2: Relation between the PTE and receiver coil radius
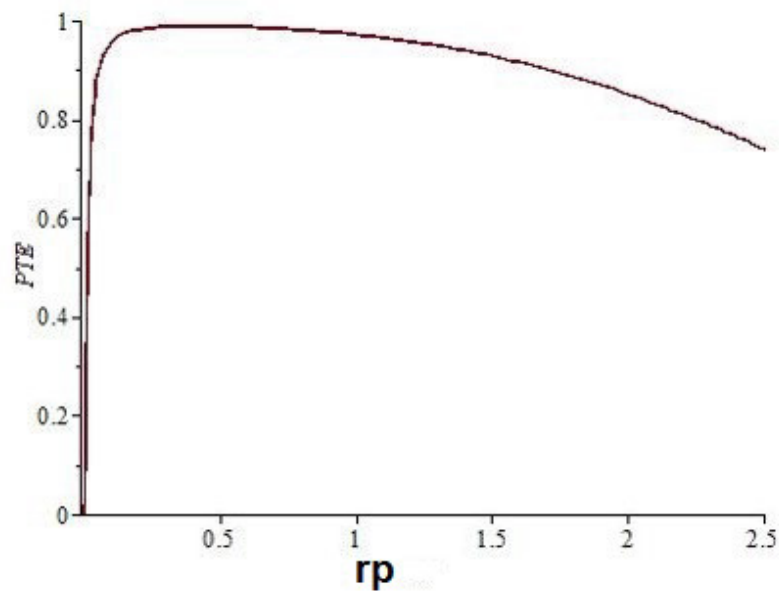
Figure 4.3: Relationship between the PTE and transfer coil radius
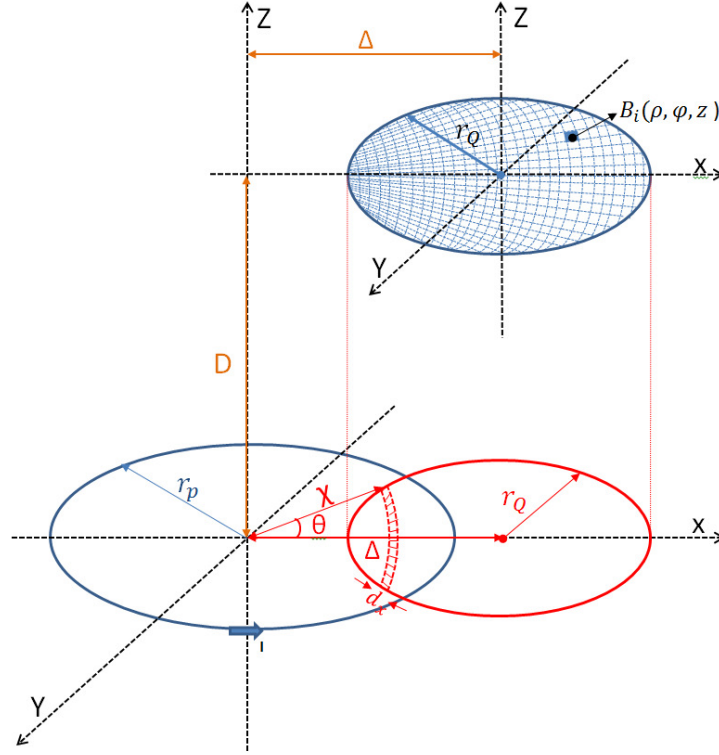
Figure 4.4: Illustration of lateral misalignment between coils where r_p is the radius of TX coil, r_Q is the radius of RX coil and Δ is the lateral misalignment distance.

4.3   MRC-WPT Misalignment Analysis

In MRC-WPT systems, the power of the TX resonant coil is transmitted to the RX resonant coil through an alternating magnetic field. Numerous experiments have established that the location of two resonant coils can affect the PTE of the whole system.

As proposed by Kyriaki [49], there are two types of misalignment, referred to as lateral and angular misalignment. Lateral misalignment involves both horizontal Δ and vertical displacement D in a parallel plane between the centers of the primary and secondary resonant coils. In angular misalignment the plane of the RX resonant coil is tilted at an angle ϑ and the coils are coaxial. Since angular misalignment is less likely to occur in a practical EV scenario, this design only considers the lateral case.

In the case of lateral misalignment, the subdivision magnetic field intensity B_i can be expressed in terms of cylindrical coordinates (ρ, φ, z), as shown in Figure 4.4.

According to Biot-Savart's law, B_i can be written as:

$$B_i(\rho) = \frac{\mu_0 z \mathbf{I}}{2\rho\pi} \cdot \frac{1}{\sqrt{(r_P + \rho)^2 + z^2}}$$
$$\cdot \left[-F(k) + \frac{r_P^2 + \rho^2 + z^2}{(r_P - \rho)^2 + z^2} \cdot E(k) \right]$$

(4.3.11)

$$B_i(z) = \frac{\mu_0 \mathbf{I}}{2\pi} \cdot \frac{1}{\sqrt{(r_P + \rho)^2 + z^2}}$$
$$\cdot \left[F(k) + \frac{r_P^2 - \rho^2 - z^2}{(r_P - \rho)^2 + z^2} \cdot E(k) \right]$$

(4.3.12)

where ρ and z are displacement in the horizontal direction and vertical direction, respectively. φ-directed fields are zero. $\mathbf{I}$ is the current in the TX resonant coil. $F(k)$ and $E(k)$ are the complete elliptical integrals of the first and second kinds, respectively, and k is the modulus. Both equations of the complete elliptical integrals are given below:

$$F(k) = \int_0^{\pi/2} \frac{d\alpha}{\sqrt{1 - k^2 sin^2(\alpha)}}$$

(4.3.13)

$$E(k) = \int_0^{\pi/2} \sqrt{1 - k^2 sin^2(\alpha)} d\alpha$$

(4.3.14)

$$k = \sqrt{\frac{4 r_P \rho}{(r_P + \rho)^2 + z^2}}.$$

(4.3.15)

In general, the mutual inductance M can be defined as:

$$M = \frac{N_1 N_2}{\mathbf{I}} \oint_s B_i(z) ds$$

(4.3.16)

where $\mathbf{I}$ is the current in the TX resonant coil.

As shown in Figure 4.4, the RX resonant coil is subdivided into several identical subdivisions and r_Q is its radius. The red circle is the projection of the receiver coil,

and it can be divided into several arc areas as magnetic field intensity areas. The magnetic field intensity B_i are same in each arc area, so that we can use integration from $\Delta - r_Q$ to $\Delta + r_Q$ to get the mutual inductance value. The mutual inductance between the TX and RX resonant coil M_{12} can be given by:

$$M_{12} = \frac{N_1 N_2}{\mathbf{I}} \int_{\Delta - r_Q}^{\Delta + r_Q} B_i(z) 2x \arccos \frac{x^2 + \Delta^2 - r_Q^2}{2x\Delta} dx \qquad (4.3.17)$$

where N_1 and N_2 are the numbers of turns of the TX and RX resonant coils, respectively. In the case of a single loop, $N_1 = N_2 = 1$. x is the distance between the origin of the TX coil and the magnetic field intensity area on the RX coil. This area can be considered as an arc with a width of dx. $B_i(z)$ is the subdivision magnetic field intensity and is given by (4.3.12).

M_{12} is a crucial parameter in calculating the PTE of a misaligned MRC-WPT system. The mutual inductance (M_{12}) can be rewritten by some rearrangement of (4.3.17):

$$M_{12} = \frac{N_1 N_2}{\mathbf{I}} \int_{\Delta - r_Q}^{\Delta + r_Q} B_i(z) \cdot 2x \sqrt{\frac{r_Q^2 - (x - \Delta)^2}{\Delta \cdot x}} dx. \qquad (4.3.18)$$

The subsequent equation for PTE can be obtained by substituting (4.3.18) into (4.2.9) and subsequently into (4.2.8), leading to equation (4.3.19)

$$\eta = \frac{\sqrt{1 + \frac{N_1^2 N_2^2 \omega^2}{\mathbf{I}^2 R_P R_Q}(\int_{\Delta - r_Q}^{\Delta + r_Q} B_i(z) \cdot 2x \sqrt{\frac{r_Q^2 - (x - \Delta)^2}{\Delta \cdot x}} d_x)^2} - 1}{\sqrt{1 + \frac{N_1^2 N_2^2 \omega^2}{\mathbf{I}^2 R_P R_Q}(\int_{\Delta - r_Q}^{\Delta + r_Q} B_i(z) \cdot 2x \sqrt{\frac{r_Q^2 - (x - \Delta)^2}{\Delta \cdot x}} d_x)^2} + 1} \qquad (4.3.19)$$

- **Advanced System Design (ADS) Simulation:**

The misaligned MRC-WPT system was simulated in Advanced Design System (ADS) 2012, shown as Figure 4.5. Advanced Design System is the world's leading electronic design automation software for RF, microwave, and high speed digital applications. Compared with other software, ADS can complete, integrated set of fast, accurate
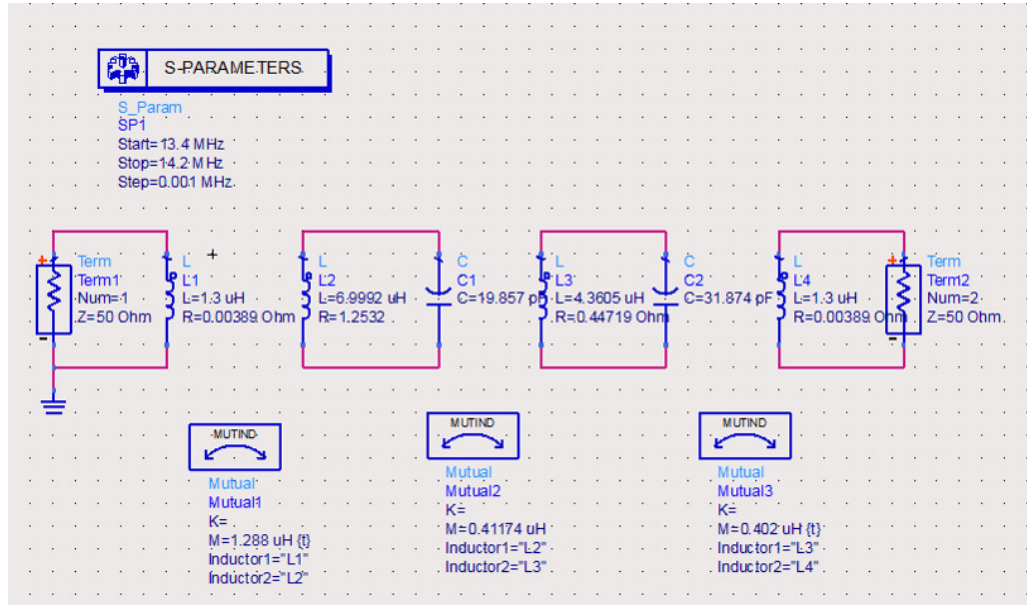
Figure 4.5: ADS Simulation

and easy-to-use circuit and EM simulators design system.

The inductance, resistance and capacitance of the resonant coils were calculated using (4.2.1), (4.2.2) (4.2.3) and (4.2.4). The resonant frequency at 13.50MHz, and decibel is defined in terms of power ratios.

The defining equation for decibels is [147]:

$$A = 10 * log10(\frac{P_1}{P_2})(dB) \tag{4.3.20}$$

where A is decibels (dB), power transfer efficiency (PTE) is equal to $\frac{P_1}{P_2}$. Using this equation can get the PTE at any misalignment position.

4.4   Novel Coil Design

In order to improve the PTE of MRC-WPT in EVs, a new primary resonant coil array is proposed in this section, which can achieve a higher PTE compared to the traditional single coil benchmark. More importantly, it can solve the misalignment issue. Compared with the previous coil-array transmitter, the proposed transmitter uses smart select program which can reduce the concerns of more magnetic harm the human body.
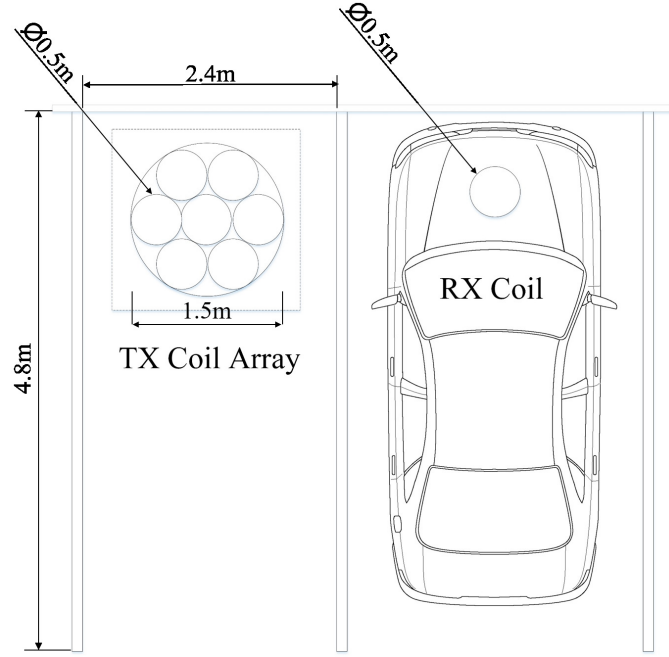
Figure 4.6: Proposed parking bay layout illustrating TX coil array (left) and vehicle-mounted RX coil (right).

The proposed coil design consists of a collection of smaller coils arranged in a grid-like fashion across a flat surface, as shown in Figure 4.7. A_{1-7} marks the centre of each inscribed circle and represent the TX array coils. The large black circle represents a traditional TX coil. R_P is the radius of the original benchmark coil, and r_P is the radius of the proposed smaller coils. As the RX coil is placed at an arbitrary location above the array, simulating the vehicle's parking misalignment, only the nearest TX coil is energized and transmits power to the EV. To illustrate this, C_1-C_n represent stopping locations at regular intervals from the arrays centre to its outer edge. When the vehicle stops at C_3, only coil A_2 is energized, for example. This adaptive switching between smaller TX coils, effectively halves the misalignment distance when compared to the larger single coil design.

Please note in this design the cross-coupling between TX coils has not been considered. According to [148] the coupling coefficient is negative when the spacing between adjacent transmitter coils is positive, while the coupling coefficient between nonadjacent transmitters is always negative. If the transmitter coils are overlapping with each other, the cross-coupling should be considered. However, in my design
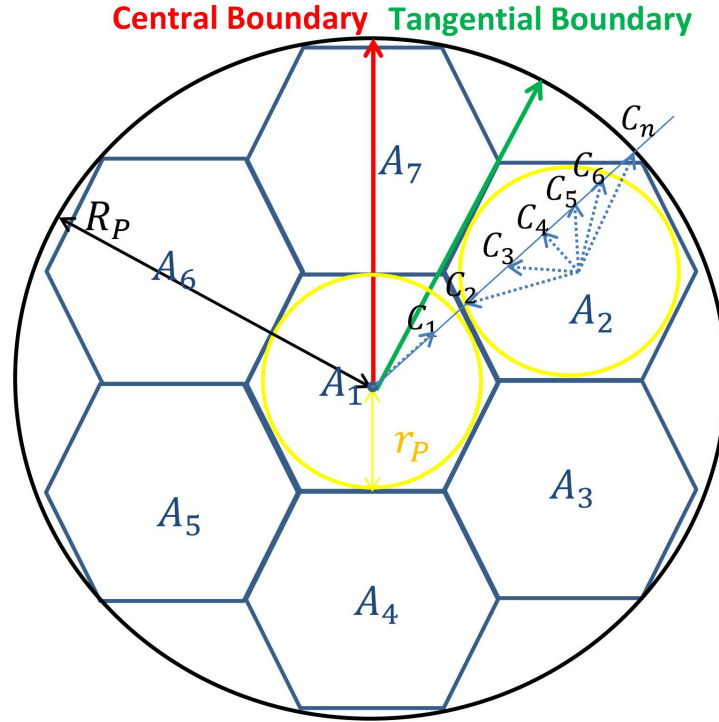
Figure 4.7: The proposed TX coil array design

since only one TX will be turned on, I do not need to consider cross-coupling.

As shown in Figure 4.7, the array has two possible paths for the RX coil to follow during misalignment, referred to as central and tangential boundaries. If the receiver (EV) stops along the central boundary, the two resonant coils will have the shortest misalignment distance, therefore maximizing PTE. The tangential boundary represents the worst case scenario as it contains a triangular gap where the misalignment distance is at its maximum and thus PTE is reduced.

4.5 Hardware Implementation

These existing EV WPT designs are either too complex, uneconomical, prone to mechanical wear or vulnerable due to potential vandalism. The novel coil array and adaptive hardware design proposed in this paper, reduces coil misalignment and improves PTE, whilst avoiding these problems. The idea is to embed an array of coils in a ground cavity beneath the parking bay surface and control them via custom designed charging circuitry. Using wireless feedback from the vehicle, the
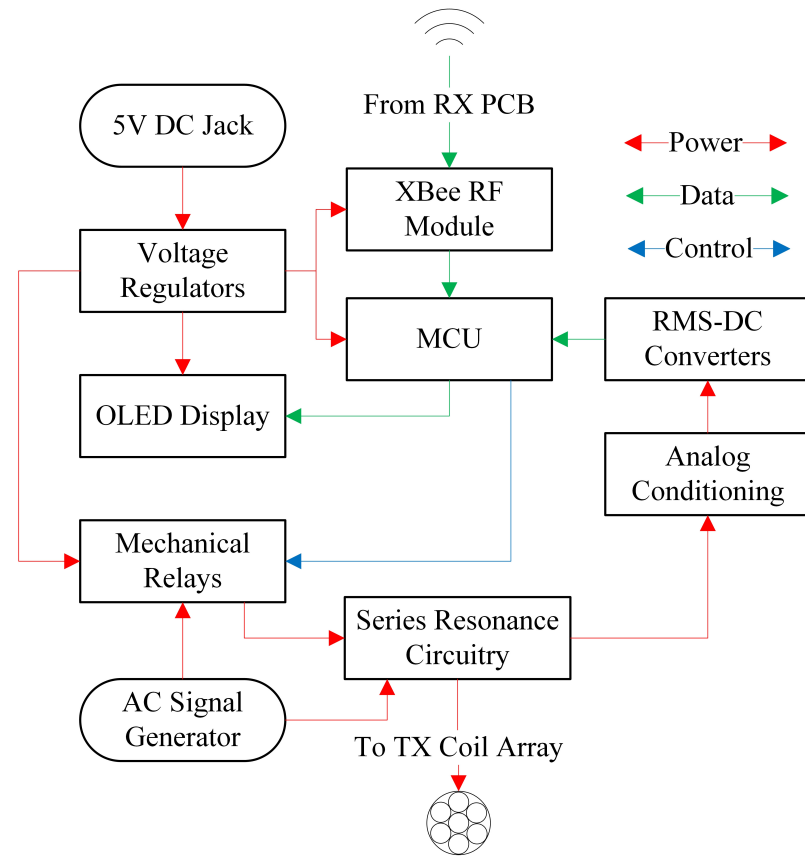
(a) Transmitter (Parking Bay)
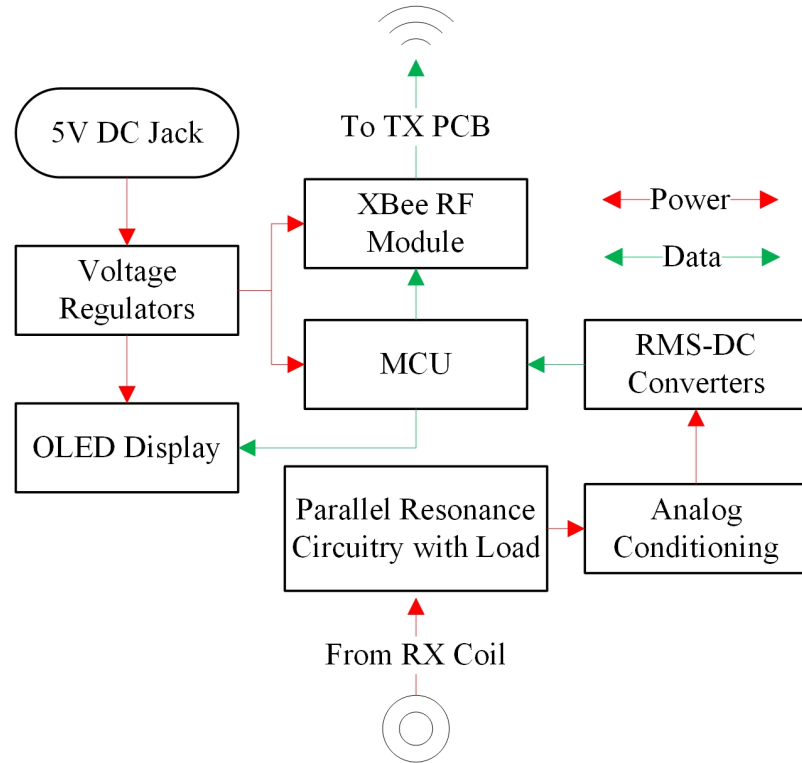
(b) Receiver (Electric Vehicle)

Figure 4.8: Block diagram of hardware setup using novel multi-coil array architecture

parking bay electronics monitor and optimize the PTE of the WPT charging process by selecting the TX coil with optimum alignment to the vehicle mounted RX coil. A system block diagram is shown in Figure 4.8.

A recent study of parking behaviour [149] reveals that only 5% of vehicles parked within alignment tolerances for WPT charging can reach a level of 80% PTE. Perfect alignment can achieve 95% peak efficiency, but the peak efficiency dropped to less than 50% at 15 - 20 cm misalignment. The study showed that drivers were more accurate at parking laterally than in the longitudinal direction, most likely by using the sides of the parking bay as an alignment guide. Moreover, alignment was superior when drivers were asked to align the front of the vehicle with the charging pad as opposed to the centre, with a mean x-displacement of 0.5 cm vs. 7.3 cm respectively.
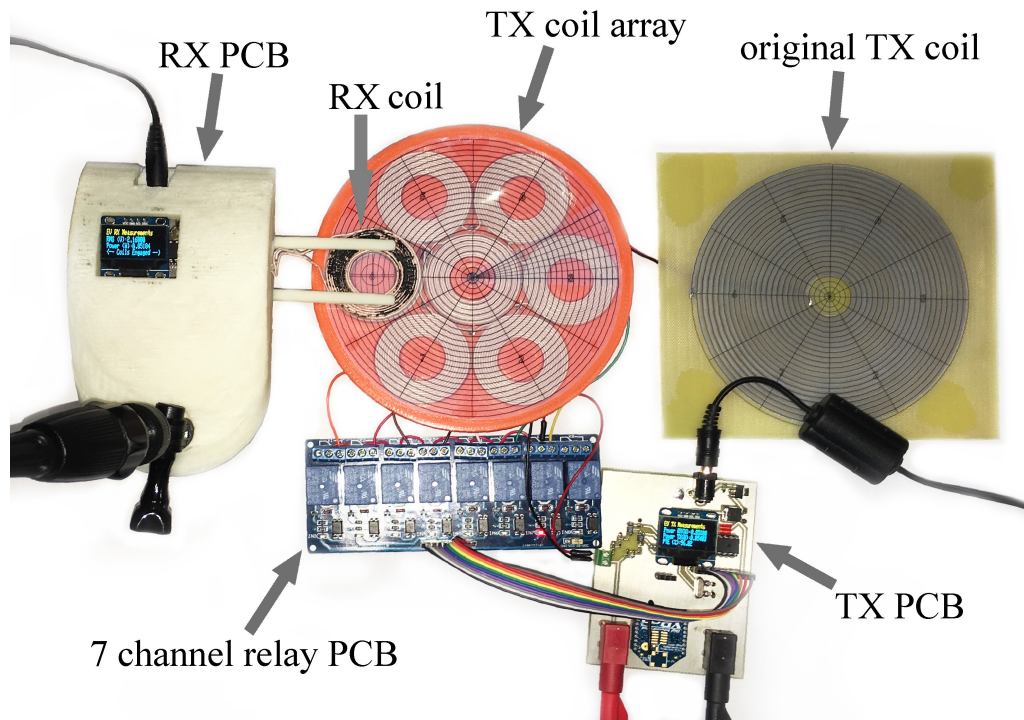
Figure 4.9: Small-scale hardware prototype of EV WPT system

According to [150], the standard space requirements of a typical car park are 2.4 m x 4.8 m with slight variations in the parking bay layout, e.g. parallel, herringbone and in-line designs. Following these recommendations, the outer diameter ($\emptyset$) of each coil in the proposed array structure is set as 0.5 m as shown in Figure 4.6. The air gap D is 0.2 m.

In practice, a 3D printed array structure as shown in Figure 4.9 acts as a container and represents a 1:11 scale version of the parking bay equivalent, and the air gap D in practice is 15 mm. A small scale lab set-up was designed as shown in Figure 4.9.

The transmitter consists of the following parts:

- 3D printed array with seven 22 mm radius TX coils;

- 65 mm radius TX PCB coil for benchmark comparison;

- TX PCB (ATMega328 microcontroller, XBee RF module (XBEE2), OLED display, RMS-DC Converter IC's (LTC1968), TX coil connection)

- 7-channel relay PCB for selecting optimum TX coil.

5V and 3.3V voltage regulators are used to condition the 5V DC jack input and power the ATMega, XBee module, OLED display and RMS-DC Converter IC's. The frequency of resonance is set at 145 kHz (note: the resonant frequency is one of the key factors determining the PTE: in practical setup you might need carefully turn this value first to achieve maximum PTE), which is also used on the signal generator. The voltage amplitude should be in the range 0-5 Vpp. I then connect the signal generator to the transmitter using the red and black banana plugs.

The receiver consists of the following parts:

- 22 mm radius RX coil without ferrite plate;

- 22 mm radius RX coil with ferrite plate;

- RX PCB (XBee RF module (XBEE2), OLED display, RMS-DC Converter IC's (LTC1968), RX coil connection, 90 Ω resistor (load))

The RX coil is connected to the 2 pin terminal on the receiver PCB. An optimum value of 90 Ω was found by varying the load impedance using a decade resistor until maximum PTE was achieved at 145 kHz (resonant frequency is key factor of PTE, it maybe has a little difference between this value and practical setup). The load is

already set on the RX PCB. There are 2 power plugs, which connect to the TX and RX PCB to power them. The OLED display should light up on both.

The vehicle-mounted power receiver measures received power P_{rx} at the load using precision RMS-DC converters, whilst the parking bay transmitter monitors transmitted power P_{tx}. XBee RF modules based on the ZigBee IEEE 802.15.4 protocol are used to establish a wireless feedback loop between the EV and parking bay. An ATMega328 microcontroller (MCU) on the TX side then calculates the current PTE. Embedded software written in C++ iteratively switches power to each of the coils using mechanical relays, until it finds the optimum alignment between TX and RX coils giving maximum coupling - an algorithmic approach.

4.5.1 Transmitter Circuitry (Parking Bay)
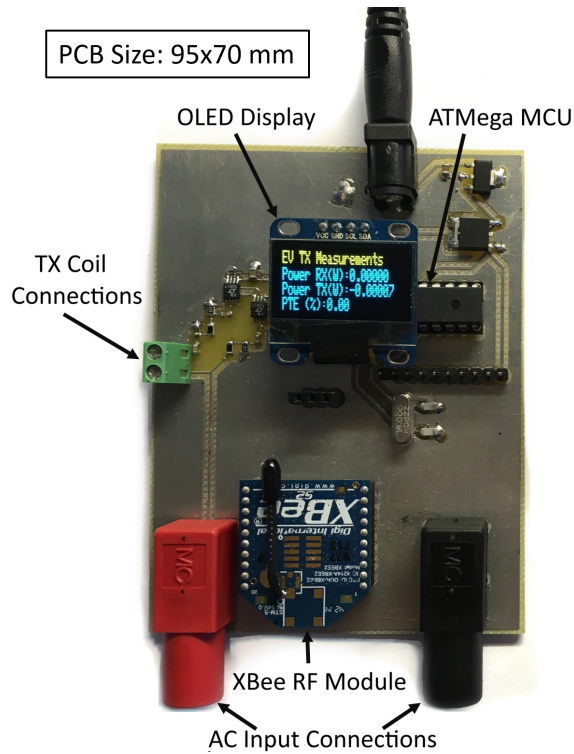
Figure 4.10: TX PCB-interface between MRC-WPT circuitry and electricity grid

To simulate a parking bay charging unit and interface to the electricity grid, a two layer TX PCB was designed in EagleCAD to monitor and control the WPT process. A picture of the working prototype can be seen in Figure 4.10.

The TX circuitry is composed of four parts:

- Microcontroller and Wireless communications

- Measurement and signal conditioning circuitry

- Power input and output

- OLED display and relay outputs

The chosen MCU is an 8-bit ATMega328 clocked at 20MHz. The XBee 802.15.4 module was chosen for wireless communication between RX and TX PCB's, as it integrates seamlessly with the RX and TX pins on the ATMega328. They are typically used for personal area networks (PAN) and provide hardware extensibility for a practical EV scenario, where WPT data, parking space availability and vehicle owner payment information could be exchanged between the vehicle and charging units more efficiently.

Two LTC1968 RMS-DC IC's measure the RMS voltage drop V_{sense} across a 1 Ω sensing resistor to give I_T and also across the entire circuit V_s. The MCU then computes P_{TX}.

The measurement and signal conditioning circuitry uses a voltage divider to reduce the signal amplitude to the input range of the RMS-DC converter. A tuning capacitor is connected to the 24 μH inductive coil in series and parallel for the TX and RX circuits respectively as proposed in Section III. Using (4.2.4), a capacitance of 47 nF was calculated to achieve resonance at 145 kHz. A 2-pin screw terminal mounted on the edge of the PCB provides the TX coil connections.

In high-power WPT EVs charging applications, an inverter is frequently used together with the AC power source. A full-bridge inverter consisting of insulated gate bipolar transistor (IGBT) or MOSFET switches is frequently used for achieving high-power capacity, ideally producing square wave voltage [18]. In addition, the matching network that is commonly referred to as an impedance matching network or a compensation network [151] [152]. A compensation network is utilized to make the system resonant and therefore increase the efficiency. An inductor connected in series to the coupling capacitor forms a series compensator circuit and it is also called a traditional compensation circuit. Moreover, the LCL topology compensation circuit is widely used in MRC-WPT system. The LCL structure is advantageous with

respect to easy control in primary side and fully compensated. A.Ong [153] proposed a LCLC topology compensation structure to reduce the frequency bifurcation effect and improve the transferred power level.

The power rating limitation in this small scale lab set-up was 5W and the traditional series compensation circuit was utilized. The two banana plug connectors took inputs from a standard sine wave generator which has a 60 Ω output impedance and simulates the AC power delivered by the electricity grid. A 128x64 OLED display module is connected via an I^2C interface to the ATMega328 and provides a GUI to monitor data such as PTE, measured RMS voltages and indicate the currently energized TX coil.

The 5 V mechanical relay PCB uses optocouplers to isolate the high frequency power signal of the waveform generator from the control and signal circuitry on the TX PCB. It is controlled from the ATMega's general purpose input/output (GPIO) pins, and is connected via a ribbon cable attached to the PCB's main Harwin connector.

4.5.2   Receiver Circuitry (Electric Vehicle)

To simulate the interface between the battery load of an EV and the MRC-WPT circuitry, a slimmed down version of the TX PCB was designed. A working prototype of the RX PCB can be seen in Figure 4.11.

The receiver differs to the transmitter in that it provides feedback of the RX coil location, hence allowing the transmitter to adapt to a change in misalignment and select a TX coil with higher PTE. A single RMS-DC converter measures the RMS voltage drop V_{RX} across a 90 Ω resistor which represents the load. The MCU then computes P_{RX} in the parallel RLC circuit.

Maximum achievable PTE at resonance depends on the value of load resistance as discussed in [154]. Hence, there exists an optimum load which maximises PTE for a given operating frequency and coupling between coils. An optimum value of 90 Ω was found by varying the load impedance using a decade resistor until maximum PTE was achieved at 145 kHz. Table 4.1 summarises the electrical and dimensional parameters of both coils.

PCB Size: 75x65 mm
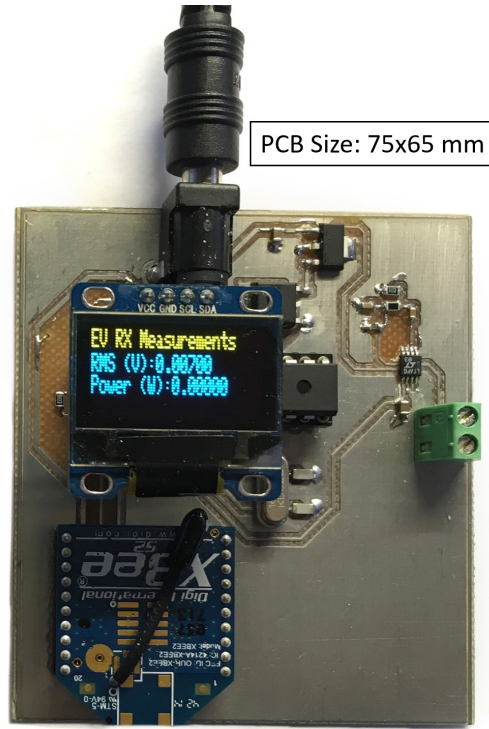
Figure 4.11: RX PCB-interface between MRC-WPT circuitry and EV load

Table 4.1: Parameters of TX coil and RX coil

Property	TX Coil (Array)	Original TX Coil
Inductance (L)	$24\mu H$	$24.47\mu H$
Q-Factor	165	120
No. of Turns & Layers	20 & 1	10 & 1
Inner Radius (r_a & r_o)	$10mm$	$10mm$
Outer Radius (R_a & R_o)	$22mm$	$65mm$
Turn Spacing (S)	0	$0.3mm$
Wire Type	Litz Wire	$1oz - Cu$
Wire or Track Thickness (t)	$1.05mm$	$1.25mm$
Property	RX without ferrite plate	RX with ferrite plate
Structure		
Inductance (L)	$23.5\mu H$	$28.8\mu H$

4.5.3   Adaptive Coil Control Algorithm

In order to optimise PTE, an adaptive algorithm was programmed in C++ and implemented on the ATMega328 MCU of the TX PCB. The main software requirements to achieve autonomous control were:

- Monitor analogue voltages V_{sense}, V_{TX}, V_{RX} and hence compute P_{TX} and P_{RX};

- Send & receive wireless data;

- Operate the mechanical relays;

- Update the OLED display with real-time data of selected TX coil, P_{TX}, P_{RX} and PTE.

The flowchart in Figure 4.12 illustrates the basic operations of the adaptive algorithm. Interrupt service routines are used to refresh the OLED screen every 250 ms and switch between relays if required. If there is a significant drop in PTE, the coil-check algorithm increments to the next coil in the array, until PTE exceeds the minimum 10% threshold. The relay needs measurement and feedback to choose the TX coil with maximized PTE, because of the random location of the receiver. 10% threshold is chosen as it provides high resolution of measurements after many experimented trials. If this threshold is greater, the relay will be continuously checking status when the receiver coil is at a tangential location. Any incoming packets stored in the serial buffer are read and used with measurements obtained from the local analog inputs to compute overall PTE. Finally, the data is displayed on a GUI using a standard OLED display library. Note, the RX PCB code has reduced functionality as it only monitors its analog inputs, displays this info via the GUI and sends serial data via the XBee feedback link to the TX PCB.

4.6   Simulation and Experimental Results

This section evaluates the experimental results from PTE measurements taken for lateral misalignment Δ between the RX coil (without ferrite plate) and TX array
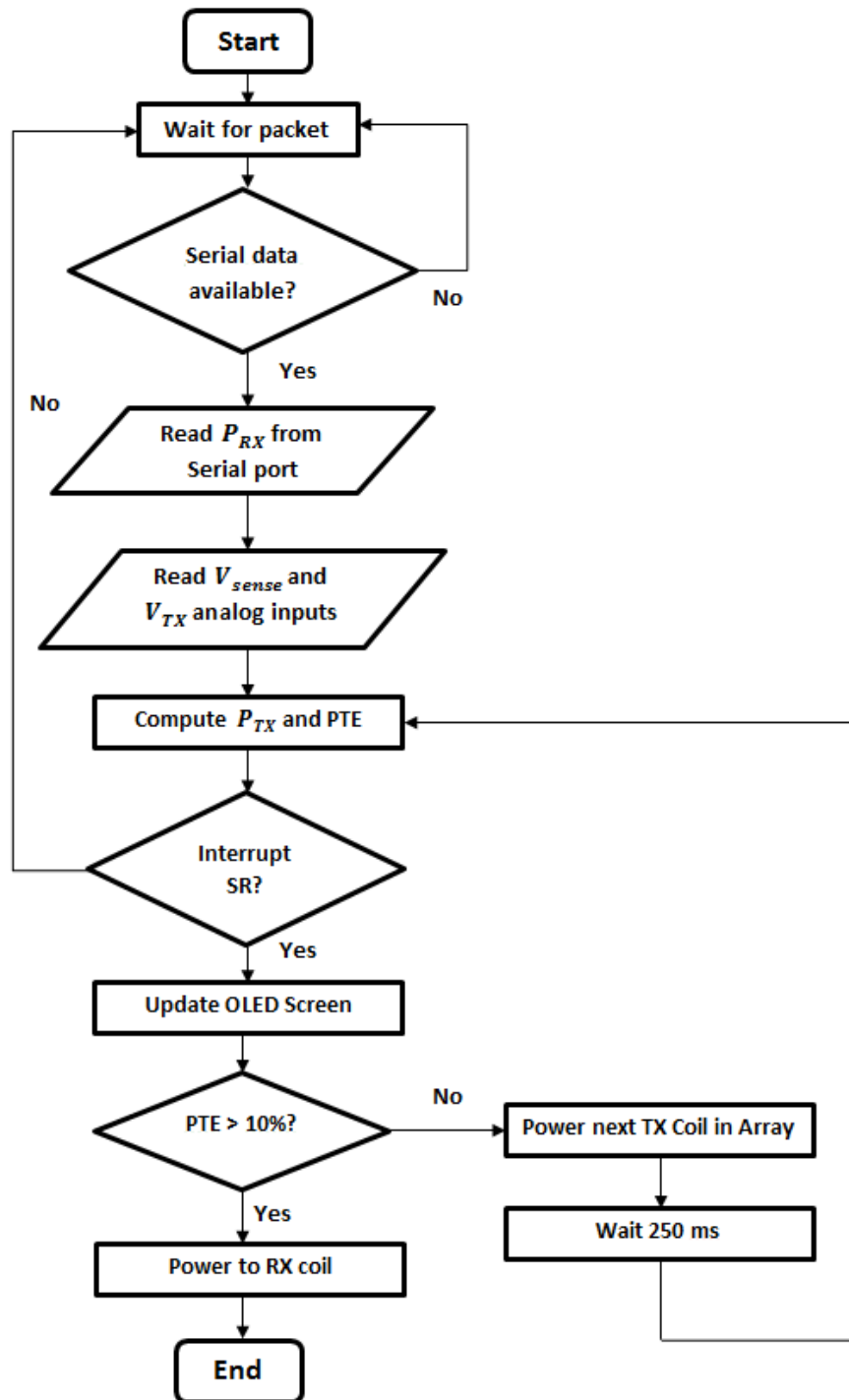
Figure 4.12: Adaptive coil selection flowchart

structure and compares these to the larger TX benchmark coil. Angular misalignment is neglected as it is unlikely to occur due to the parallel nature of charging coils in a practical EV scenario. In addition, I have performed additional experimental test considering the receiver coil with a ferrite plate in central boundary case. Note

that [16] presented a discussion about the different ferrite structures for the transmitter coil and receiver coil: when the size of the ferrite plate has the same receiver coil area, it results in higher magnetic field intensity. So in this design, the ferrite plate size is chosen the same as the receiver coil size.

Using the mathematical model for PTE discussed in Section 4.3, and the software package MAPLE16, theoretical PTE values for each point C_n were calculated, where subscript n represents regular points along the radius of the array as shown in Figure 4.7. An equivalent circuit of the misaligned MRC-WPT system was then simulated in ADS 2012. The inductance, resistance and capacitance of the resonant coils were calculated using (4.2.1), (4.2.2) (4.2.3) and (4.2.4).

This section includes three comparison results:

- comparison result between proposed two-coil system and existing four-coil system in case of misalignment (receiver coil without ferrite plate).

- comparison result between experimental data, simulation result and theory result in original case, array coil central boundary case, and array coil tangential boundary case, respectively (receiver coil without ferrite plate).

- comparison experimental result between the receiver coil with ferrite plate and receiver coil without ferrite plate in central boundary case.

Figure 4.13 shows the comparison result between the two-coil system and four-coil system in misalignment case [155]. The gap distance is 20 cm. In either two-coil system or four-coil system, the value of PTE significantly drops down as the misalignment distance increases.

Figure 4.14a shows the implementation result. The simulated model and small-scale experimental setup used a RX coil radius R_o of 22 mm. The results obtained from experiment broadly agree with the theory and simulations and show that:

1) The proposed coil array achieves a higher PTE compared to a single TX coil benchmark in each misaligned position, with an increase of 30% and 90% at the centre and outer edges respectively as shown in Figure 4.14a.
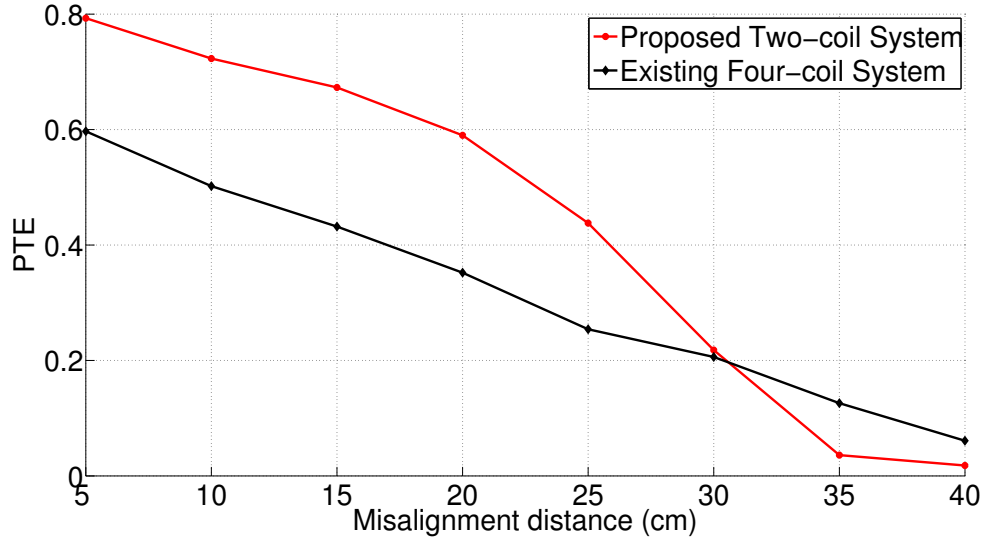
Figure 4.13: comparison between proposed two-coil system and existing four-coil system in case of misalignment

2) The PTE of two peak points in proposed TX coil array can reach 95%, mainly because in these points, the receiver and small transmitter are under alignment location without considering AC/DC conversion. Once AC-DC converters were used on the transmitting side and receiver side rectification and subsequent voltage conditioning for the battery load, this PTE may become lower.

3) A "valley" exists in the proposed coil array between $\Delta = 20$ mm and 30 mm, as this is where the RX coil's centre is furthest away from any array coil.

Figure 4.14b shows the relation between the PTE and misaligned distance Δ for the original benchmark coil. Figure 4.15a and Figure 4.15b show the relationship between PTE and the misaligned distance Δ for the proposed system with the array coil central boundary and array coil tangential boundary in theoretical calculation, simulation and experimental result respectively. The new array design successfully achieved a higher PTE in different scenarios whilst confirming identical trends for PTE vs Δ. We note the theoretical results are lower than the simulation results and experimental results at some points, particularly at misalignment Δ between 15 cm to 35 cm. This is because these positions are located at the edge of the transmitter coil (the coil winding closely), and the coil winding density is ignored in theoretical analysis. This was also evidenced by [156] which presented that the
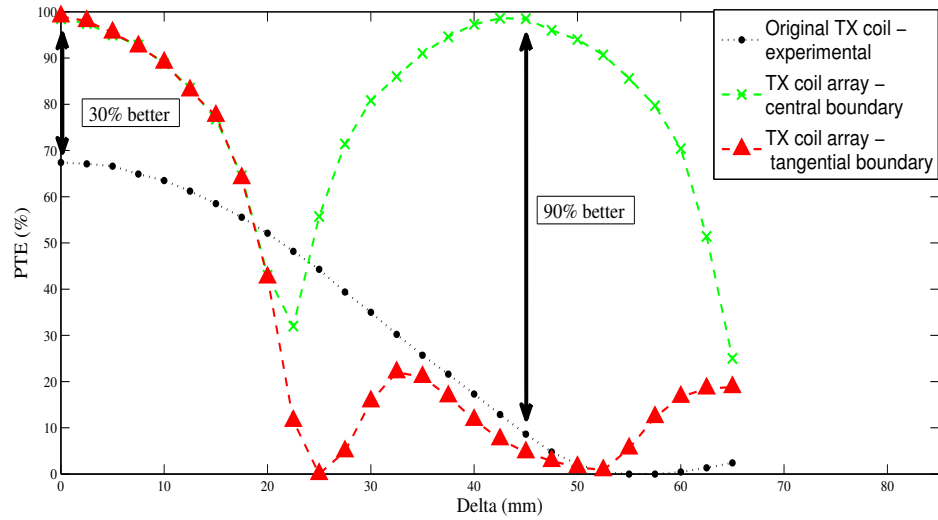
(a) Experimental results
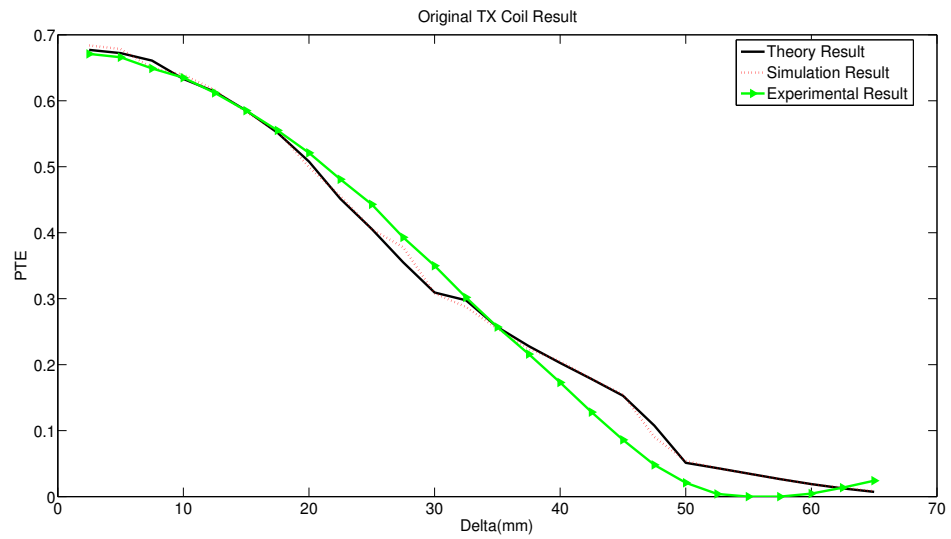
(b) Results comparison when using a single benchmark TX coil

Figure 4.14: PTE when the misalignment distance Δ varies.
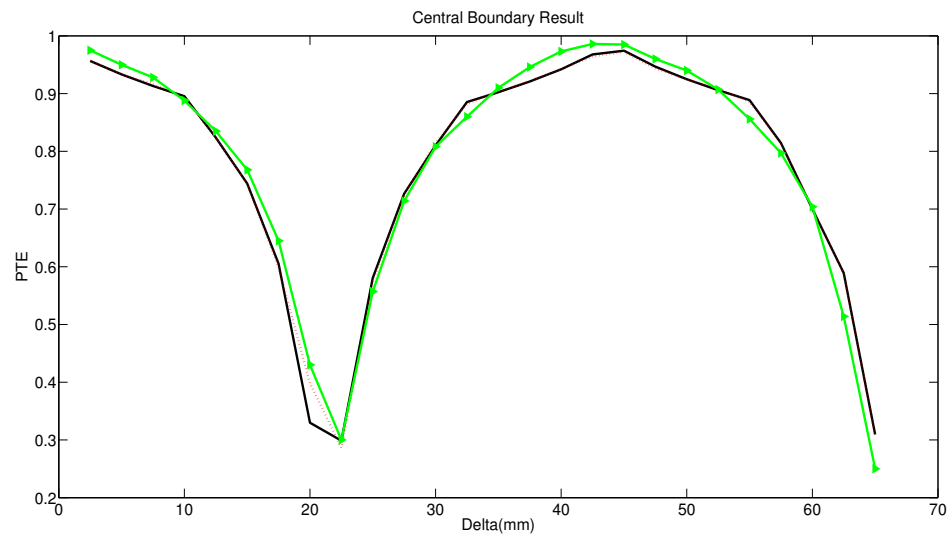
(a) Results of proposed system with RX coil at central boundary
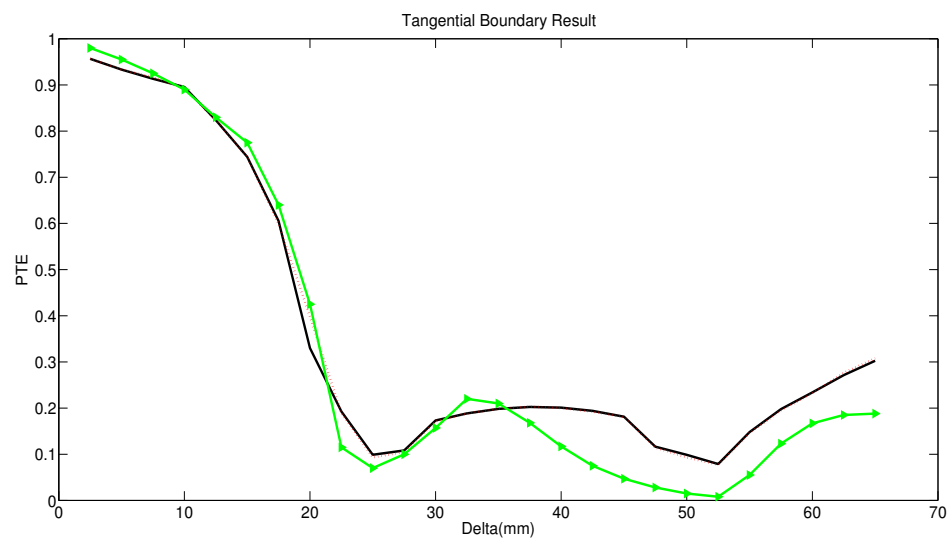
(b) Results of proposed system with RX coil at tangential boundary

Figure 4.15: PTE when the misalignment distance Δ varies.

coil winding density can affect the magnetic field intensity of the spiral coil. The practical magnetic field intensity at these positions a little higher than the theoretical calculating value, thus, the PTE is a little higher than theoretical results.

Figure 4.15a shows the relationship between PTE and the misaligned distance Δ for the proposed system with the array coil central boundary. Additionally, we consider the effects of adding a ferrite plate. In Figure 4.15a, we can see that compared with the case of receiver coil without ferrite plate, the receiver coil with a ferrite plate can improve the PTE. This is because a ferrite plate is generally useful for enhancing the magnetic coupling, leading to high PTE and low EMF/EMI.

For the experimental setup, PTE readings were taken along a horizontal line from the array's centre to its outer radius ($R_o = 65$ mm) in 2.5 mm intervals and were repeated for $0 - 360°$ at increments of $5°$. The vertical displacement (D) between the TX and RX coils was kept constant at 1 mm. The results were plotted on a 2D graph and on a heat map using MATLAB.

As shown in the heat map in Figure 4.16, the tangential boundary contains a triangular gap between $\Delta = 22.5$ to 30 mm, where the PTE was shown to dip below 15% due to a lower coupling coefficient between TX and RX coils.

The central boundary, however, marks a region where PTE was much higher for any given location of the RX coil along this line. The heat map shows that the PTE achieved at $\Delta = 45$ mm was 98.5%, whereas the benchmark single coil only achieved 8.5%. Thus an increase of 90% PTE was observed even when the RX coil was misaligned by 3/4 of the array radius.

4.7   Summary

The success of MRC-WPT in EV's relies on adequate alignment of TX and RX coils, to ensure high PTE and to minimize the losses incurred by both customers and electricity providers. There are many parameters of the coils that affect PTE such as its location, dimensions and geometry. This chapter has introduced a novel array-type primary resonant coil design, which solves the misalignment issue in MRC-WPT and achieves a higher PTE. In practice, the coil misalignment is inevitable, since it
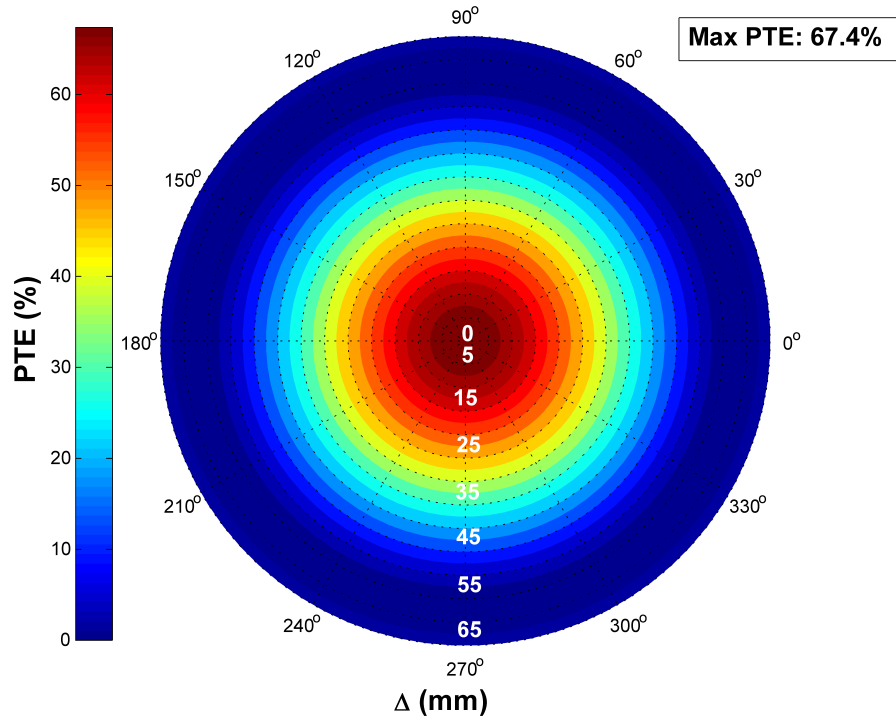
(a) Benchmark single TX coil
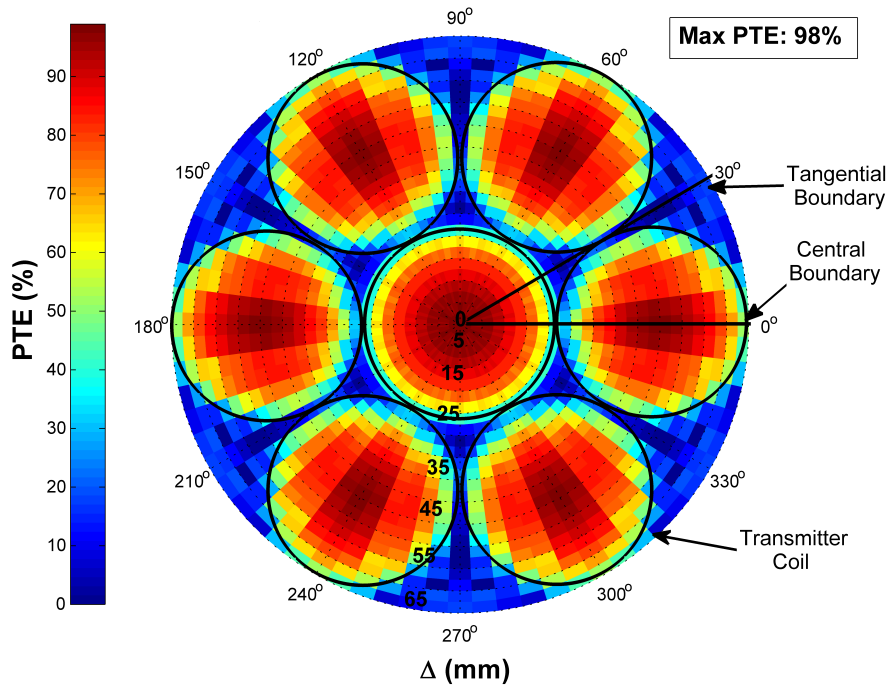
(b) Proposed TX coil array

Figure 4.16: Heat map showing relationship between PTE and misalignment distance Δ when using (a) single benchmark TX coil and (b) the proposed TX array coils. The radius of benchmark TX coil $R_p = 65$ mm and that of the proposed array coil $r_p = 22$ mm.

is difficult for drivers to accurately park their car above a designated charging point or stay within dynamic charging boundaries. Experimental results are obtained using custom designed hardware and have shown a clear match between the theory and real-world implementation of the proposed array design. PTE improvements were observed, of up to 30-90% in the experimental setup. Furthermore, the array design can reduce the RX coil radius and thus reduce the cars weight. Another advantage is the flexibility in choosing any number of TX array coils and varying their arrangement. However, this chapter only considers the case where a single TX coil in the array is energized at any time.

The sharp drop in PTE between coils along the tangential boundary could be resolved using an overlapping array or hexagonally shaped coils. Although the overall array radius in an overlapping configuration would be reduced, the maximum possible misalignment distance between coils would also be reduced. Hence, the red areas marking high PTE on the color map in Figure 4.16b would merge together, resulting in an increased average PTE of the array. This would also reduce the slight PTE drop seen at coil transitions along the central boundary.

Chapter 5

Dynamic Wireless Power Transfer for EVs Charging

Plug-in EV charging continues to roll out across the world with service and parking areas and garages of private homes finding roles as top-up locations. But range anxiety (drivers fearing that they will run out of power between charging points) continues to prove a major deterrent to wider EV take-up. In order to solve this problem, wireless EVs charging has been proposed. Dynamic EVs charging means that the vehicle can be charged while it is actually moving. Multiple segmented transmitters rail for dynamic wireless power transfer (DWPT) electric vehicles (EVs) charging can supply high power transfer efficiency (PTE). Previous research discussed the vehicles' speed is a key factor that can affect the design of the rail (especially, the distance between two neighboring segmented transmitters T) to maximize the system's PTE. However, I find out it is not the vehicle's speed but the size of the transmitter rail that can affect the design of T for optimizing the PTE. Moreover, in order to reduce the pressure of a large number of EVs to the power grid, we proposes an adaptive renewable (wind) energy-powered dynamic wireless charging system. It is benefited to expand the EVs market and let more consumers to accept the EVs by extending its range and using renewable energy.

5.1 Analysis of Multiple Segmented Transmitters Design

5.1.1 Introduction

Although Electric Vehicles (EVs) have been widely accepted in many countries, EV charging has become a challenge for facilitating long-lasting development of EVs. EV charging technologies can be classified as conventional plug-in charging and wireless EV charging. Compared to plug-in EV charging, wireless EV charging makes the car charged automatically and conveniently. In literature, there are two types of transmitter rail design: long transmitter rail, shown as in Figure 5.1 the rail a and multiple segmented transmitters rail, shown as in Figure 5.1 the rail b, c and d. The long transmitter rail provides steady power flow for certain distance. But its power transfer efficiency (PTE) is lower than that of using the segmented transmitters rail [157] [158]. [148] Lu *et al.* proposed multiple rectangular transmitter coils at the primary side as the transmitter rail, with a complete system design and experiment setup. However, how to design the distance between the segmented transmitters has not been studied. O.Smiai *et al.* discussed the speed limit is necessary with the charging pad design in order to maximize the PTE [159]. However, we find out the vehicle's speed cannot affect the design of T for maximizing the PTE. In this section, we propose a new theoretic model for addressing the different cases of multiple segmented transmitters rail design in DWPT EV charging. Simulation results show that not the vehicle's speed but the size of the transmitter rail can affect the design of T for optimizing the PTE.

5.1.2 System Model

As shown in Figure 5.1 rail b, c and d, the blue coil and black coil are the adjacent segmented transmitters. The length of the segmented transmitter is w_1, and the width of the segmented transmitter is h_1. The red coil is the receiver which is fixed in the car. It is a rectangular coil, the length of the receiver coil is w_2 and the width h_2 of the receiver is the same as transmitter width h_1. When the receiver coil arrives
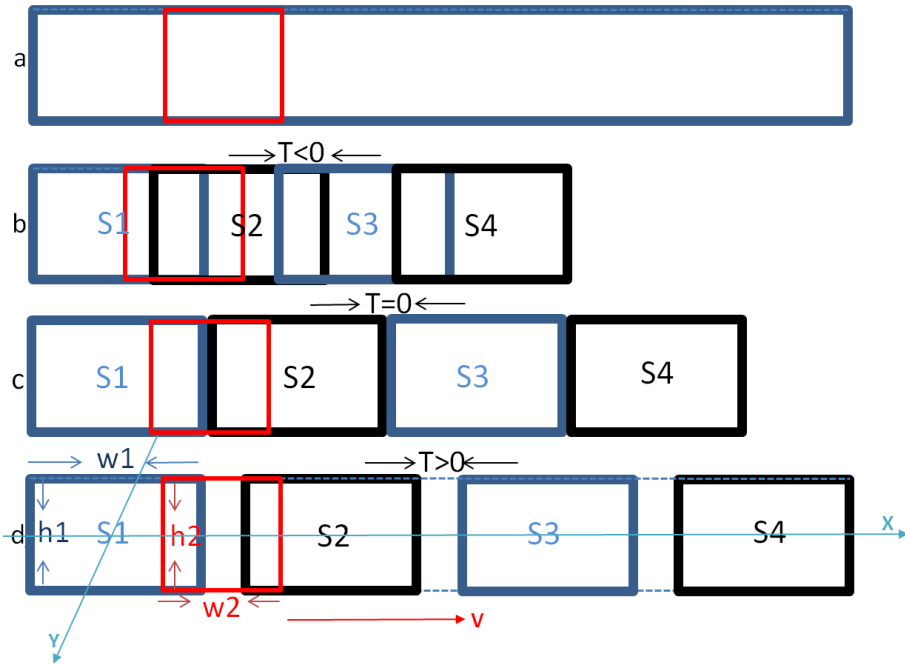
Figure 5.1: Long transmitter rail (a) and Multiple segmented transmitters rail (b, c and d) using same receiver (red coil)

at the transmitter, the previous transmitter will be switched off at the same time. The distance between two neighboring segmented transmitters is T, the speed of the vehicle is v km/h, and the time is t. $T < 0$ means two segmented transmitters are overlapped; $T = 0$, means two segmented transmitters are next to each other; $T > 0$ indicates there is a gap between two segmented transmitters.

Assuming the speed of the vehicle is v km/h, and the time is t, shown as Figure 5.1 rail d. The time of the receiver coil enters into the first segmented transmitter is $t = t_0$, the horizontal coordinate of the receiver coil center point at $-\frac{1}{2}w_1 - \frac{1}{2}w_2$. The receiver coil arrives at the second segmented transmitter in time $t = t_1$, the horizontal coordinate of the receiver coil center point is $T + \frac{1}{2}w_1 - \frac{1}{2}w_2$. So the horizontal displacement of the receiver coil is $T + w_1$. The horizontal coordinate of the receiver coil center point x_0 can be written as:

$$x_0 = v \cdot t - \frac{1}{2} \cdot w_1 - \frac{1}{2} \cdot w_2, t \in (0, \frac{T + w_1}{v}) \tag{5.1.1}$$

5.1.3   Proposed Method
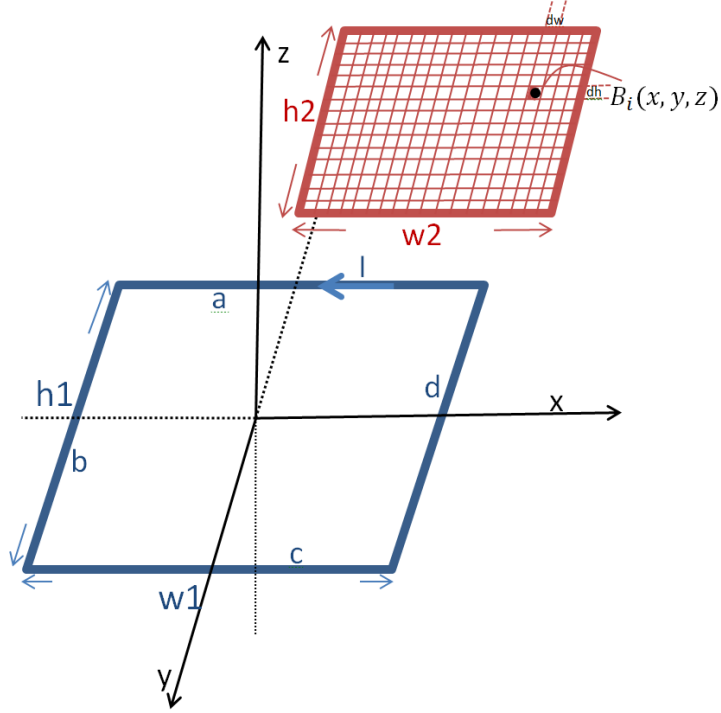
Figure 5.2: Structure of two resonant coils

Figure 5.2 is a schematic illustration of two resonant coils. The blue rectangular coil is the transmitter coil, and the red rectangular coil is the receiver coil. The transmitter coil has four parts (line a, line b, line c and line d). The transmitter coil with N_1 turns is w_1 in length and h_1 in width, respectively. The receiver coil with N_2 turns is w_2 in length and h_2 in width, respectively. **I** is the current in the transmitter coil. The receiver coil is subdivided to many little rectangles and each subdivision with d_w length and d_h width. B_i is the subdivision magnetic field density in each subdivision [160], and only z direct flux can affect the mutual inductance. Subsequently B_i can be written as:

$$B_i = B_{zi}(a) + B_{zi}(b) + B_{zi}(c) + B_{zi}(d) \tag{5.1.2}$$

where $B_{zi}(a)$, $B_{zi}(b)$, $B_{zi}(c)$, and $B_{zi}(d)$ denote the magnetic field density due to current in lines a, b, c, d, respectively. According to Biot-Savart's Law, they can be written as:

$$B_{zi}(a) = \frac{\mu_0 N_1 \mathbf{I}}{4\pi} \cdot \frac{y + h_1/2}{(y + h_1/2)^2 + z^2}$$
$$\cdot \left[\frac{x + w_1/2}{\sqrt{(y + h_1/2)^2 + z^2 + (x + w_1)^2}} - \frac{x - w_1/2}{\sqrt{(y + h_1/2)^2 + z^2 + (x - w_1)^2}} \right] \tag{5.1.3}$$

$$B_{zi}(b) = \frac{\mu_0 N_1 \mathbf{I}}{4\pi} \cdot \frac{x + w_1/2}{(x + w_1/2)^2 + z^2}$$
$$\cdot \left[\frac{y + h_1/2}{\sqrt{(y + h_1/2)^2 + z^2 + (x + w_1)^2}} - \frac{y - h_1/2}{\sqrt{(y - h_1/2)^2 + z^2 + (x + w_1)^2}} \right] \tag{5.1.4}$$

$$B_{zi}(c) = \frac{\mu_0 N_1 \mathbf{I}}{4\pi} \cdot \frac{-(y - h_1/2)}{(y - h_1/2)^2 + z^2}$$
$$\cdot \left[\frac{x + w_1/2}{\sqrt{(y - h_1/2)^2 + z^2 + (x + w_1)^2}} - \frac{x - w_1/2}{\sqrt{(y - h_1/2)^2 + z^2 + (x - w_1)^2}} \right] \tag{5.1.5}$$

$$B_{zi}(d) = \frac{\mu_0 N_1 \mathbf{I}}{4\pi} \cdot \frac{-(x - w_1/2)}{(x - w_1/2)^2 + z^2}$$
$$\cdot \left[\frac{y + h_1/2}{\sqrt{(y + h_1/2)^2 + z^2 + (x - w_1)^2}} - \frac{y - h_1/2}{\sqrt{(y - h_1/2)^2 + z^2 + (x - w_1)^2}} \right] \tag{5.1.6}$$

where μ_0 is the permeability of free space. x, y and z are the center point's coordinates of an arbitrary subdivision. The mutual inductance M_{12} can be written as the sum of each subdivision [160]:

$$M_{12} = \frac{N_1 N_2 d_w d_h}{\mathbf{I}} \sum_{i=1}^{N_w = w_2/d_w} \sum_{i=1}^{N_h = h_2/d_h} |B_i| \tag{5.1.7}$$

According to [4], the power transfer efficiency (PTE) η can be written as:

$$\eta = \frac{\frac{\Gamma_W}{\Gamma_Q}\frac{K^2}{\Gamma_P\Gamma_Q}}{(1 + \frac{\Gamma_W}{\Gamma_Q})^2 + (1 + \frac{\Gamma_W}{\Gamma_Q})\frac{K^2}{\Gamma_P\Gamma_Q}} \tag{5.1.8}$$

where

$$\Gamma_P = \frac{R_P}{2L_P}, \Gamma_Q = \frac{R_Q}{2L_Q}, K = \frac{M_{12}\omega}{2\sqrt{L_P L_Q}} \tag{5.1.9}$$

The subscripts P and Q denote the primary resonant coil and the secondary resonant coil. W denotes the load. Γ is the intrinsic decay rate, and it depends on the resistance and self-inductance of the resonant coils. R_P is the total resistance of the primary resonant coil, L_P is the self-inductance of the primary resonant coil. R_Q is the total resistance of the secondary resonant coil, L_Q is the self-inductance of the secondary resonant coil. K is the coupling coefficient between the two resonant coils. The PTE η can be maximized when $\Gamma_W = \Gamma_Q\sqrt{1 + (K^2/\Gamma_P\Gamma_Q)}$, and η can be rewritten as:

$$\eta = \frac{\sqrt{1 + \frac{K^2}{L_P L_Q}} - 1}{\sqrt{1 + \frac{K^2}{L_P L_Q}} + 1} \tag{5.1.10}$$

For convenience, I use j as a subscript to denote two values: $j = P$ means the primary resonant coil, and $j = Q$ represents the secondary resonant coil. The parameters of resonant coils can be given by [161]:

$$L_j = \frac{\mu_0\mu_r}{\pi}\left[w\cosh^{-1}\frac{h}{2a} - h\cosh^{-1}\frac{w}{2a}\right] \tag{5.1.11}$$

$$R_j = \frac{w+h}{a\pi}\sqrt{\frac{2f\pi\mu_0\mu_r}{2\sigma}} + 20\left\{\left[\frac{2f\pi}{c}\right]^2 \cdot w \cdot h\right\}^2 \qquad (5.1.12)$$

where μ_r is the relative permeability, w is the length of the rectangular coil, and h is the width of the rectangular coil. a is the wire radius of the coil. c is the speed of light, σ is the conductivity of the conductor and f is the resonant frequency. L_j and R_j are the self-inductance and the resistance of resonant coils, respectively.

Overall, I use the following Algorithm 1 to calculate the system PTE.

Algorithm 1

Require:
1: Set all parameters' value w_1, w_2, h_1, h_2, μ_0, μ_r, a, f, σ;
2: Substitute $x = x_0$, y, z into the equation (5.1.2);
3: Substitute the resultant B_i of (5.1.2) into the equation (5.1.7), then get the mutual inductance M_{12};
4: Set $w = w_1$, $h = h_1$, and substitute them into (5.1.11), (5.1.12) to calculate L_P, R_P;
5: Set $w = w_2$, $h = h_2$, and substitute them into (5.1.11), (5.1.12) to calculate L_Q, R_Q;
6: Substitute L_P, L_Q, R_P, R_Q, M_{12} into (5.1.9) to get Γ_P, Γ_Q, K for calculating PTE using equation (5.1.8);

Ensure:
η;

5.1.4   Results

Figure 5.3 shows the relation between PTE and two neighboring segmented transmitters distance T, when the speed v increases from 0 km/h to 100 km/h. It can be seen that when the sizes of transmitter rail and receiver are fixed, no matter what the vehicle's speed v is, the values of the PTE are same. The vehicle's speed v can not affect the design of the distance T to optimize the PTE. $T = 0.2m$ is the case d in the Figure 5.1, and the PTE is around 93%; $T = 0$ is the case c in the Figure 5.1, and the PTE is 96.4%; $T = -0.5m$ is the case b in the Figure 5.1, and the PTE is 97%. The different distances T can affect the PTE.

Figure 5.4 shows the relation between PTE and T when the vehicle's speed v is 30km/h. The difference between them is the size of transmitter rail. Red line (a)
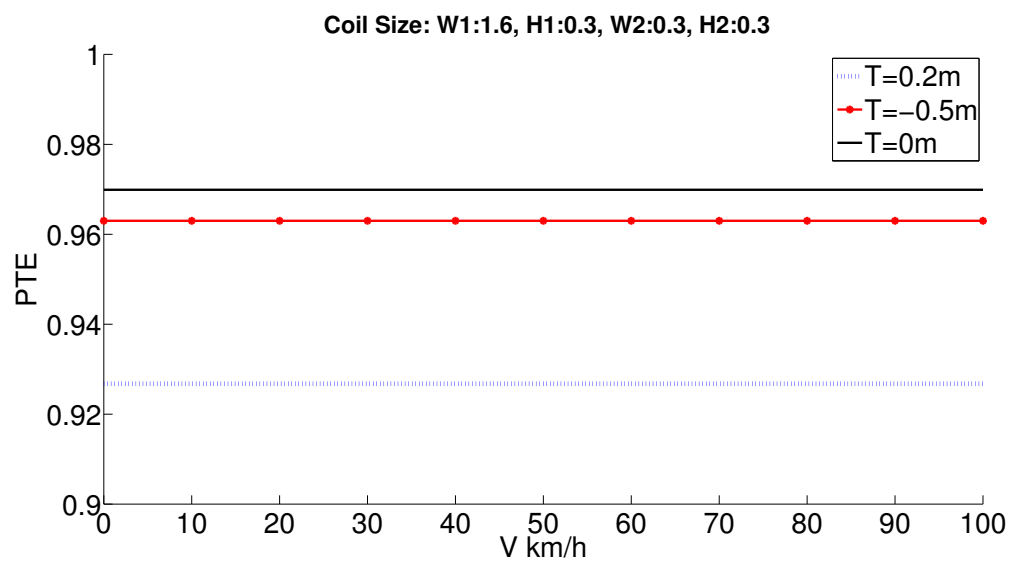
Figure 5.3: The relation between PTE and T in different v
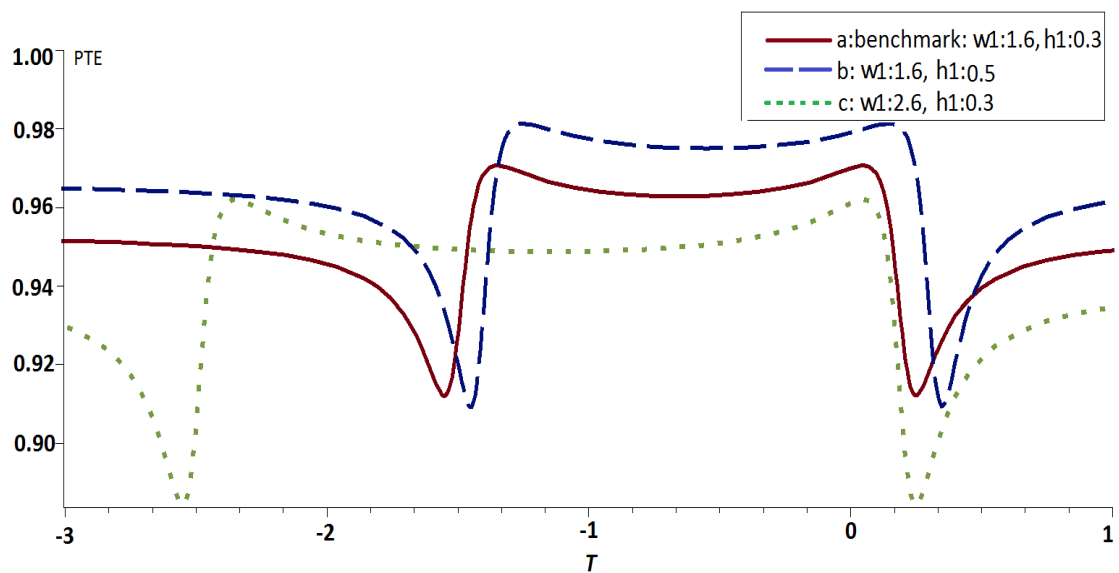
Figure 5.4: The relation between PTE and T in different size of segmented transmitters

serves as the benchmark with the length w_1= 1.6m, the width h_1= 0.3m. For blue line (b), the length w_1 is same, but the width h_1 is bigger. The average PTE is higher than that of the benchmark. The width h_1 of green line (c) is same as the benchmark, but the length w_1 is longer. The average PTE is lower than that of the benchmark. In a word, the size of the transmitter rail can affect the design of the distance T for optimizing the PTE.

5.1.5 Summary

This section has modeled multiple segmented transmitters' design in DWPT EVs charging. Based on the proposed theory and simulation results, the vehicle's speed v is not a determinant factor of T design. The size of the transmitter rail can affect the design of T for optimizing the PTE. In the future work, we will use this theory to choose an optimal distance between the neighboring transmitter T that maximizes the PTE for EVs charging.

5.2 Renewable energy-powered dynamic wireless charging system Design

5.2.1 Introduction

Dynamic wireless EV charging aims at increasing EV range. Moreover, as electrification of transport ultimately targets CO2 emissions reduction, increased utilization of renewable energy sources is likely to provide the means for reaching the decarbonization objective [162]. T.V.Theodoropoulos *et al.* [162] proposed a Demand-side management (DSM) architecture for dynamic EVs wireless charging. The objective of DSM is to balance supply with demand and minimize the total cost of consuming energy. The dynamic wireless EVs charging scenario has been set up based on The Additive Increase Multiplicative Decrease (AIMD) and VEINS. The AIMD concept is used to control EV charging rates. VEINS is an open source framework for vehicular network simulations. In this scenario, vehicle speed at 50km/h, and vehicles

enter the charging lane every 2s. However, 50km/h is very low speed if it is driving on the motorway. The wind power plant was added in the system as the power generator, however, it is not enough to provide supply energy from wind alone, especially in no windy weather. H.Aliyu [163] *et al.* proposed a prediction and dispatch of electric energy from a large wind power plant and a solar thermal plant. The turbines in the wind power plant shall be grouped according to types, power output and geographic location. Neural Network methods shall be employed to predict the power output from each group and the entire wind farm. The wind electric heating system shall operate alongside solar thermal heating system to compliment for periods when wind is insufficient. This model shall mitigate issues of power stability on the grid due to variability and intermittency of wind energy supply.

- Segmentation of Power Supply Rail Design: The segmentation power supply rail was an optimal choice for a dynamic EV charging rail. Each segment should be independently turned ON and OFF. The length of the segment rail was an important design issue because it would be too expensive if the length was very short due to an increased number of inverters or switch boxes. Otherwise, the power transfer efficiency would decrease if the length was very long due to increased resistance. Besides these issues, the amount of segments, the distance between neighboring segments and car length should be considered in dynamic wireless EVs charging scheme.

- Charger Switch Frequency: Dynamic EVs charging was survived on the road, due to traffic conditions, weather, control the charger switching frequency has many difficulties. It is difficult to control the quick opening and closing of the segment chargers when the speed of the EV is very fast, *e.g.*on the motorway.

- Energy Distribution: Large-scale EVs charging will put pressure on the grid. Nowadays, renewable energy (*e.g.* wind) power generation is a trend in the world. How to distribute the energy source according the requirement energy is a typical research topic, because the wind energy output is limited by the weather.

Considering above design issues, this paper proposed an adaptive renewable (wind) energy-powered dynamic wireless charging system for electric vehicles (EVs)

which can maximize the utilization of wind energy and further mitigating the intermittent influence from both demand and renewable energy on the grid.

The objectives of this system are:

- To reduce carbon emissions (ideally achieving zero carbon emission) caused by EV charging, which typically uses electricity generated by generation mix (coal, gas etc.), through the integration of renewable energy.

- To increase the range of EVs (ideally infinity range) by using dynamic and wireless EV charging infrastructure.

5.2.2 Renewable Energy-powered System Model

The suggested dynamic wireless EVs charging system can be directly powered by renewable energy, particularly the wind energy. Meanwhile, it also can be powered by the utility power grid if renewable energy is insufficient, show as in Fig. 5.5. Because one aim of this system is most efficient use of wind energy, so the energy storage device is not concerned. The charging demand is predicted using the traffic flow data and traffic condition classification methods. Both distributed wind energy and the centralized grid provide electricity to the charging system but wind energy is the prioritized supply source so electricity will be imported from the grid only when wind energy is inadequate to meet all charging demands. The charging lane adopts the multiple segmented transmitters rail design due to its higher power transfer efficiency comparing with long transmitter rail configuration (The segmented transmitter will be referred to as 'charging pad' or 'pad' in later parts of this paper). Each charging pad is controlled by a switch that can be turned on/off via the automatic selection module.

Fig. 5.6 describes the key components and operation principles of our adaptive dynamic wireless charging system for EVs driving on highways. The system consists of four parts: wind energy prediction module, charging demand prediction module, demand response optimization module and automatic selection module. The detail of operating the whole system is as following:
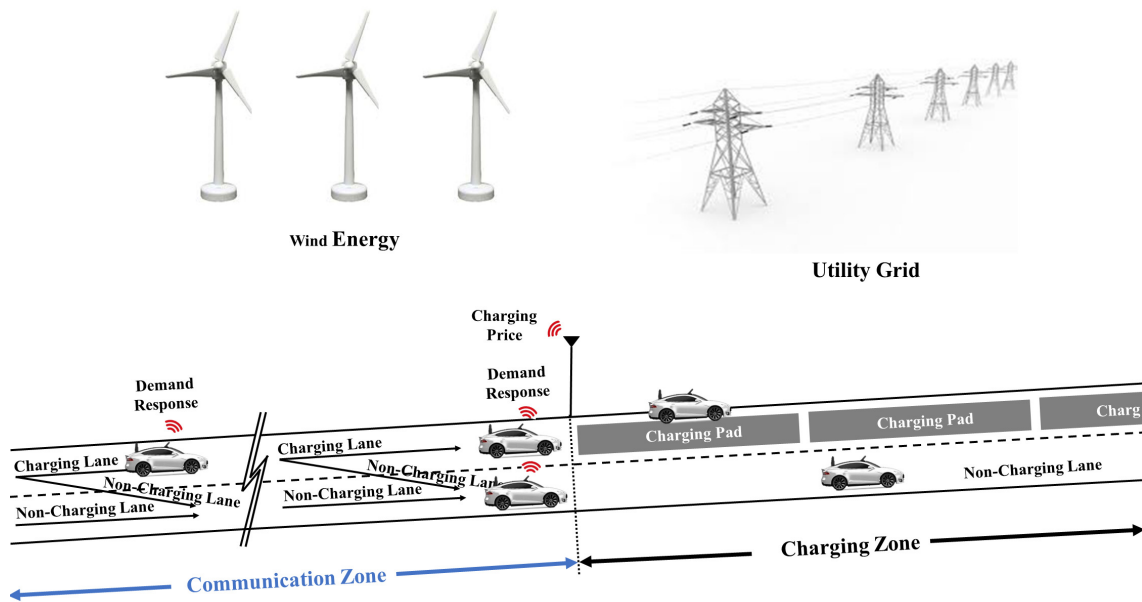
(a) Wind powered dynamic EVs wirless charging system
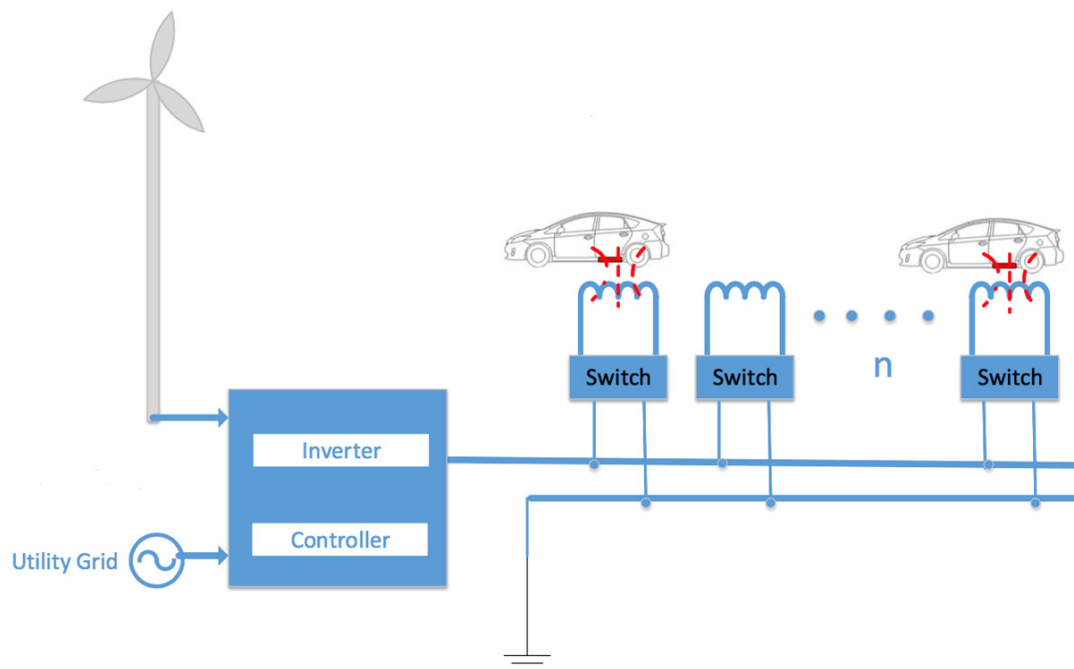
(b) Schematic diagram of charging system

Figure 5.5: Wind powered dynamic EVs wirless charging system
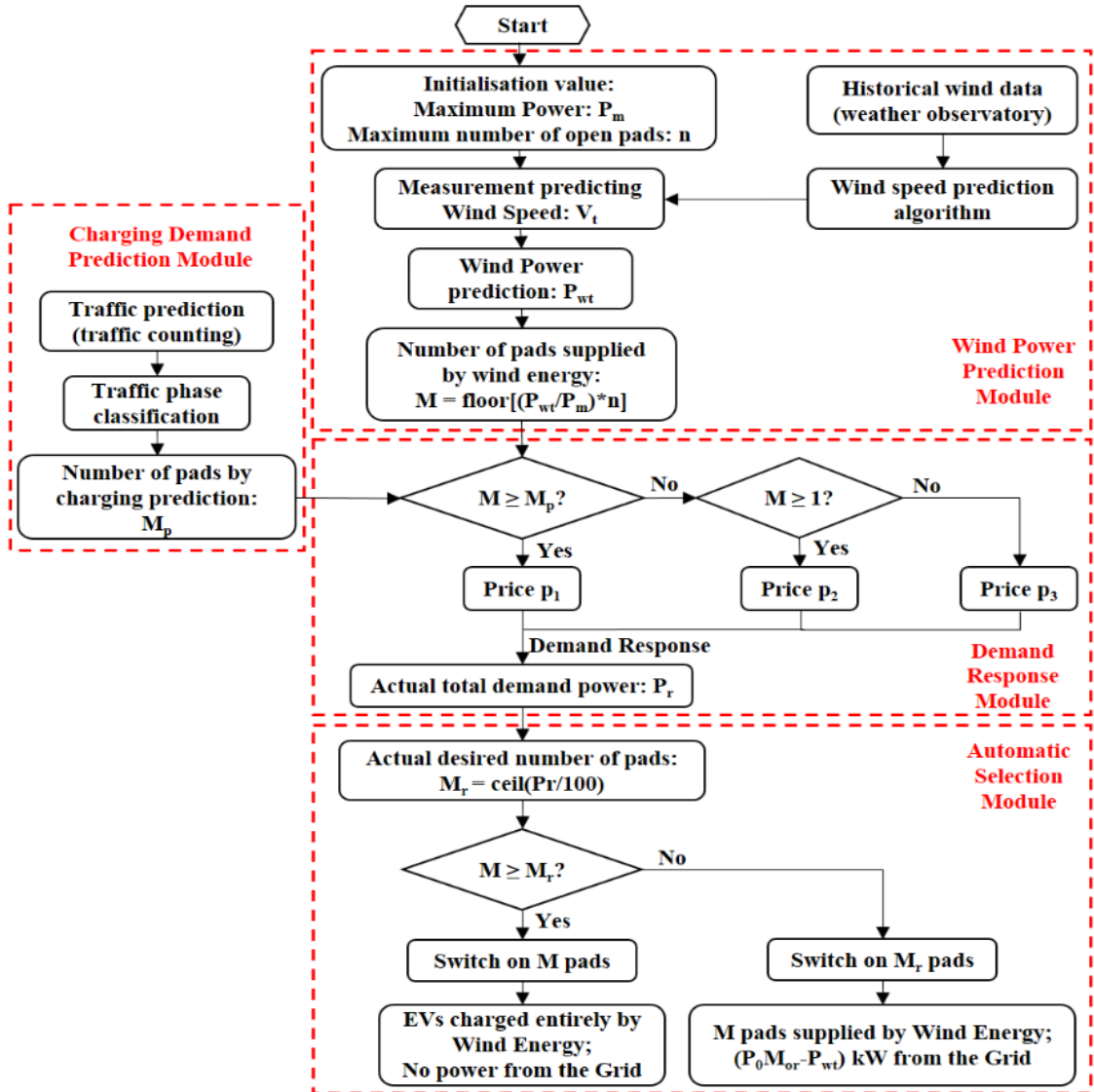
Figure 5.6: System function flowchart

1. Initialise the maximum power (P_m) that is the sum of rated power of all wind turbines, and then calculating the maximum number of pads that P_m can supply, *i.e. n*.

2. Forecasting future (time scale depending on system design) wind energy (P_{wt}) via wind speed (V) prediction which can be obtained from the historical wind data and wind speed prediction algorithm such as Auto Regression Algorithm.

3. Decide the number of pads that P_{wt} can supply (M) according to the algorithm: $M = Floor[(P_{wt}/P_m) * n]$.

4. Forecasting future (time scale depending on system design) traffic flow (N) using traffic flow counting infrastructure.

5. Decide the desired number of pads (M_p) according to the traffic phase classification and charging demand prediction programme.

6. Decide the charging price (p) based on the values of M and M_p, and then communicate p to potential consumers in the communication zone in order to operate price-incentivised Demand Response and collect the total demand power (P_r) and calculate the number of pads (M_r) required to supply these charging demand.

7. Decide the appropriate number of pads to be switched on by comparing demand and supply powers, *i.e.* P_{wt} and P_r. At this stage, P_{wt} is fully used aiming at maximize the utilisation of wind energy and eliminate the interference to the grid due to the wind power surplus.

8. Decide the energy supply model, independent wind energy or wind energy plus energy from the utility grid.

There are two supply models that system can choose:

- Case 1: $M \geq M_r$, switching on M pads. This means wind energy can independently meet all charging demand and all available wind energy is used up.

- Case 2: $M < M_r$, switching on M_r pads. This means wind energy is insufficient to supply all charging demand so M pads are charged by wind energy and $(M_r - M)$ pads are charged by the Grid, consuming $(P_r - P_{wt})$ kW electricity.

Charging Demand Predication Module

Since traffic flow reflects the potential charging demand to some extent, particularly when the entire vehicle fleet is EVs in the future, it can be used as an easy demand prediction approach. This could make better use of the existing traffic flow counting infrastructure and improve the efficiency and accuracy of charging demand prediction.

According to [164], traffic conditions are commonly classified into two, three or five phases: congested/ non-congested (two phases), congested/ medium congested/ non-congested (three phases) and free flow/ non-congested/ lightly congested/ congested/ heavily congested (five phases). Hence, charging demand prediction programmes can be proposed based on these traffic condition classifications. In the multiple segmented transmitters rail configuration, the corresponding desired number of charging pads by demand prediction can then be determined in a controlled manner. For example, Table 5.1 shows a five-phase charging demand prediction programme which will be applied in the case study in Section III.

In the programme, N is the traffic flow, M_p is the predicted desired number of charging pads by charging demand prediction programme, N_{max} is the maximum traffic flow in a specified time period and a_1, a_2, a_3 and a_4 are the upper limits of traffic flow at each phase. N_{max}, a_1, a_2, a_3 and a_4 can be defined by analyzing historical traffic data or traffic flow forecasting and they may vary with places, climate and regulations *etc*. For the former four phases, the values of M_p are obtained by multiplying the upper limit of traffic flow of that phase by a safety factor of 1.2 while for the last phase, the value of M_p, *i.e.* the maximum number of pads required to be switched on by demand prediction (notated as $'s'$), is obtained by multiplying the maximum traffic flow N_{max} by a safety factor of 1.2. In practical operation, M_p shall be rounded-ceiling to integers.

Traffic flow, N	Traffic phase	Desired number of charging pads, M_p
$N \leq a_i$	Free flow	$1.2a_1$
$a_1 < N \leq a_2$	No-congested	$1.2a_2$
$a_2 < N \leq a_3$	Lightly congested	$1.2a_3$
$a_3 < N \leq a_4$	congested	$1.2a_4$
$N > a_4$	Heavily congested	$1.2N_{max}$

Table 5.1: Five-phase charging demand prediction program

Demand Response Optimization Module

The electricity demand curve reflects that demand declines with the price rise, so price-based Demand Response (DR) techniques are commonly used in solving DR optimization problems. There are existing researches about flat pricing [7], peak load pricing [165] and adaptive pricing (real-time) [166], [167] for household DR and static EV charging DR. Unfortunately, these DR algorithms do not suit the highway traffic conditions such as fast speed, short charging duration and dynamic entry and leaving. In our system, a three-layer pricing scheme is formulated as (7), aiming at encouraging more charging demand when wind energy is sufficient while reducing charging demand when wind energy is insufficient.

$$
p = \begin{cases}
p_1, & M \geq M_p \\
p_2, & 1 \leq M < M_p \\
p_3, & M = 0
\end{cases}
\tag{5.2.13}
$$

where p is the charging price sending to customers, p_1 is the lowest price when wind energy is adequate to supply all predicted demand, p_2 is the medium price when wind energy can supply parts of the predicted demand and the Grid compensates for the supply deficit and p_3 is the highest price when no wind energy is available and the Grid is required to supply all charging demand. Therefore, $p_1 < p_2 < p_3$.

The charging price will be communicated to potential consumers when they enter the communication zone. The response of consumer i to the charging price is

modelled by carefully selected Utility Function as shown by (8)

$$U_i(\chi_i, \omega_i) = \omega_i \log \chi_i, i = 1, 2, .., N \tag{5.2.14}$$

where $U_i(\chi_i, \omega_i)$ is the utility function of consumer i, χ_i is the amount of electricity used by consumer i and ω_i is the willingness to pay parameter which varies between different customers. We assume ω_i is a random integer ranging between 1 and N.

The welfare of consumer i would then be:

$$W_i(\chi_i, \omega_i) = U_i(\chi_i, \omega_i) - p\chi_i \tag{5.2.15}$$

Assuming all consumers maximize their own welfare, the optimization problem at the consumer side is presented as:

$$\begin{cases} \text{maximize} & \sum_{i=1}^{N} W_i(\chi_i, \omega_i) \\ \text{subject to} & \chi_i \geq 0 \end{cases} \tag{5.2.16}$$

The solution to the optimization problem is obtained by solving equation (11):

$$\frac{\partial W_i(\chi_i, \omega_i)}{\partial \chi_i} = 0 \tag{5.2.17}$$

i.e. the optimal amount of electricity consumption for the maximum welfare of consumer i is:

$$\chi_i = \frac{\omega_i}{p \times (\ln 10)} \tag{5.2.18}$$

Once the optimal amount of electricity of all potential consumers are obtained, the welfare of each potential customer at the given charging price will then be calculated. It is assumed that only customers with positive maximum welfare, *i.e.*, $W_i(\chi_i, \omega_i) \geq 0$ will accept the charging price and get charged in the charging zone.

Among all available commercial EVs, the required charging power varies dramatically, ranging from 60-80 kW (low power, such as Smart [168], Volkswagen [169] and Nissan [170]) to 266-581 kW (high power, such as Tesla [171], Volvo [172] and

BMW [173]). In our system, we consider low-power EVs. Assuming the number of EVs responding for charging is $j(j \in [0, N])$, the required power of the batteries on these EVs are modelled as random integers below 100 kW. Hence, the total demand power becomes:

$$P_r = \sum_{k=1}^{j} 100 \times rand(1)_k \qquad (5.2.19)$$

where P_r is the total demand power and k is the serial number of EVs responding for charging.

Automatic Selection Module

In the automatic selection module, the corresponding number of pads for providing those demand power is first calculated:

$$M_r = \lceil \frac{P_r}{P_o} \rceil \qquad (5.2.20)$$

where M_r is the number of pads for providing P_r demand power and P_o is the nominal power of each pad.

By comparing the value of supply power and demand power, *i.e.* P_r and P_{wt}, the final number of pads to be turned on and the supply source(s) are determined aiming at maximizing the utilization of wind energy as well as minimizing the interference to the Grid. At this stage, the system performs in two cases as follows.

- Case 1: $P_{wt} \geq P_r$, switching on M pads. This means wind energy can independently meet all charging demand so all wind energy is used to encourage customers to charge and eliminate interference to the Grid due to wind energy surplus. Denoting the amount of power imported from the gird as P_g and then $P_g = 0$ in this case.

- Case 2: $P_{wt} < P_r$, switching on M_r pads. This means wind energy can not meet all charging demand and the grid is required to compensate the power

deficit. The amount of compensation power from the grid is calculated as:

$$P_g = P_r - P_{wt} \qquad (5.2.21)$$

5.2.3 Case study

In this section, a case study of the adaptive dynamic wireless charging system on a British motorway is demonstrated and the simulation results of different traffic and wind scenarios are discussed. The communication zone is set to 5 km and operation interval is three minutes.

Traffic Flow

MIDAS Site 9203 (LM4) on British Motorway A1 (M) was selected as the sample charging lane. The charging lane is 1 km long and the traffic flow counting infrastructure locates at the entry point of this lane. The historical traffic flow data in 2014 was obtained from [174], which showed that the double-lane three-minute traffic flow fluctuated between 2 and 71 vehicles. It was also noted that there existed different traffic patterns between weekdays and weekends as displayed in Fig. 5.7. The average three-minute traffic flow of Mondays to Fridays is generally higher than that of Saturdays and Sundays. In addition, there are two distinguishing traffic flow peaks during weekdays, one around 40 vehicles from 7 am to 9 am and the other between 50 and 62 vehicles from 4 pm to 6 pm. However, no significant peak occurs at weekends and the highest traffic flow reaches only 30 to 40 vehicles between 11 am and 5 pm.

On the other hand, it was found that there was no significant correlation between traffic flow and the driving speed. For instance, for driving speed at 110 km/h (68 mph), the three minute traffic flow ranged from 2 vehicles to 63 vehicles and the speed could occur at any time of a day. In majority intervals, the driving speed was relatively stable between 103 km/h (64 mph) and 120 km/h (75 mph), which complied with the speed limit of British motorways at 112 km/h (70 mph) [175]. In addition, [176] proved that the driving speeds had no impact on the power transfer efficiency of multiple segmented dynamic charging systems. Therefore, it is
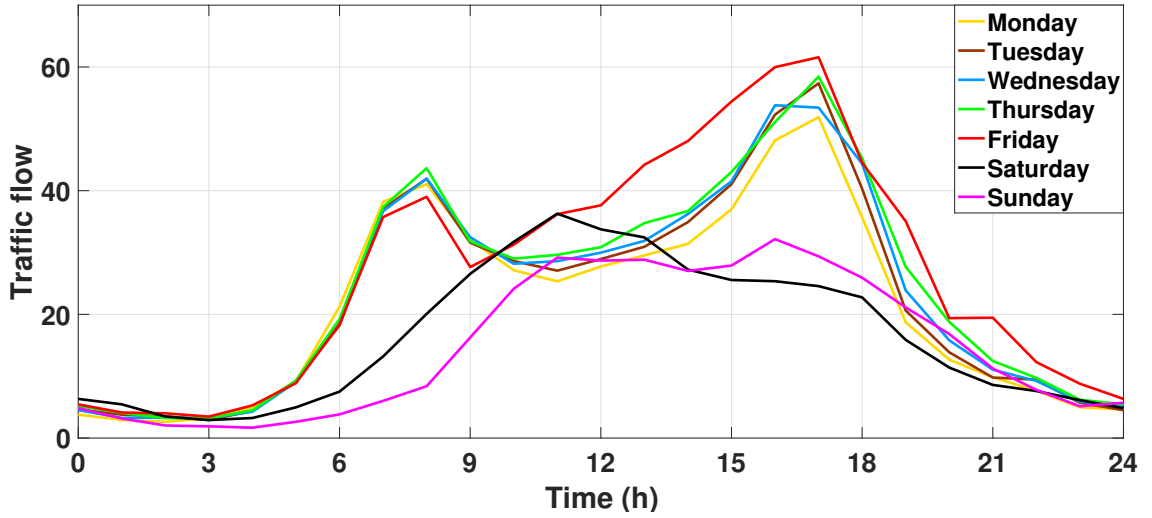
Figure 5.7: 24-hour traffic flow data

reasonable for our adaptive dynamic wireless charging system to operate based on the traffic flow rather than the driving speed.

The five-phase charging demand prediction programme is deployed in the case study. Parameters are set as: a_1=15, a_2=30, a_3=45, a_4=60 and N_{max}=75. Accordingly, the maximum desired number of charging pads by demand prediction is 90, *i.e.* n=90.

Wind Energy

According to the maximum desired number of charging pads by demand prediction (n=90) and the nominal charging power of each pad (P_o=100 kW), the maximum charging demand became 9000 kW. Hence, three 3 MW Permanent Magnet Direct Drive (PMDD) Wind Turbines from Goldwind Americas Inc. [177] were adopted with rated wind speed at 10.5 m/s. The dynamic power curve of the turbine is depicted in Fig. 5.8a. The historical observatory profiles in 2016 was obtained from Weybourne Atmospheric Observatory, University of East Anglia [178] and data of 21 March, 21 June, 21 September and 21 December were selected to represent wind conditions in spring, summer, autumn and winter, respectively. Fig. 5.8b and Fig. 5.8c shows the 24 hours wind power out in June and December.
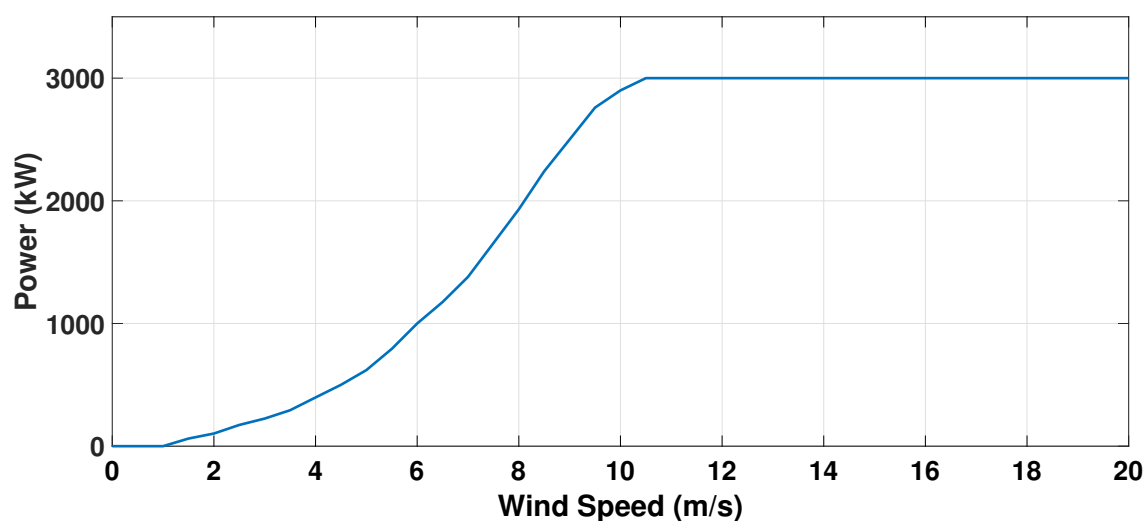
(a) Dynamic power curve of the Goldwind 3MW PMDD Wind Turbine
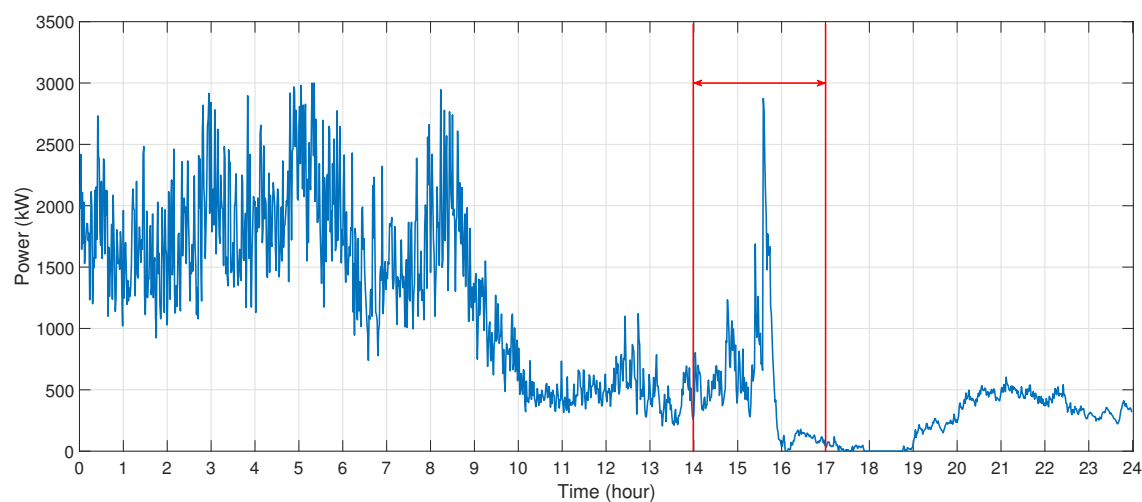
(b) 24-hour wind power out of 21 June 2016
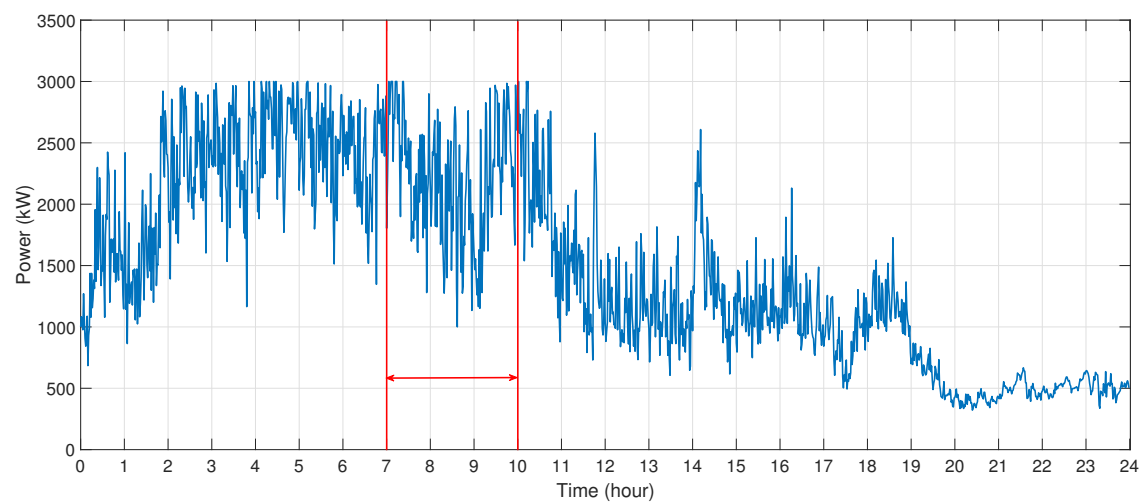
(c) 24-hour wind power out of 18 December 2016

Figure 5.8: 24-hour wind power out of different seasons

Normal Charging Power of Each Pad

Table 5.2 shows the charging pad parameters. The nominal charging power of each pad was set to 100 kW, *i.e.* P_o=100 kW, which could provide adequate power for low-power EVs considering the efficiency of wireless power transfer. The 100 charging pads are evenly installed along the charging lane. Each pad is designed as 9 m long and the distance between two pads is 1 m. Once the final number of pads to be turned on is obtained, *i.e.* M_r or M, the specified working pads will also be determined on an even manner:

$$s_1 = 1$$
$$s_2 = s_1 + \frac{100}{\lceil M_r or M \rceil}$$
$$s_3 = s_2 + \frac{100}{\lceil M_r or M \rceil}$$
$$...$$
$$s_{M_r[or M]} = s_{M_r - 1[or M - 1]} + \frac{100}{\lceil M_r or M \rceil}$$

For example, if 20 pads are required to be turned on, the system will automatically calculate the serial number of them: 1, 6, 11, 16, 21, 26, 31, 36, 41, 46, 51, 56, 61, 66, 71, 76, 81, 86, 91, 96.

Then the sensors at both ends of EVs and pads will be activated. When EVs approach the specified charging pads within the sensing range, the pads will be automatically turned on and the EVs drivers will receive speed reduction signal to ensure enough charging time and high charging efficiency. By contrast, when EVs pass the activated pads and go out of the sensing range, the pad will automatically turn off and EVs drivers will receive normal speed signal which means they could drive at any speed within the official speed limits.
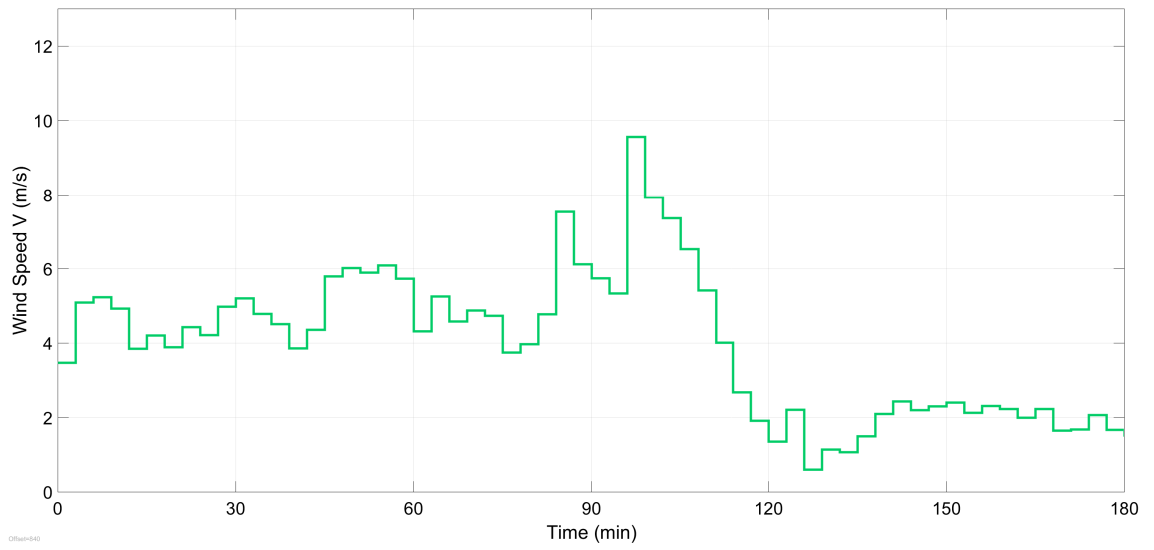
(a) Wind Speed
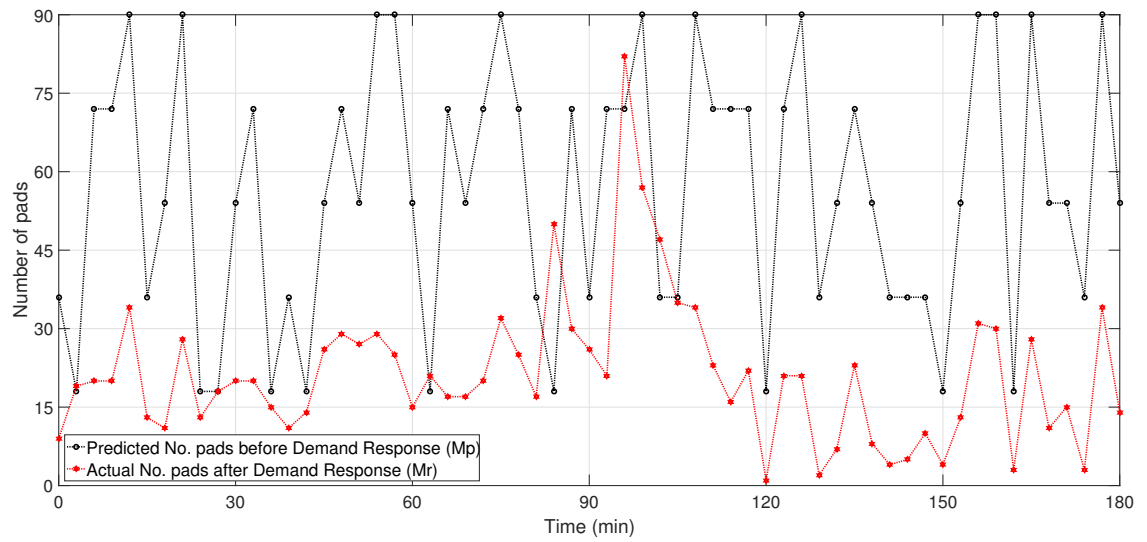
(b) The results of charging pad number
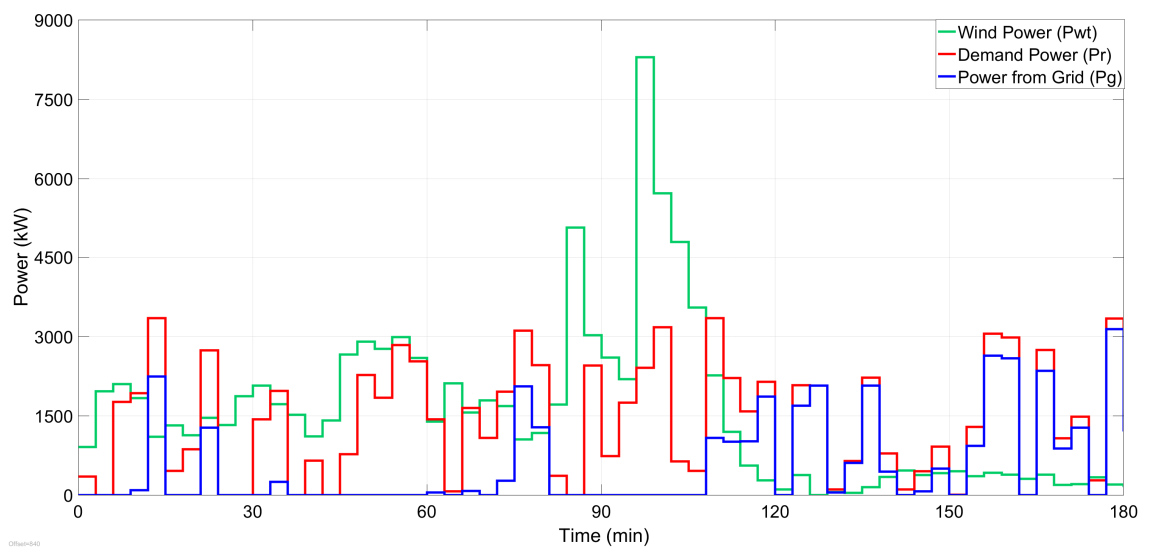
(c) The results of power

Figure 5.9: The results of system at 21th/June/2016
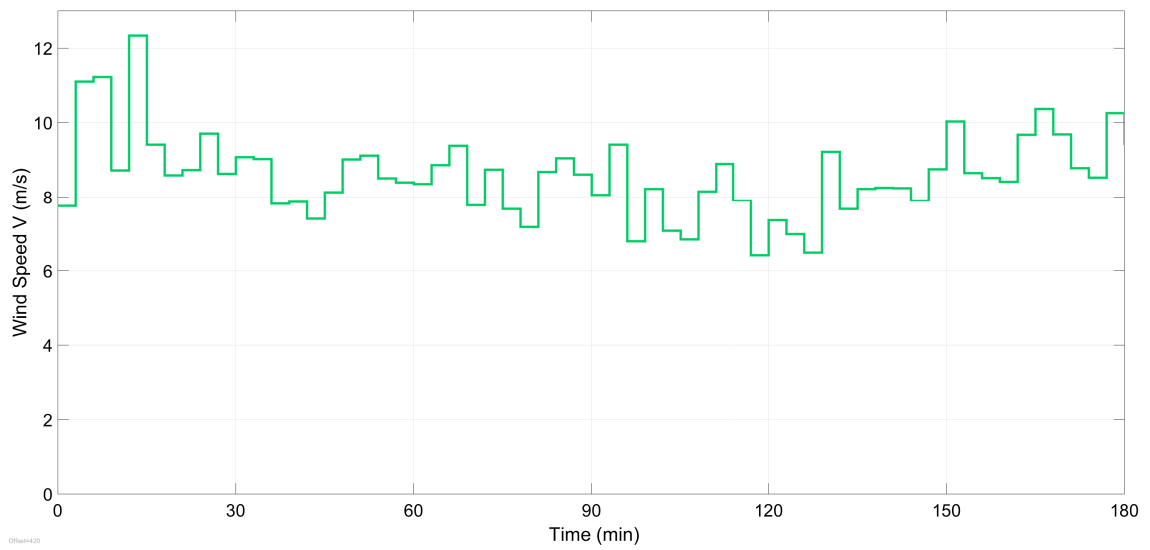
(a) Wind Speed
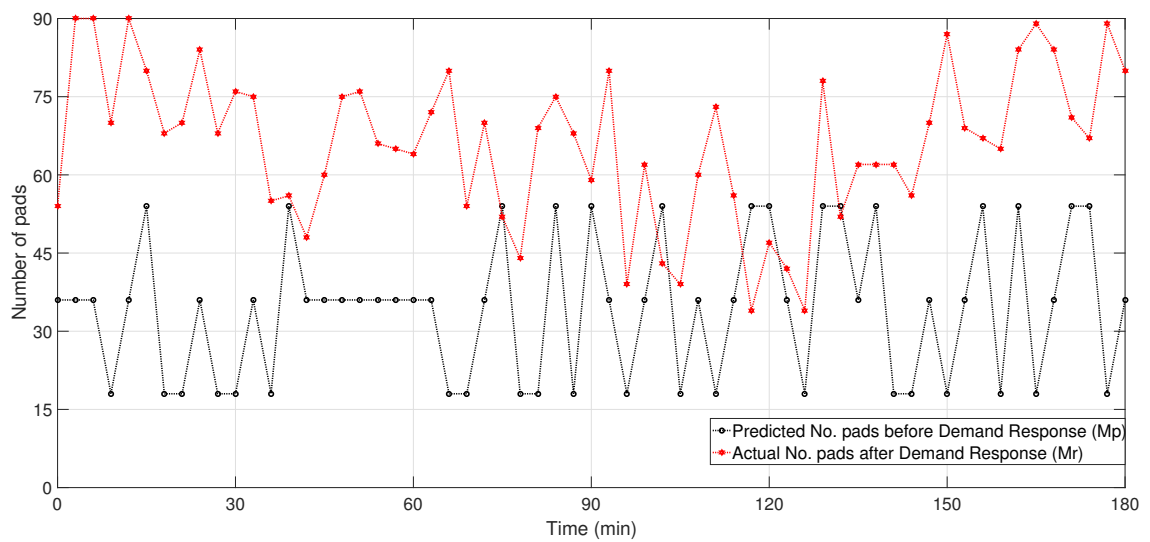
(b) The results of charging pad number
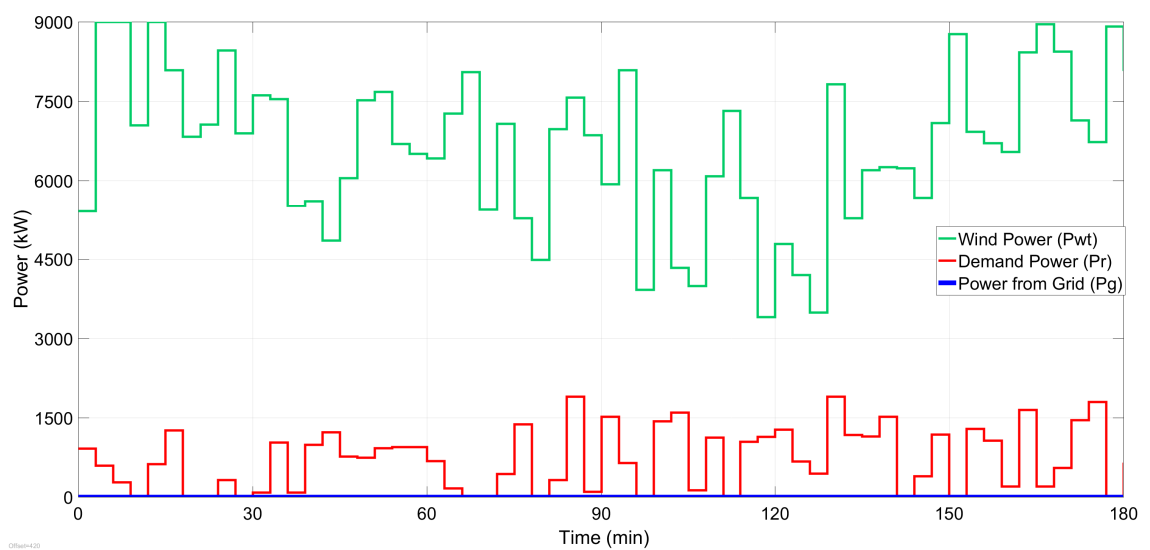
(c) The results of power

Figure 5.10: The results of system at 18th/December/2016

Table 5.2: Charging Pad Parameters

Charging lane length	1 km
Charging pad length	9 m
Distance between pads	1 m
Number of pads installed on the charging lane	100
Nominal power per pad	100 kw

5.3 Result

The simulation result of summer weekday scenario with wind profile from 2 pm to 5 pm on 21th June 2016 in the weekday traffic flow condition is selected as an example to illustrate the performance of the system. It can be seen from Fig.5.9 that although both wind speed and traffic flow vary intermittently, the system reacts sensitively and adaptively to the variation of the two inputs. Taking the consecutive intervals from 57 minutes to 60 minutes as example. The wind speed is 5.74 m/s so near 2600 kW wind power is generated by three turbines and 25 charging pads (M) can be supplied. However, at this time, the traffic flow reaches 64 vehicles requiring 90 charging pads (M_p) according to the five-phase charging demand prediction programme. Since $1 < M < M_p$, the system automatically give price P_2 to all customers, and after demand side response management, only 25 charging pads M_r are required. So the total wind power output is nearly 2600 kW, the power requirement from demand side is nearly 2500 kW, and the power from grid is zero. The system can adaptive the demand side response to reduce the utility grid stress.

It is also noted from Fig.5.9 that the five-phase charging demand prediction programme can mitigate the intermittency of charging demand due to the dynamic nature of traffic flow though more power is consumed. In addition, the prioritization of wind energy supply helps to mitigate the interference to the grid for half of the simulation time as well as reduce the electricity demand on the grid. With total consumption of 15.7 MWh for three hours, only 5 MWh electricity is supplied by the Grid. More than 10 MWh electricity is saved by integrating wind energy. This means 6.5 tons CO2 can be reduced according to [179].

Fig. 5.10 is the simulation result of winter weekend scenario with wind profile from 7:00 am to 10:00 am on 18th December 2016. The traffic flow is free at the

weekend, and the maximum traffic flow reaches 45 vehicles. However, at this time the average wind speed reaches 8 m/s, and the average wind power output is 6000 kW. The number of pads by traffic prediction is much less than the number of pads supplied by wind power. From the demand response module, the system provides a lower price to customers to encourage the charging. So Fig. 5.10b shows the number of pads after demand response (M_r) more than the number of pads before the demand response (M_p). The power supply from grid is zero, and the whole wind energy uses to EVs charging. This could help maximize the utilization of wind energy, reduce the additional cost for purchasing electricity from the grid and mitigate the intermittent impact to the grid.

5.3.1 Summary

Electrification of transport is an effective approach to alleviating the impact of energy crisis and climate change. Dynamic wireless charging shows promising potentions in addressing the driving range and battery concerns on EVs, but its dynamic nature in charging demand and higher operation requirements may pose higher pressure on the grid and lead to carbon emission growth. An adaptive dynamic wireless charging system for EVs driving on highways, integrating distributed wind energy supply and using traffic flow for charging demand prediction, has been presented in this paper. Demand response via price signals between customers and operators are investigated, which can optimize the energy generation, minimize the system cost and maximize customers' satisfaction. It is proved that the hierarchical charging demand prediction programme response fast and can mitigate the demand intermittancy to some extent. The prioritization of wind energy supply largely helps reduce the electricity demand from the grid as well as the corresponding carbon emissions. Future work will include the detailed configuration of the charging pads with high power transfer efficiency. Moreover, experimental tests will be performed in order to examine the commercial feasibility of this system.

Chapter 6

Conclusion and Future Work

6.1 Conclusion

Wireless power transfer technology in principle can be divided into three types: inductive coupling WPT, magnetic resonant coupling WPT, electromagnetic radiation WPT. The first two belong to near field transmission, and the last one is far field transmission. The operation of inductive coupling WPT is simple, but limited in the transmission distance, and high accurate alignment in the charging direction. Magnetic resonant coupling WPT's transmission distance longer than inductive coupling WPT, but more complex in the circuit implementation and multiple devices charged. Electromagnetic radiation WPT has high efficiency, long transmission distance merits. The disadvantage is radiation, and Line of Sight requirement. The most significant drawback of all WPT systems is the low efficiency of the energy transferred. Most losses happen during the transfer from coil to coil, summarized as:

1. **Improving the transmission efficiency and distance:**
   Coil design and coil material: coil size, coil geometry, coil alignment (lateral misalignment and angle misalignment)
   Circuit design and frequency
   Compensating circuit
   Environmental analysis and temperature, humidity
   Ferrite Core

2. Multiple transmitters/receivers design

Wireless EV charging has to face charging efficiency problems, too. Theoretical calculations show: increasing the radius of the receiver coil can improve the mutual inductance, thus improve the power transfer efficiency. However, there has a decreasing trend of power transfer efficiency when increasing the radius of the transmitter coil. That means large transmitter coil maybe can not lead to higher efficiency. So there has a design trade off among the coil size and the power transfer efficiency for the system. In addition, the magnetic coupling decreases rapidly with misaligned. The misalignment between transmitter coil and receiver coil is inevitable, especially in dynamic EVs charging case. In addition to the wireless charging will have to face the charging efficiency problem, wireless EVs charging will face the electrical standards and other issues, there are a lot of people worried about the electromagnetic radiation of wireless charging.

This thesis introduces a novel array type primary resonant coil design, which solves the misalignment issue in MRC-WPT and achieves a higher PTE. In practice, coil misalignment is inevitable, since it is difficult for drivers to accurately park their car above a designated charging point or stay within dynamic charging boundaries. MAPLE16 was used to calculate the theoretical PTE values and ADS 2012 to implement an equivalent circuit. Experimental results were obtained using custom designed hardware and showed a clear trend between the theory and real-world implementation of the proposed array design. PTE improvements were observed, of up to 20% in simulations and between 30-90% in the experimental set-up. Furthermore the array design can reduce the RX coil radius and thus reduce the cars weight. Another advantage is the flexibility in choosing any number of TX array coils and varying their arrangement. However, this thesis only considers the case where a single TX coil in the array is energized at any time.

Dynamic EVs charging is another research topic in this thesis. The segmentation power supply rail was an optimal choice for dynamic EVs charging rail. Each segment should be independently turned ON and OFF. The length of the segment rail was an important design issue because it would be too expensive if the length was very short due to an increased number of inverters or switch boxes. Otherwise, the

power transfer efficiency would decrease if the length was very long due to increased resistance. Besides these issues, the amount of segments, the distance between neighboring segments and car length should be considered in dynamic EVs charging scheme. We modeled multiple segmented transmitters' design in dynamic wireless EVs charging. Based on the proposed theory and simulation results, the vehicle's speed v is not a determinant factor of distance between the neighboring transmitter T design. The size of the transmitter rail can affect the design of T for optimizing the PTE.

Dynamic wireless charging for Electric Vehicles (EVs) is promising to promote the take-up of EVs by extending the driving range and reducing the size and cost of batteries of EVs. However, its dynamic charging demand and rigorous operation requirements may stress the Grid and increase carbon emissions. This thesis proposes a novel adaptive dynamic wireless charging system for EVs driving on highways which integrates wind energy supply and traffic flow-based charging demand prediction programme aiming at cutting down the system cost and carbon emissions, realizing fast demand prediction and supply response as well as relieving the demand on the Grid. lower speed limit is imposed to enhance the customers' satisfaction. The hierarchical charging demand prediction programme is proved effective in demand intermittent mitigation. Electricity supply from the Grid and the corresponding carbon emission can be reduced due to the prioritization of wind energy.

6.2 Future Work

In the future we have some further work on the coil design for static EV charging:

1) Overlapping Coil Design

   The sharp drop in PTE between coils along the tangential boundary (in chapter 3) could be resolved using an overlapping array or hexagonally shaped coils as shown in Figure 6.1. Although the overall array radius in an overlapping configuration would be reduced, the maximum possible misalignment distance between coils would also be reduced. Hence, the red areas marking high PTE on the color

map in Figure 4.16b would merge together, resulting in an increased average PTE of the array. This would also reduce the slight PTE drop seen at coil transitions along the central boundary.

2) High Power Hardware Implementation

   The hardware implementation is a prototype, future work will verify it in high power EV implementation. The adaptive hardware design presented in chapter 3 focuses only on PTE improvements related to the coil misalignment and neglects the losses incurred by additional circuitry required in a complete EV charging system. These might include AC-DC converters on the transmitting side and receiver side rectification and subsequent voltage conditioning for the battery load. Hence the proposed design would need further work to include these functions and to analyze their effects on the overall PTE.

3) Battery analysis

   Battery modelling is another main work in the design.
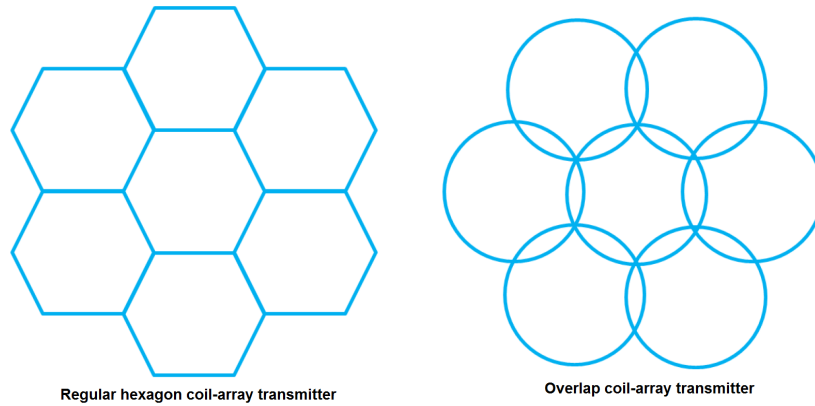
Figure 6.1: Future Work of TX coil array design

For dynamic wireless power transfer for electric vehicle charging:

1) Optimize segmented transmitters design for dynamic EVs charging In the dynamic EVs charging, I proposed that the size of the transmitter rail can affect the design of T for optimizing the power transfer efficiency. In the future work, I will give a detail model design talk about the relationship between the transmitter size, distance T and power transfer efficiency. We hope we can do the hardware circuit test in the future work.

2) Renewable dynamic EVs charging system analysis In future work, I will do more analysis about customers communication in demand response and charging rails design.

Publications List

Journal Publications

1 **Xiaolin Mou**, Oliver Groling, Hongjian Sun, "Energy Efficient and Adaptive Design for Wireless Power Transfer in Electric Vehicles," accepted: *IEEE Transaction on industrial electronics.(05/Mar/2017),* doi : 10.1109/TIE.2017.2686299

2 **Xiaolin Mou**, Hongjian Sun, "Analysis of Multiple Segmented Transmitters Design in Dynamic Wireless Power Transfer for Electric Vehicles Charging," accepted: *Electronics Letters (22/May/2017),* doi :10.1049/el.2016.3340

Conference Publications

1 **Xiaolin Mou**, Oliver Groling, Andrew Gallant, Hongjian Sun, "Energy Efficient and Adaptive Design for Wireless Power Transfer in Electric Vehicles," *in Proc. 2016 IEEE 83rd Vehicular Technology Conference (VTC Spring)*, Nanjing, China, 2016, pp.1-5. doi:10.1109/VTCSpring.2016.7504220

2 Minglei You, **Xiaolin Mou**, Hongjian Sun,"Effective capacity analysis of smart grid communication networks," *in Proc. 2015 IEEE 20th International Workshop on Computer Aided Modelling and Design of Communication Links and Networks (CAMAD)*, Guildford, UK, 2015, pp. 196-200. doi: 10.1109/CAMAD 2015.7390508

3 **Xiaolin Mou**, Hongjian Sun, "Wireless Power Transfer: Survey and Roadmap," *in Proc. 2015 IEEE 81st Vehicular Technology Conference (VTC Spring)*, Glasgow, UK, 2015, pp. 1-5. doi: 10.1109/VTCSpring.2015.7146165

References

[1] T. Nikola, "System of electric lighting," 1891, US Patent 454'622.

[2] A. Waser, "Nikola tesla's wireless systems." [Online]. Available: http://www.andre-waser.ch/Publications/NikolaTeslasWirelessSystems.pdf

[3] T. Nikola, "Electrical transformer," 1897, US Patent 593'138.

[4] A. Kurs, "Wireless power transfer via strongly coupled magnetic resonances," *Science express*, pp. 83–86, June 2007.

[5] â. Agreement, "United nations framework convention on climate change." [Online]. Available: http://unfccc.int/files/essential_background/convention/application/pdf/english_paris_agreement.pdf,accessedMar.2017

[6] I. E. Agency, "Global ev outlook 2016: Beyond one million electric cars." [Online]. Available: https://www.iea.org/publications/freepublications/publicationGlobal_EV_Outlook_2016.pdf,assessedMar.2017

[7] C. A. GarcÃŋa-VÃązquez, F. Llorens-Iborra, L. M. FernÃąndez-RamÃŋrez, H. SÃąnchez-Sainz, and F. Jurado, "Evaluating dynamic wireless charging of electric vehicles moving along a stretch of highway," in *2016 International Symposium on Power Electronics, Electrical Drives, Automation and Motion (SPEEDAM)*, June 2016, pp. 61–66.

[8] R. Bosshard and J. W. Kolar, "Inductive power transfer for electric vehicle charging: Technical challenges and tradeoffs," *IEEE Power Electronics Magazine*, vol. 3, no. 3, pp. 22–30, Sept 2016.

[9] F. T. *et al*, "Dynamic wireless ev charging fed from railway grid: Grid connection concept," in *Proc. 2015 International Conference on Electrical Systems for Aircraft, Railway, Ship Propulsion and Road Vehicles (ESARS)*, March 2015, pp. 1–5.

[10] B. Kallel, T. Keutel, and O. Kanoun, "Miso configuration efficiency in inductive power transmission for supplying wireless sensors," in *Proc. 2014 11th International Multi-Conference on Systems, Signals Devices (SSD)*, Feb 2014, pp. 1–5.

[11] S. L. *et al*, "Design and implementation of shaped magnetic-resonance-based wireless power transfer system for roadway-powered moving electric vehicles," *IEEE Transactions on Industrial Electronics*, vol. 61, Part 3, pp. 1179–1192, 2014.

[12] S. Y. R. Hui, W. Zhong, and C. K. Lee, "A critical review of recent progress in mid-range wireless power transfer," *IEEE Trans. Power Electronics*, vol. 29, no. 9, pp. 4500–4511, Sept 2014.

[13] T. Theodoropoulos, Y. Damousis, and A. Amditis, "A load balancing control algorithm for EV static and dynamic wireless charging," in *Proc. 2015 IEEE 81st VTC*, 2015, pp. 1–5.

[14] B. Esteban, M. Sid-Ahmed, and N. C. Kar, "A comparative study of power supply architectures in wireless ev charging systems," *IEEE Trans. Power Electronics*, vol. 30, no. 11, pp. 6408–6422, Nov 2015.

[15] Y. D. Chung, C. Y. Lee, H. Kang, and Y. G. Park, "Design considerations of superconducting wireless power transfer for electric vehicle at different inserted resonators," *IEEE Trans. Applied Superconductivity*, vol. 26, no. 4, pp. 1–5, June 2016.

[16] W. Zhang, J. C. White, A. M. Abraham, and C. C. Mi, "Loosely coupled transformer structure and interoperability study for EV wireless charging systems," *IEEE Trans. Power Electronics*, vol. 30, no. 11, pp. 6356–6367, Nov 2015.

[17] J. Kim, H. C. Son, D. H. Kim, K. H. Kim, and Y. J. Park, "Efficiency of magnetic resonance wpt with two off-axis self-resonators," in *Proc. 2011 IEEE MTT-S International Microwave Workshop Series on Innovative Wireless Power Transmission: Technologies, Systems, and Applications*, May 2011, pp. 127–130.

[18] H. K. *et al*, "Coil design and measurements of automotive magnetic resonant wireless charging system for high-efficiency and low magnetic field leakage," *Proc. IEEE Transactions on Microwave Theory and Techniques*, vol. 64, no. 2, pp. 383–400, Feb 2016.

[19] J. D. *et al*, "Compact and efficient bipolar coupler for wireless power chargers: Design and analysis," *Proc. IEEE Transactions on Power Electronics*, vol. 30, no. 11, pp. 6130–6140, Nov 2015.

[20] Z. Dang and J. Qahouq, "Modeling and investigation of magnetic resonance coupled wireless power transfer system with lateral misalignment," *Proc. 29th Annual IEEE Applied Power Electronics Conference and Exposition (APEC)*, pp. 1313–1322, 2014.

[21] K. Fotopoulou and B. Flynn, "Wireless power transfer in loosely coupled links," *in Proc. IEEE Transactions on Magnetics*, vol. 47, no. 2, pp. 413–430, 2011.

[22] R. C. Fernandes and A. de Oliveira, "Iterative design method of weakly coupled magnetic elements for inductive power transfer," *Proc. Brazilian Power Electronics Conference (COBEP)*, pp. 1088–1093, 2013.

[23] R. J. *et al*, "Overcoming coil misalignment using magnetic fields of induced currents in wireless power transmission," *Proc. IEEE International Microwave Symposium Digest (MTT)*, pp. 1–4, 2012.

[24] Z. H. *et al*, "Field distribution models of spiral coil for misalignment analysis in wpt systems," *Proc. IEEE Transactions on Microwave Theory and Techniques*, vol. 62, no. 4, pp. 920–933, 2014.

[25] X. Mou and H. Sun, "Wireless power transfer: Survey and roadmap," in *Proc. of IEEE 81st VTC*, 2015, pp. 1–5.

[26] Y. C. H. Hoang and F. Bien, "Efficiency improvement for magnetic resonance based wireless power transfer with axial-misalignment," *Electronics Letters*, vol. 48, no. 6, pp. 339–341, 2012.

[27] J. K. *et al*, "Consideration of use of arrayed transmitting coils in wireless power transfer with magnetically coupled resonance," *Proc. International Symposium on Antennas and Progagation (ISAP)*, pp. 451–454, 2012.

[28] S. I. *et al*, "Positioning-free resonant wireless power transmission sheet with staggered repeater coil array," *Proc. IEEE Antennas and Wireless Propagation Letters*, vol. 11, pp. 1710–1714, 2012.

[29] H. M. *et al*, "A consideration of efficiency improvement of transmitting coil array in wireless power transfer with magnetically coupled resonance," *Proc. IEEE Wireless Power Transfer (WPT)*, pp. 13–16, 2013.

[30] M. Fu, H. Yin, X. Zhu, and C. Ma, "Analysis and tracking of optimal load in wireless power transfer systems," *IEEE Trans. Power Electronics*, vol. 30, no. 7, pp. 3952–3963, July 2015.

[31] Y. Lim, H. Tang, S. Lim, and J. Park, "An adaptive impedance-matching network based on a novel capacitor matrix for wireless power transfer," *IEEE Trans. Power Electronics*, vol. 29, no. 8, pp. 4403–4413, Aug 2014.

[32] L. C. Meng, K. W. E. Cheng, and S. L. Ho, "Multicoils design for induction cookers with applying switched exciting method," *IEEE Trans. Magnetics*, vol. 48, no. 11, pp. 4503–4506, Nov 2012.

[33] S. Y. Hui, "Planar wireless charging technology for portable electronic products and qi," *Proc. Proceedings of the IEEE*, vol. 101, no. 6, pp. 1290–1301, June 2013.

[34] W. X. Zhong, X. Liu, and S. Y. R. Hui, "A novel single-layer winding array and receiver coil structure for contactless battery charging systems with

free-positioning and localized charging features," *IEEE Trans. Industrial Electronics*, vol. 58, no. 9, pp. 4136–4144, Sept 2011.

[35] S. Y. R. Hui and W. W. C. Ho, "A new generation of universal contactless battery charging platform for portable consumer electronic equipment," *IEEE Trans. Power Electronics*, vol. 20, no. 3, pp. 620–627, May 2005.

[36] "System description wireless power transfer, volume i : low pawer, part1: Interface definition." [Online]. Available: http://www.wirelesspowerconsortium.com

[37] T. Nakamura and S. Ichikawa, "Vehicle parking assist system, vehicle including the same, and vehicle parking assist method," Apr. 16 2013, US Patent 8,423,223.

[38] M. Bruni and E. Davenport, "Self-aligning inductive charger," 1996, US Patent 5,498,948. [Online]. Available: http://www.google.com/patents/US5498948

[39] J. Welschholz, "Charging system for vehicles where the charging coils are coupled through the vehicle license plate," 2015, US Patent 9,145,063.

[40] [Online]. Available: http://www.ecofriend.com/wireless-charging-electric-cars.html

[41] [Online]. Available: http://www.evmeerkat.com/tag/wireless/

[42] F. Musavi and W. Eberle, "Overview of wireless power transfer technologies for electric vehicle battery charging," *IET Power Electronics*, vol. 7, no. 1, pp. 60–66, January 2014.

[43] M. Hassan and A. E. Zawawi, "Wireless power transfer (wireless lighting)," in *Proc. 2015 5th International Conference on Information Communication Technology and Accessibility (ICTA)*, Dec 2015, pp. 1–4.

[44] J. Dai and D. C. Ludois, "A survey of wireless power transfer and a critical comparison of inductive and capacitive coupling for small gap applications," *IEEE Trans. Power Electronics*, vol. 30, no. 11, pp. 6017–6029, Nov 2015.

[45] M. Debbou and F. Colet, "Inductive wireless power transfer for electric vehicle dynamic charging," in *Proc. 2016 IEEE PELS Workshop on Emerging Technologies: Wireless Power Transfer (WoW)*, Oct 2016, pp. 118–122.

[46] J. Dai and D. C. Ludois, "Wireless electric vehicle charging via capacitive power transfer through a conformal bumper," in *Proc. APEC*, March 2015, pp. 3307–3313.

[47] Y. Zhang, Z. Zhao, and K. Chen, "Frequency decrease analysis of resonant wireless power transfer," *IEEE Trans. Power Electronics*, vol. 29, no. 3, pp. 1058–1063, March 2014.

[48] B. Kallel, T. Keutel, and O. Kanoun, "Miso configuration efficiency in inductive power transmission for supplying wireless sensors," in *Proc. 2014 11th International Multi-Conference on Systems, Signals Devices (SSD)*, Feb 2014, pp. 1–5.

[49] K. Fotopoulou and B. Flynn, "Wireless power transfer in loosely coupled links: Coil misalignment model," *Proc. IEEE Transactions on Magnetics*, vol. 47, no. 2, pp. 416–430, Feb 2011.

[50] L. Xie, Y. Shi, Y. Hou, and A. Lou, "Wireless power transfer and applications to sensor networks," *IEEE Wireless Communications*, vol. 20, no. 4, pp. 140–145, August 2013.

[51] J. D. Kim, C. Sun, and I. S. Suh, "A proposal on wireless power transfer for medical implantable applications based on reviews," in *Proc. Wireless Power Transfer Conference (WPTC), 2014 IEEE*, May 2014, pp. 166–169.

[52] C. R. Valenta and G. D. Durgin, "Harvesting wireless power: Survey of energy-harvester conversion efficiency in far-field, wireless power transfer systems," *IEEE Microwave Magazine*, vol. 15, no. 4, pp. 108–120, June 2014.

[53] A. Sahai and D. Graham, "Optical wireless power transmission at long wavelengths," in *Proc. 2011 International Conference on Space Optical Systems and Applications (ICSOS)*, May 2011, pp. 164–170.

[54] A. Massa, G. Oliveri, F. Viani, and P. Rocca, "Array designs for long-distance wireless power transmission: State-of-the-art and innovative solutions," *Proceedings of the IEEE*, vol. 101, no. 6, pp. 1464–1481, June 2013.

[55] R. M. Dickinson, "Power in the sky: Requirements for microwave wireless power beamers for powering high-altitude platforms," *IEEE Microwave Magazine*, vol. 14, no. 2, pp. 36–47, March 2013.

[56] P. Jaffe and J. McSpadden, "Energy conversion and transmission modules for space solar power," *Proceedings of the IEEE*, vol. 101, no. 6, pp. 1424–1437, June 2013.

[57] S. Bi, C. K. Ho, and R. Zhang, "Recent advances in joint wireless energy and information transfer," in *Proc. 2014 IEEE Information Theory Workshop (ITW)*, Nov 2014, pp. 341–345.

[58] L. Liu, R. Zhang, and K. C. Chua, "Wireless information and power transfer: A dynamic power splitting approach," *IEEE Transactions on Communications*, vol. 61, no. 9, pp. 3990–4001, September 2013.

[59] S. K. Samanta and C. K. Chanda, "Wireless power network design through smart grid transmission system model," in *Proc. 2015 International Conference on Energy, Power and Environment: Towards Sustainable Growth (ICEPE)*, June 2015, pp. 1–5.

[60] C. Zhang, N. Tang, W. Zhong, C. K. Lee, and R. S. Y. Hui, "A new energy harvesting and wireless power transfer system for smart grid," in *Proc. 2016 IEEE 7th International Symposium on Power Electronics for Distributed Generation Systems (PEDG)*, June 2016, pp. 1–5.

[61] C. Kyprianou, C. Psomas, and I. Krikidis, "A green wireless powered sensor network: An experimental approach," in *Proc. 2016 18th Mediterranean Electrotechnical Conference (MELECON)*, April 2016, pp. 1–6.

[62] Q. Liu, K. S. Yildirim, P. Pawe?czak, and M. Warnier, "Safe and secure wireless power transfer networks: challenges and opportunities in rf-based systems," *IEEE Communications Magazine*, vol. 54, no. 9, pp. 74–79, September 2016.

[63] K. Huang and V. K. N. Lau, "Enabling wireless power transfer in cellular networks: Architecture, modeling and deployment," *IEEE Transactions on Wireless Communications*, vol. 13, no. 2, pp. 902–912, February 2014.

[64] N. Shinohara and T. Ichihara, "Coexistence of wireless power transfer via microwaves and wireless communication for battery-less zigbee sensors," in *Proc. 2014 International Symposium on Electromagnetic Compatibility, Tokyo (EMC'14/Tokyo)*, May 2014, pp. 445–448.

[65] S. Bi, C. K. Ho, and R. Zhang, "Wireless powered communication: opportunities and challenges," *IEEE Communications Magazine*, vol. 53, no. 4, pp. 117–125, April 2015.

[66] T. He, K.-W. Chin, and S. Soh, "On using wireless power transfer to increase the max flow of rechargeable wireless sensor networks," in *Proc.2015 IEEE Tenth International Conference on Intelligent Sensors, Sensor Networks and Information Processing (ISSNIP)*, April 2015, pp. 1–6.

[67] T. He, K. W. Chin, and S. Soh, "On wireless power transfer and max flow in rechargeable wireless sensor networks," *IEEE Access*, vol. 4, pp. 4155–4167, 2016.

[68] M. Kiani, U. M. Jow, and M. Ghovanloo, "Design and optimization of a 3-coil inductive link for efficient wireless power transmission," *IEEE Transactions on Biomedical Circuits and Systems*, vol. 5, no. 6, pp. 579–591, Dec 2011.

[69] C.-S. Wang, G. A. Covic, and O. H. Stielau, "Power transfer capability and bifurcation phenomena of loosely coupled inductive power transfer systems," *IEEE Transactions on Industrial Electronics*, vol. 51, no. 1, pp. 148–157, Feb 2004.

[70] O. H. Stielau and G. A. Covic, "Design of loosely coupled inductive power transfer systems," in *Proc. International Conference on Power System Technology, 2000. Proceedings. PowerCon 2000*, vol. 1, 2000, pp. 85–90 vol.1.

[71] H. H. Wu, A. Gilchrist, K. Sealy, P. Israelsen, and J. Muhs, "Design of symmetric voltage cancellation control for lcl converters in inductive power transfer systems," in *Proc. 2011 IEEE International Electric Machines Drives Conference (IEMDC)*, May 2011, pp. 866–871.

[72] F. Liu, Y. Zhang, K. Chen, Z. Zhao, and L. Yuan, "A comparative study of load characteristics of resonance types in wireless transmission systems," in *Proc. 2016 Asia-Pacific International Symposium on Electromagnetic Compatibility (APEMC)*, vol. 01, May 2016, pp. 203–206.

[73] T. Kan, T. D. Nguyen, J. C. Wjite, R. K. Malhan, and C. Mi, "A new integration method for an electric vehicle wireless charging system using lcc compensation topology," *IEEE Transactions on Power Electronics*, vol. PP, no. 99, pp. 1–1, 2016.

[74] F. Lu, H. Zhang, H. Hofmann, and C. C. Mi, "A dynamic charging system with reduced output power pulsation for electric vehicles," *IEEE Transactions on Industrial Electronics*, vol. 63, no. 10, pp. 6580–6590, Oct 2016.

[75] J. Deng, F. Lu, W. Li, R. Ma, and C. Mi, "Zvs double-side lcc compensated resonant inverter with magnetic integration for electric vehicle wireless charger," in *Proc. 2015 IEEE Applied Power Electronics Conference and Exposition (APEC)*, March 2015, pp. 1131–1136.

[76] A. O. *et al*, "Analysis of impedance matched circuit for wireless power transfer," in *Proc. 2014 - 40th Annual Conference of the IEEE Industrial Electronics Society*, Oct 2014, pp. 2965–2970.

[77] Y. Li, X. Li, F. Peng, H. Zhang, W. Guo, W. Zhu, and T. Yang, "Wireless energy transfer system based on high q flexible planar-litz mems coils," in *Proc. 2013 8th IEEE International Conference on Nano/Micro Engineered and Molecular Systems (NEMS)*, April 2013, pp. 837–840.

[78] T. Mizuno, S. Yachi, A. Kamiya, and D. Yamamoto, "Improvement in efficiency of wireless power transfer of magnetic resonant coupling using magneto-plated wire," *IEEE Transactions on Magnetics*, vol. 47, no. 10, pp. 4445–4448, Oct 2011.

[79] D. Kurschner, C. Rathge, and U. Jumar, "Design methodology for high efficient inductive power transfer systems with high coil positioning flexibility," *IEEE Transactions on Industrial Electronics*, vol. 60, no. 1, pp. 372–381, Jan 2013.

[80] J. P. K. Sampath, A. Alphones, L. Y. Y. Kenneth, and D. M. Vilathgamuwa, "Analysis on normalized distance and scalability in designing wireless power transfer," in *Proc. 2015 IEEE PELS Workshop on Emerging Technologies: Wireless Power (WoW),*, June 2015, pp. 1–6.

[81] S. Xianjin, L. Guoqiang, L. Yanhong, Z. Chao, and X. Xiaoyu, "Analyses and experiments of field-circuit coupling equations for wireless power transfer using solenoidal coils," in *Proc. 2015 IEEE International Wireless Symposium (IWS)*, March 2015, pp. 1–4.

[82] Z. Pantic and S. Lukic, "Computationally-efficient, generalized expressions for the proximity-effect in multi-layer, multi-turn tubular coils for wireless power transfer systems," *IEEE Transactions on Magnetics*, vol. 49, no. 11, pp. 5404–5416, Nov 2013.

[83] M. Q. Nguyen, Z. Hughes, P. Woods, Y. S. Seo, S. Rao, and J. C. Chiao, "Field distribution models of spiral coil for misalignment analysis in wireless power transfer systems," *IEEE Transactions on Microwave Theory and Techniques*, vol. 62, no. 4, pp. 920–930, April 2014.

[84] T. Ishizaki, D. Fukada, and I. Awai, "A novel concept for 2-dimensional free-access wireless power transfer system using asymmetric coupling resonators with different sizes," in *Proc. 2011 IEEE MTT-S International Microwave Workshop Series on Innovative Wireless Power Transmission: Technologies, Systems, and Applications (IMWS)*, May 2011, pp. 243–246.

[85] S. Mehri, A. C. Ammari, J. B. H. Slama, and L. Ladhar, "Performance characterization of variable width square coils for inductive link wireless power transfer," in *Proc. 2016 18th Mediterranean Electrotechnical Conference (MELECON)*, April 2016, pp. 1–6.

[86] F. Jolani, Y. q. Yu, and Z. D. Chen, "Electromagnetic modeling and optimization of magnetic resonant coupling wireless power transfer using coil array," in *Proc. 2015 IEEE MTT-S International Conference on Numerical Electromagnetic and Multiphysics Modeling and Optimization (NEMO)*, Aug 2015, pp. 1–3.

[87] Z. Dang and J. Qahouq, "Modeling and investigation of magnetic resonance coupled wireless power transfer system with lateral misalignment," in *Proc. 2014 Twenty-Ninth Annual IEEE Applied Power Electronics Conference and Exposition (APEC)*, March 2014, pp. 1317–1322.

[88] K. Fotopoulou and B. Flynn, "Wireless power transfer in loosely coupled links: Coil misalignment model," *IEEE Transactions on Magnetics*, vol. 47, no. 2, pp. 416–430, Feb 2011.

[89] A. Sample, D. Meyer, and J. Smith, "Analysis, experimental results, and range adaptation of magnetically coupled resonators for wireless power transfer," *IEEE Transactions on Industrial Electronics*, vol. 58, no. 2, pp. 544–554, Feb 2011.

[90] L. Chen, S. Liu, Y. C. Zhou, and T. J. Cui, "An optimizable circuit structure for high-efficiency wireless power transfer," *IEEE Transactions on Industrial Electronics*, vol. 60, no. 1, pp. 339–349, Jan 2013.

[91] O. Jonah and S. Georgakopoulos, "Wireless power transfer in concrete via strongly coupled magnetic resonance," *IEEE Transactions on Antennas and Propagation*, vol. 61, no. 3, pp. 1378–1384, March 2013.

[92] S. Moon, B.-C. Kim, S.-Y. Cho, C.-H. Ahn, and G.-W. Moon, "Analysis and design of a wireless power transfer system with an intermediate coil for high

efficiency," *IEEE Transactions on Industrial Electronics*, vol. 61, no. 11, pp. 5861–5870, Nov 2014.

[93] K. Knaisch, M. Springmann, and P. Gratzfeld, "Comparison of coil topologies for inductive power transfer under the influence of ferrite and aluminum," in *Proc. 2016 Eleventh International Conference on Ecological Vehicles and Renewable Energies (EVER)*, April 2016, pp. 1–9.

[94] E. Kilinc, C. Dehollaini, and F. Maloberti, "Design and optimization of inductive power transmission for implantable sensor system," in *Proc. 2010 XIth International Workshop on Symbolic and Numerical Methods, Modeling and Applications to Circuit Design (SM2ACD)*, Oct 2010, pp. 1–5.

[95] R. Castanho Fernandes and A. de Oliveira, "Iterative design method of weakly coupled magnetic elements for inductive power transfer," in *Proc. 2013 Brazilian Power Electronics Conference (COBEP)*, Oct 2013, pp. 1088–1094.

[96] R. Jegadeesan, Y.-X. Guo, and M. Je, "Overcoming coil misalignment using magnetic fields of induced currents in wireless power transmission," in *Proc. 2012 IEEE MTT-S International Microwave Symposium Digest (MTT)*, June 2012, pp. 1–3.

[97] D. Liu, H. Hu, and S. Georgakopoulos, "Misalignment sensitivity of strongly coupled wireless power transfer systems," *IEEE Transactions on Power Electronics*, vol. PP, no. 99, pp. 1–1, 2016.

[98] J. McLean and R. Sutton, "The multipole nature of the extraneous field of a magnetic field wireless power transfer system," in *Proc. 2016 IEEE International Symposium on Electromagnetic Compatibility (EMC)*, July 2016, pp. 582–587.

[99] D. Ahn and S. Hong, "Effect of coupling between multiple transmitters or multiple receivers on wireless power transfer," *IEEE Transactions on Industrial Electronics*, vol. 60, no. 7, pp. 2602–2613, July 2013.

[100] K. Miwa, H. Mori, N. Kikuma, H. Hirayama, and K. Sakakibara, "A consideration of efficiency improvement of transmitting coil array in wireless power transfer with magnetically coupled resonance," in *Proc. 2013 IEEE Wireless Power Transfer (WPT)*, May 2013, pp. 13–16.

[101] K. Koh, T. Beh, T. Imura, and Y. Hori, "Multi-receiver and repeater wireless power transfer via magnetic resonance coupling," in *Proc. 2012 15th International Conference on Electrical Machines and Systems (ICEMS)*, Oct 2012, pp. 1–6.

[102] K. Miwa, H. Mori, N. Kikuma, H. Hirayama, and K. Sakakibara, "A consideration of efficiency improvement of transmitting coil array in wireless power transfer with magnetically coupled resonance," in *Proc. 2013 IEEE Wireless Power Transfer (WPT)*, May 2013, pp. 13–16.

[103] J. Kim, H.-C. Son, D.-H. Kim, and Y.-J. Park, "Optimal design of a wireless power transfer system with multiple self-resonators for an LED TV," *IEEE Transactions on Consumer Electronics*, vol. 58, no. 3, pp. 775–780, August 2012.

[104] J. Shin, S. Shin, Y. Kim, S. Ahn, S. Lee, G. Jung, S.-J. Jeon, and D.-H. Cho, "Design and implementation of shaped magnetic-resonance-based wireless power transfer system for roadway-powered moving electric vehicles," *IEEE Transactions on Industrial Electronics*, vol. 61, no. 3, pp. 1179–1192, March 2014.

[105] S. Li and C. C. Mi, "Wireless power transfer for electric vehicle applications," *IEEE Journal of Emerging and Selected Topics in Power Electronics*, vol. 3, no. 1, pp. 4–17, March 2015.

[106] S. Y. R. Hui, W. Zhong, and C. K. Lee, "A critical review of recent progress in mid-range wireless power transfer," *IEEE Transactions on Power Electronics*, vol. 29, no. 9, pp. 4500–4511, Sept 2014.

[107] T. T. *et al*, "A load balancing control algorithm for EV static and dynamic wireless charging," in *Proc. 2015 IEEE 81st Vehicular Technology Conference*, 2015, pp. 1–5.

[108] B. Esteban, M. Sid-Ahmed, and N. C. Kar, "A comparative study of power supply architectures in wireless ev charging systems," *IEEE Transactions on Power Electronics*, vol. 30, no. 11, pp. 6408–6422, Nov 2015.

[109] Y. D. C. *et al*, "Design considerations of superconducting wireless power transfer for electric vehicle at different inserted resonators," *IEEE Transactions on Applied Superconductivity*, vol. 26, no. 4, pp. 1–5, June 2016.

[110] W. Z. *et al*, "Loosely coupled transformer structure and interoperability study for ev wireless charging systems," *IEEE Transactions on Power Electronics*, vol. 30, no. 11, pp. 6356–6367, Nov 2015.

[111] J. K. *et al*, "Efficiency of magnetic resonance wpt with two off-axis self-resonators," in *Proc. 2011 IEEE MTT-S International Microwave Workshop Series on Innovative Wireless Power Transmission: Technologies, Systems, and Applications (IMWS)*, May 2011, pp. 127–130.

[112] H. K. *et al*, "Coil design and measurements of automotive magnetic resonant wireless charging system for high-efficiency and low magnetic field leakage," *IEEE Transactions on Microwave Theory and Techniques*, vol. 64, no. 2, pp. 383–400, Feb 2016.

[113] Z. Dang and J. Qahouq, "Modeling and investigation of magnetic resonance coupled wireless power transfer system with lateral misalignment," *Proc. 29th Annual IEEE Applied Power Electronics Conference and Exposition (APEC)*, pp. 1313–1322, 2014.

[114] K. Fotopoulou and B. Flynn, "Wireless power transfer in loosely coupled links," *Proc. IEEE Transactions on Magnetics*, vol. 47, no. 2, pp. 413–430, 2011.

[115] R. C. Fernandes and A. de Oliveira, "Iterative design method of weakly coupled magnetic elements for inductive power transfer," *Proc. Brazilian Power Electronics Conference (COBEP)*, pp. 1088–1093, 2013.

[116] R. J. *et al*, "Overcoming coil misalignment using magnetic fields of induced currents in wireless power transmission," *Proc. IEEE International Microwave Symposium Digest (MTT)*, pp. 1–4, 2012.

[117] Z. H. *et al*, "Field distribution models of spiral coil for misalignment analysis in wpt systems," *IEEE Transactions on Microwave Theory and Techniques*, vol. 62, no. 4, pp. 920–933, 2014.

[118] X. Mou and H. Sun, "Wireless power transfer: Survey and roadmap," in *Proc. of 81st IEEE Vehicular Technology Conference*, 2015, pp. 1–5.

[119] Y. C. H. Hoang and F. Bien, "Efficiency improvement for magnetic resonance based wireless power transfer with axial-misalignment," *Electronics Letters*, vol. 48, no. 6, pp. 339–341, 2012.

[120] J. K. *et al*, "Consideration of use of arrayed transmitting coils in wireless power transfer with magnetically coupled resonance," *Proc. International Symposium on Antennas and Progagation (ISAP)*, pp. 451–454, 2012.

[121] S. I. *et al*, "Positioning-free resonant wireless power transmission sheet with staggered repeater coil array," *IEEE Antennas and Wireless Propagation Letters*, vol. 11, pp. 1710–1714, 2012.

[122] H. M. *et al*, "A consideration of efficiency improvement of transmitting coil array in wireless power transfer with magnetically coupled resonance," *IEEE Wireless Power Transfer (WPT)*, pp. 13–16, 2013.

[123] M. Budhia, G. Covic, and J. Boys, "A new ipt magnetic coupler for electric vehicle charging systems," in *Proc. IECON 2010 - 36th Annual Conference on IEEE Industrial Electronics Society*, Nov 2010, pp. 2487–2492.

[124] H. Takanashi, Y. Sato, Y. Kaneko, S. Abe, and T. Yasuda, "A large air gap 3 kw wireless power transfer system for electric vehicles," in *Proc. 2012 IEEE Energy Conversion Congress and Exposition (ECCE)*, Sept 2012, pp. 269–274.

[125] T. D. Nguyen, S. Li, W. Li, and C. C. Mi, "Feasibility study on bipolar pads for efficient wireless power chargers," in *Proc. 2014 IEEE Applied Power Electronics Conference and Exposition - APEC 2014*, March 2014, pp. 1676–1682.

[126] W. Zhang, J. C. White, A. M. Abraham, and C. C. Mi, "Loosely coupled transformer structure and interoperability study for ev wireless charging systems," *IEEE Transactions on Power Electronics*, vol. 30, no. 11, pp. 6356–6367, Nov 2015.

[127] S. Y. Choi, B. W. Gu, S. Y. Jeong, and C. T. Rim, "Advances in wireless power transfer systems for roadway-powered electric vehicles," *IEEE Journal of Emerging and Selected Topics in Power Electronics*, vol. 3, no. 1, pp. 18–36, March 2015.

[128] S. Lee, J. Huh, C. Park, N. S. Choi, G. H. Cho, and C. T. Rim, "On-line electric vehicle using inductive power transfer system," in *Proc. 2010 IEEE Energy Conversion Congress and Exposition*, Sept 2010, pp. 1598–1601.

[129] J. Huh, S. W. Lee, W. Y. Lee, G. H. Cho, and C. T. Rim, "Narrow-width inductive power transfer system for online electrical vehicles," *IEEE Transactions on Power Electronics*, vol. 26, no. 12, pp. 3666–3679, Dec 2011.

[130] C. Park, S. Lee, S. Y. Jeong, G. H. Cho, and C. T. Rim, "Uniform power i-type inductive power transfer system with dq-power supply rails for on-line electric vehicles," *IEEE Transactions on Power Electronics*, vol. 30, no. 11, pp. 6446–6455, Nov 2015.

[131] S. Y. Choi, S. Y. Jeong, B. W. Gu, G. C. Lim, and C. T. Rim, "Ultraslim s-type power supply rails for roadway-powered electric vehicles," *IEEE Transactions on Power Electronics*, vol. 30, no. 11, pp. 6456–6468, Nov 2015.

[132] C. C. Mi, G. Buja, S. Y. Choi, and C. T. Rim, "Modern advances in wireless power transfer systems for roadway powered electric vehicles," *IEEE Transactions on Industrial Electronics*, vol. 63, no. 10, pp. 6533–6545, Oct 2016.

[133] V. X. Thai, S. Y. Choi, B. H. Choi, J. H. Kim, and C. T. Rim, "Coreless power supply rails compatible with both stationary and dynamic charging of electric vehicles," in *Proc. 2015 IEEE 2nd International Future Energy Electronics Conference (IFEEC)*, Nov 2015, pp. 1–5.

[134] J. M. Miller, P. T. Jones, J. M. Li, and O. C. Onar, "Ornl experience and challenges facing dynamic wireless power charging of ev's," *IEEE Circuits and Systems Magazine*, vol. 15, no. 2, pp. 40–53, Secondquarter 2015.

[135] J. M. Miller, O. C. Onar, C. White, S. Campbell, C. Coomer, L. Seiber, R. Sepe, and A. Steyerl, "Demonstrating dynamic wireless charging of an electric vehicle: The benefit of electrochemical capacitor smoothing," *IEEE Power Electronics Magazine*, vol. 1, no. 1, pp. 12–24, March 2014.

[136] M. Budhia, G. A. Covic, and J. T. Boys, "Design and optimization of circular magnetic structures for lumped inductive power transfer systems," *IEEE Transactions on Power Electronics*, vol. 26, no. 11, pp. 3096–3108, Nov 2011.

[137] G. A. Covic, M. L. G. Kissin, D. Kacprzak, N. Clausen, and H. Hao, "A bipolar primary pad topology for ev stationary charging and highway power by inductive coupling," in *Proc. 2011 IEEE Energy Conversion Congress and Exposition*, Sept 2011, pp. 1832–1838.

[138] S. Shin, J. Shin, Y. Kim, S. Lee, B. Song, G. Jung, and S. Jeon, "Hybrid inverter segmentation control for online electric vehicle," in *Proc. 2012 IEEE International Electric Vehicle Conference*, March 2012, pp. 1–6.

[139] H. Z. Z. Beh, G. A. Covic, and J. T. Boys, "Wireless fleet charging system for electric bicycles," *IEEE Journal of Emerging and Selected Topics in Power Electronics*, vol. 3, no. 1, pp. 75–86, March 2015.

[140] G. R. Nagendra, J. T. Boys, G. A. Covic, B. S. Riar, and A. Sondhi, "Design of a double coupled ipt ev highway," in *Proc. IECON 2013 - 39th Annual Conference of the IEEE Industrial Electronics Society*, Nov 2013, pp. 4606–4611.

[141] S. Choi, J. Huh, W. Y. Lee, S. W. Lee, and C. T. Rim, "New cross-segmented power supply rails for roadway-powered electric vehicles," *IEEE Transactions on Power Electronics*, vol. 28, no. 12, pp. 5832–5841, Dec 2013.

[142] L. Chen, G. R. Nagendra, J. T. Boys, and G. A. Covic, "Double-coupled systems for ipt roadway applications," *IEEE Journal of Emerging and Selected Topics in Power Electronics*, vol. 3, no. 1, pp. 37–49, March 2015.

[143] K. Y. K. *et al*, "Power transfer efficiency of magnetic resonance wireless power link with misaligned relay resonator," in *Proc. 42nd European Microwave Conference*, Oct 2012, pp. 217–220.

[144] Z. Dang and J. Qahouq, "Modeling and investigation of magnetic resonance coupled wireless power transfer system with lateral misalignment," in *Proc. 29th Applied Power Electronics Conference and Exposition*, March 2014, pp. 1317–1322.

[145] R. e. Jegadeesan, "Overcoming coil misalignment using magnetic fields of induced currents in wireless power transmission," in *Proc. 2012 IEEE MTT-S International in Microwave Symposium Digest*, June 2012, pp. 1–3.

[146] X. Zhang, Z. Yuan, Q. Yang, Y. Li, J. Zhu, and Y. Li, "Coil design and efficiency analysis for dynamic wireless charging system for electric vehicles," *IEEE Trans. Magnetics*, vol. 52, no. 7, pp. 1–4, July 2016.

[147] H. C. Son, J. W. Kim, Y. J. Park, and K. H. Kim, "Efficiency analysis and optimal design of a circular loop resonant coil for wireless power transfer," in *Proc. 2010 Asia-Pacific Microwave Conference*, Dec 2010, pp. 849–852.

[148] F. Lu, H. Zhang, H. Hofmann, and C. C. Mi, "A dynamic charging system with reduced output power pulsation for electric vehicles," *IEEE Transactions on Industrial Electronics*, vol. 63, no. 10, pp. 6580–6590, Oct 2016.

[149] S. A. B. *et al*, "How driver behaviour and parking alignment affects inductive charging systems for electric vehicles," *Transportation Research Part C: Emerging Technologies*, vol. 58, Part D, pp. 721–731, 2015.

[150] J. Kim, H.-C. Son, D.-H. Kim, and Y.-J. Park, "Optimal design of a wireless power transfer system with multiple self-resonators for an LED TV," *IEEE Transactions on Consumer Electronics*, vol. 58, no. 3, pp. 775–780, August 2012.

[151] B. E. *et al*, "A comparative study of power supply architectures in wireless ev charging systems," *Proc. IEEE Transactions on Power Electronics*, vol. 30, no. 11, pp. 6408–6422, Nov 2015.

[152] S. L. *et al.*, "Wireless power transfer by electric field resonance and its application in dynamic charging," *Proc. IEEE Transactions on Industrial Electronics*, vol. 63, no. 10, pp. 6602–6612, Oct 2016.

[153] A. O. *et al*, "Analysis of impedance matched circuit for wireless power transfer," in *Proc. 2014 - 40th Annual Conference of the IEEE Industrial Electronics Society*, Oct 2014, pp. 2965–2970.

[154] V. *et al*, "Wireless power transfer for electric vehicles - present and future trends," in *Proc. Electric Vehicles in Smart Grids*. Springer, 2015, pp. 33–60.

[155] Y. Cao, Z. Dang, J. A. A. Qahouq, and E. Phillips, "Dynamic efficiency tracking controller for reconfigurable four-coil wireless power transfer system," in *Proc. 2016 IEEE APEC*, March 2016, pp. 3684–3689.

[156] M. Q. Nguyen, Z. Hughes, P. Woods, Y. S. Seo, S. Rao, and J. C. Chiao, "Field distribution models of spiral coil for misalignment analysis in wireless power transfer systems," *IEEE Trans. Microwave Theory and Techniques*, vol. 62, no. 4, pp. 920–930, April 2014.

[157] K. Song, C. Zhu, K. E. Koh, T. Imura, and Y. Hori, "Wireless power transfer for running ev powering using multi-parallel segmented rails," in *Proc. 2015 IEEE PELS Workshop on Emerging Technologies: Wireless Power (2015 WoW)*, June 2015, pp. 1–6.

[158] K. K. Ean, S. Kai, P. Sukprasert, T. Imura, and Y. Hori, "Two-transmitter wireless power transfer with lcl circuit for continuous power in dynamic charging," in *Proc. 2015 IEEE PELS Workshop on Emerging Technologies: Wireless Power (2015 WoW)*, June 2015, pp. 1–6.

[159] O. Smiai, F. Bellotti, A. D. Gloria, R. Berta, A. Amditis, Y. Damousis, and A. Winder, "Information and communication technology research opportunities in dynamic charging for electric vehicle," in *Proc. 2015 Euromicro Conference on Digital System Design*, Aug 2015, pp. 297–300.

[160] J. Kim, H. C. Son, D. H. Kim, K. H. Kim, and Y. J. Park, "Efficiency of magnetic resonance wpt with two off-axis self-resonators," in *Proc. 2011 IEEE MTT-S International Microwave Workshop Series on Innovative Wireless Power Transmission: Technologies, Systems, and Applications*, May 2011, pp. 127–130.

[161] G. A. Warren L. Stutzman, Thiele, *Antenna Theory and Design.* John Wiley and Sons, 2007.

[162] T. V. Theodoropoulos, I. G. Damousis, and A. J. Amditis, "Demand-side management ict for dynamic wireless ev charging," *IEEE Transactions on Industrial Electronics*, vol. 63, no. 10, pp. 6623–6630, Oct 2016.

[163] H. Aliyu and J. T. Agee, "Electric energy from the hybrid wind-solar thermal power plants," in *Proc. 2016 IEEE PES PowerAfrica*, June 2016, pp. 264–268.

[164] H. Yi, H. Jung, and S. Bae, "Deep neural networks for traffic flow prediction," in *2017 IEEE International Conference on Big Data and Smart Computing (BigComp)*, Feb 2017, pp. 328–331.

[165] K. M. T. Jia Ying Yong, Vigna K. Ramachandaramurthy and N. Mithulananthan, "A review on the state-of-the-art technologies of electric vehicle, its impacts and prospects," *In Renewable and Sustainable Energy Reviews*, vol. 49, pp. 365–385, 2015.

[166] U. F. Limited, "âĂIJev city casebook 50 big ideas shaping the future of electric mobility." [Online]. Available: http://urbanforesight.org/projects/case-studies/detail/ev-city-casebook-50-big-ideas-shaping-future-electric-mobility/,accessedMar. 2017

[167] T. Theodoropoulos, Y. Damousis, and A. Amditis, "A load balancing control algorithm for ev static and dynamic wireless charging," in *2015 IEEE 81st Vehicular Technology Conference (VTC Spring)*, May 2015, pp. 1–5.

[168] Smart, "Electric drive." [Online]. Available: http://uk.smart.com/uk/en/index/smartelectric-drive.html,accessedJune2017

[169] Volkswagen, "Electric-hybrid cars." [Online]. Available: http://www.volkswagen.co.uk/new/electric-hybrid,accessedJune2017

[170] Nissan, "Leaf." [Online]. Available: https://www.nissan.co.uk/vehicles/newvehicles/leaf.html,accessedJune2017

[171] Tesla, "Tesla." [Online]. Available: https://www.tesla.com/en_GB/,accessedJune2017

[172] Volvo, "Xc90." [Online]. Available: http://www.volvocars.com/uk/cars/newmodels/xc90-twin-engine,accessedJune2017

[173] BMW, "Bmw." [Online]. Available: http://www.bmw.co.uk/en_GB/topics/new-cars/explore-our-model-types/electric/introduction.html, accessedJune2017

[174] Data.gov.uk, "Highways england network journey time and traffic flow data." [Online]. Available: https://data.gov.uk/

dataset/highways-englandnetwork-journey-time-and-traffic-flow-data, accessedJune2017

[175] GOV.UK, "Speed limits." [Online]. Available: https://www.gov.uk/speed-limits,accessedJune2017

[176] X. Mou and H. Sun, "Analysis of multiple segmented transmitters design in dynamic wireless power transfer for electric vehicles charging," *Electronics Letters*, vol. 53, no. 14, pp. 941–943, 2017.

[177] G. Americas, "3.0 mw(s) pmdd wind turbine brochure." [Online]. Available: http://www.goldwindamericas.com/sites/default/files/Gold-wind%20Americas_Goldwind%203.0MW%28S%29%20Brochure%20%282017%29.pdf,accessedJune2017.

[178] U. of East Anglia, "Centre for environmental data analysis." [Online]. Available: https://services.ceda.ac.uk/cedasite/myceda/user/,accessedJune2017

[179] P. O. of Science and Technology, "Carbon footprint of electricity generation." [Online]. Available: https://www.parliament.uk/documents/post/postpn_383-carbon-footprint-electricity-generation.pdf